รายงานวิจัยฉบับสมบูรณ์

โครงการ การศึกษาโครงสร้างและกลไกการเกิดปฏิกิริยาของสารประกอบ oxiranes บน Nanoporous และ Mesoporous Zeolites

โดย อ.ดร.บุญเดช เบิกฟ้า

มิถุนายน 2556 สัญญาเลขที่ MRG5480239

รายงานวิจัยฉบับสมบูรณ์

โครงการ การศึกษาโครงสร้างและกลไกการเกิดปฏิกิริยาของสารประกอบ oxiranes บน Nanoporous และ Mesoporous Zeolites

ผู้วิจัย
อ.ดร.บุญเดช เบิกฟ้า

สังกัด
มหาวิทยาลัยเกษตรศาสตร์

สนับสนุนโดยสำนักงานคณะกรรมการการอุดมศึกษา
สำนักงานกองทุนสนับสนุนการวิจัยและมหาวิทยาลัยเกษตรศาสตร์

บทคัดย่อ

รหัสโครงการ : MRG5480239
ชื่อโครงการ : การศึกษาโครงสร้างและกลไกการเกิดปฏิกิริยาของสารประกอบ oxiranes บน Nanoporous และ Mesoporous Zeolites
ชื่อนักวิจัย : อ.ดร.บุญเดช เบิกฟ้า
อีเมลล์ : bundet.b@ku.ac.th
ระยะเวลาโครงการ : 1 กรกฎาคม 2554 – 30 มิถุนายน 2556

บทคัดย่อ:

ซีโอไลต์มีความสำคัญเป็นอย่างมากในอุตสาหกรรม เนื่องจากความสามารถของตัวมันที่ใช้ในการเป็นตัวดูดซับ ตัวแยก และตัวเร่งปฏิกิริยา ซีโอไลต์มีมากมายหลายชนิด ZSM-5 เป็นซีโอไลต์ชนิดหนึ่งที่สำคัญมาก และใช้ในปฏิกิริยาเคมีอินทรีย์มากมาย อาทิ butene isomerization, propexe oxide isomerization เป็นต้น

เริ่มแรกนั้นเราศึกษาการดูดซับและการเกิดปฏิกิริยาของ 1-butene ไปเป็น isobutene ด้วยตัวเร่งปฏิกิริยา H-ZSM-5 ด้วยการคำนวณแบบ ONIOM(MP2:M06-2X) พบว่าพลังงานการดูดซับของ 1-butene มีค่า -16.5 kcal/mol สำหรับปฏิกิริยานั้นทำการคำนวณกลไก 4 ขั้นตอน 1) การเกิด protonation ของตัวดูดซับ 1-butene ไปเป็น seconday alkoxide intermediate 2) การเกิด methyl shift จาก secondary alkoxide ไปเป็น primary alkoxide 3) การเกิด proton transfer ไปเป็น tert-butyl carbenium ion และ 4) ปฏิกิริยา deprotonation ไปเป็นผลิตภัณฑ์ isobutene พบว่าขั้นกำหนดอัตราการเกิดปฏิกิริยาคือขั้นที่ 3 ด้วยค่าพลังงานกระตุ้น 34.7 kcal/mol สอดคล้องกับการทดลอง

ต่อมาได้ศึกษาการเกิดปฏิกิริยา isomerization ของ propene oxide (methyl oxirane) บนตัวเร่งปฏิกิริยา H-FER พลังงานการดูดซับของ propene oxide, propanal and propanone มีค่า -25.5, -24.5 and -26.0 kcal/mol ตามลำดับ สอดคล้องการค่าการทดลอง (propanone บน H-ZSM-5 -31.1 kcal/mol) กลไกการเกิดปฏิกิริยาแบ่งออกเป็น 2 ขั้นตอน คือ 1) ปฏิกิริยา protonation เพื่อเกิด ring-opening และ 2) เกิด 1,2-hydride shift ผลิตภัณฑ์ที่ได้ มี2 ประเภทคือ propanal และ propanone สำหรับ propanal นั้น ค่าพลังงานกระตุ้น 31.6 kcal/mol มีค่าต่ำกว่า propanone ที่มีค่าพลังงานกระตุ้น 48.9 kcal/mol

คำหลัก: Zeolite, H-ZSM-5, butene isomerization, propene oxide isomerization, M06-2X

Abstract

Project Code : MRG5480239
Project Title : Structure and Reaction Mechanism of Oxiranes over Nanoporous and Mesoporous Zeolites
Investigator : Dr. Bundet Boekfa
E-mail Address : bundet.b@ku.ac.th
Project Period : 1 July 2011 – 30 June 2013

Abstract:

Zeolites have a high impact in chemical industries because of their wide range of applications in adsorption, separation and particularly as they regarded as catalysts. Among the various pore zeolites, ZSM-5 is one of the most important zeolite for being used for many organic reactions such as butene isomerization and propene oxide isomerization.

Firstly, the adsorption and skeletal isomerization of 1-butene to isobutene on the nanoporous H-ZSM-5 catalyst has been studied by ONIOM calculations. The adsorption energy of 1-butene from ONIOM (MP2:M06-2X) calculations is -16.5 kcal/mol. This and other results obtained with the M06-2X functional are in better agreement with the experiment than corresponding ones from the ωB97X-D functional. The reaction mechanism of the skeletal isomerization of 1-butene is proposed to proceed in four steps: 1) protonation of adsorbed 1-butene to a secondary alkoxide intermediate, 2) methyl shift between adjacent carbon-carbon atoms of the secondary alkoxide to form the primary alkoxide, 3) proton transfer to form the tert-butyl carbenium ion, and 4) deprotonation of the carbenium intermediate, leading to isobutene as the reaction product. The third step of the reaction is rate determining with an activation energy of 34.7 kcal/mol, in good agreement well with the experimental value of 30.0 kcal/mol.

Next, the reaction mechanism of propene oxide on H-FER has been studied with quantum calculation. The adsorption of propene oxide, propanal and propanone on H-FER zeolite are calculated and found to be -25.5, -24.5 and -26.0 kcal/mol, which agree well with experimental data for the propanone interacted with zeolite (-31.1 kcal/mol). The isomerization reaction mechanism of propene oxide is considered to proceed through a stepwise mechanism: (1) the epoxide ring protonation, and, concurrently, the ring-opening, and (2), the 1,2-hydride shift formatting the adsorbed carbonyl compound. Two different types of product, propanal and propanone, were observed. For the propanal product, the ring opening step is found to be the rate-determining step with an activation barrier of 31.6 kcal/mol, whereas for the propanone product, the hydride shift formatting step is found to be the rate-determining step with a higher activation barrier of 48.9 kcal/mol.

Keywords : Zeolite, H-ZSM-5, butene isomerization, propene oxide isomerization, M06-2X

บทสรุปผู้บริหาร (Executive Summary)

Zeolites have a high impact in chemical industries because of their wide range of applications in adsorption, separation and particularly as they regarded as catalysts. Their outstanding properties, such as shape selectivity, thermal stability and the intrinsic acidity, make this type of materials the frontier catalyst of choice for important hydrocarbon reactions such as cracking, dehydration and isomerization [1-8]. Among the various pore zeolites, ZSM-5 is a particularly significant catalyst for being used for many organic reactions such as isomerization, aldol condensation.[2-3,9-16]

Isobutene is a raw material for the production of methyl tert-butyl ether (MTBE) and ethyl tert-butyl ether (ETBE), both of which are used as additives in lead-free gasoline. Isobutene can be produced from more abundant butene isomers such as 1-butene and 2-butene via skeletal isomerization. A survey of the literature suggests that zeolites with a pore diameter between 4 and 5.5 Å are suitable catalysts for this reaction.[7,17-25] This corresponds to 8- to 10-membered ring channels such as those found in Ferrierite, Theta-1 and ZSM-5. The latter showed satisfactory results with an isobutene conversion rate of nearly 90%.[24] For systems with a low number of acidic sites and at high temperature, a monomolecular mechanism is reported while otherwise dimerization followed by cracking into light hydrocarbons is believed to take place.[25] In former computational studies on the skeletal isomerization of 1-butene on various zeolites the reaction was found to proceed via secondary linear butoxide, primary isobutoxide, and tert-butyl cation intermediates.[26-28] First part of our present work is to investigate the skeletal isomerization of 1-butene on H-ZSM-5 zeolite by ONIOM(MP2:DFT) calculations on a 34T quantum cluster. We compare the results where M06 is used in the framework region with results from the B3LYP, cam-B3LYP, M06-2X and ωB97X-D functionals. Its goal is to elucidate the effect of H-ZSM-5 on the skeletal isomerization of 1-butane.

Oxiranes, commonly called expoxides, are cyclic ethers with three member rings are widely used for synthesizing organic compounds and are key intermediates in petrochemical processes [29-32]. The ring strain initiates the high reactivity toward nucleophilic substitution. The useful reaction of oxiranes is the “ring-opening isomerization” catalyzed by either homogeneous or heterogeneous catalysts such as Al_2O_3, Al_2O_3-SiO_2, ZnO, WO_3, ZrO_2 etc. [33-47]. This reaction can be applied to synthesize organic compounds, polymers and macromolecules [29-32]. In recent years, there have been numerous experimental and theoretical studies on reactions and mechansims of the ring-opening isomerization[33-35,39-44,48-49]. In the case of unsymmetrical oxiranes, the selection of suitable catalysts plays an important role on the regioselectivity in the ring-opening isomerization. In general, two different carbonyl compounds are products from “ring-opening isomerization” of unsymmetrical oxiranes [35-36,44]. For example, propanal and propanone are the only two carbonyl compounds from the reaction of propene oxide. Among reported catalysts, zeolites are one of the interesting candidates due to their high catalytic performance, stability and green chemistry

concept. In second part, the reaction mechanisms of the isomerization of propene oxide is investigated. The aim of the study is to compare the catalytic activity and regioselectivity of zeolite structures on the isomerization.

References

(1) Smit, B.; Maesen, T. L. M. *Nature (London, U. K.)* 2008, *451*, 671.

(2) Bhan, A.; Iglesia, E. *Acc. Chem. Res.* 2008, *41*, 559.

(3) Yaluris, G.; Rekoske, J. E.; Aparicio, L. M.; Madon, R. J.; Dumesic, J. A. *J. Catal.* 1995, *153*, 65.

(4) Luzgin, M. V.; Rogov, V. A.; Arzumanov, S. S.; Toktarev, A. V.; Stepanov, A. G.; Parmon, V. N. *Angew. Chem., Int. Ed.* 2008, *47*, 4559.

(5) Corma, A.; Garcia, H. *Chem. Rev. (Washington, DC, U. S.)* 2003, *103*, 4307.

(6) Chen, C. S. H.; Bridger, R. F. *J. Catal.* 1996, *161*, 687.

(7) Andy, P.; Gnep, N. S.; Guisnet, M.; Benazzi, E.; Travers, C. *J. Catal.* 1998, *173*, 322.

(8) Venuto, P. B. *Microporous Mater.* 1994, *2*, 297.

(9) Smit, B.; Maesen, T. L. M. *Nature* 2008, *451*, 671.

(10) Luzgin, M. V.; Rogov, V. A.; Arzumanov, S. S.; Toktarev, A. V.; Stepanov, A. G.; Parmon, V. N. *Angewandte Chemie - International Edition* 2008, *47*, 4559.

(11) Corma, A. *J. Catal.* 2003, *216*, 298.

(12) Andy, P.; Gnep, N. S.; Guisnet, M.; Benazzi, E.; Travers, C. *J. Catal.* 1998, *173*, 322.

(13) Venuto, P. B. *Microporous Materials* 1994, *2*, 297.

(14) Evans, D. A.; Nelson, J. V.; Vogel, E.; Taber, T. R. *J. Am. Chem. Soc.* 1981, *103*, 3099.

(15) Salvapati, G. S.; Ramanamurty, K. V.; Janardanarao, M. *J. Mol. Catal.* 1989, *54*, 9.

(16) Li, C. J. Chem. Rev. (Washington, DC, U. S.) 1993, 93, 2023.

(17) Asensi, M. A.; Corma, A.; Martíez, A. *Journal of Catalysis* 1996, *158*, 561.

(18) Guisnet, M.; Andy, P.; Gnep, N. S.; Benazzi, E.; Travers, C. *Journal of Catalysis* 1996, *158*, 551.

(19) Houžvička, J.; Hansildaar, S.; Ponec, V. *Journal of Catalysis* 1997, *167*, 273.

(20) Jousse, F.; Leherte, L.; Vercauteren, D. P. *Journal of Molecular Catalysis A: Chemical* 1997, *119*, 165.

(21) Mériaudeau, P.; Tuan, V. A.; Le, N. H.; Szabo, G. *Journal of Catalysis* 1997, *169*, 397.

(22) Trombetta, M.; Busca, G.; Rossini, S.; Piccoli, V.; Cornaro, U. *Journal of Catalysis* 1997, *168*, 349.

(23) De Ménorval, B.; Ayrault, P.; Gnep, N. S.; Guisnet, M. *Journal of Catalysis* 2005, *230*, 38.

(24) Rutenbeck, D.; Papp, H.; Freude, D.; Schwieger, W. *Applied Catalysis A: General* 2001, *206*, 57.

(25) Rutenbeck, D.; Papp, H.; Ernst, H.; Schwieger, W. *Applied Catalysis A: General* 2001, *208*, 153.

(26) Boronat, M.; Corma, A. *Applied Catalysis A: General* 2008, *336*, 2.

(27) Boronat, M.; Viruela, P.; Corma, A. *Physical Chemistry Chemical Physics* 2001, *3*, 3235.

(28) Tuma, C.; Kerber, T.; Sauer, J. *Angewandte Chemie - International Edition* 2010, *49*, 4678.

(29) Katsuki, T.; Sharpless, K. B. *J. Am. Chem. Soc.* 1980, *102*, 5974.

(30) Smith, J. G. *Synthesis* 1984, 629.

(31) Cheng, Z.; Zhu, X.; Fu, G. D.; Kang, E. T.; Neoh, K. G. *Macromolecules* 2005, *38*, 7187.

(32) Carlier, P. R. *Angew. Chem., Int. Ed.* 2004, *43*, 2602.

(33) Fási, A.; Gömöry, A.; Pálinkó, I.; Kiricsi, I. *J. Catal.* 2001, *200*, 340.

(34) Fási, A.; Kiss, J. T.; Török, B.; Pálinkó, I. *Appl Catal A Gen* 2000, *200*, 189.

(35) Fási, A.; Notheisz, F.; Bartók, M. *J. Catal.* 1997, *167*, 242.

(36) Fási, A.; Pálinkó, I. *J. Catal.* 1999, *181*, 28.

(37) Fási, A.; Pálinkó, I. *Catal. Lett.* 1999, *58*, 103.

(38) Fási, A.; Pálinkó, I.; Gömöry, A.; Kiricsi, I. *Stud. Surf. Sci. Catal.* 2004, *154 C*, 2711.

(39) Fási, A.; Pálinkó, I.; Gömöry, A.; Kiricsi, I. *J. Mol. Catal. A: Chem.* 2004, *208*, 307.

(40) Fási, A.; Pálinkó, I.; Hernadi, K.; Kiricsi, I. *Catal. Lett.* 2002, *81*, 237.

(41) Fási, A.; Pálinkó, I.; Kiricsi, I. *Stud. Surf. Sci. Catal.* 1999, *125*, 391.

(42) Fási, A.; Pálinkó, I.; Kiricsi, I. *J. Catal.* 1999, *188*, 385.

(43) Fási, A.; Pálinkó, I.; Kiricsi, I. *Stud. Surf. Sci. Catal.* 2000, *130 A*, 839.

(44) Fási, A.; Pálinkó, I.; Kiricsi, I. *React. Kinet. Catal. Lett.* 2001, *74*, 187.

(45) Fási, A.; Pálinkó, I.; Kiricsi, I. *Stud. Surf. Sci. Catal.* 2005, *158 B*, 1303.

(46) Fási, A.; Pálinkó, I.; Kiricsi, I. *Catal. Lett.* 2005, *101*, 105.

(47) Molnár, Á.; Bucsi, I.; Bartók, M.; Resofszki, G.; Gáti, G. *J. Catal.* 1991, *129*, 303.

(48) Fási, A.; Pálinko, I.; Gömöry, Á.; Kiricsi, I. *Cent. Eur. J. Chem.* 2005, *3*, 230.

(49) Namuangruk, S.; Khongpracha, P.; Pantu, P.; Limtrakul, J. *J. Phys. Chem. B* 2006, *110*, 25950.

วัตถุประสงค์งานวิจัย

- To develop a suitable methodology for studying adsorption and reaction on acidic zeolite.
- To study the reaction mechanisms of isomerization on acidic zeolite.

ระเบียบวิธีวิจัย

The cluster models were taken from the lattice structure of ZSM-5 Zeolite. The 34T (T being Si or Al tetrahedral atoms) model is large enough to cover the intersection channel of H-ZSM-5 zeolite where the probe molecules resides. An Al atom replaces Si at the most favored position T12. A two-layer ONIOM scheme is employed. The inner layer, the Brønsted acid site, consists of five tetrahedral atoms (Si_4O_4AlH) that are considered as the active region and treated by means of MP2 perturbation theory. The outer layer is a 34T framework and is treated with the B3LYP, cam-B3LYP, M06-2X and **ω**B97X-D density functionals. The combination of MP2 and M06-2X has been already applied to predict adsorption and reaction mechanisms in ZSM-5 zeolite. The geometries of the inner-layer and the probe molecule were optimized with the 6-31G(d,p) basis set which was also used in the outer layer. For more reliable interaction energies, this was followed by single-point calculations with the 6-311+G(2df,2p) basis set. The outer layer atoms were always kept fixed at the crystallographic positions.

First, the ONIOM(MP2:B3LYP), ONIOM(MP2:cam-B3LYP), ONIOM(MP2:M06-2X) and ONIOM(MP2: **ω**B97X-D) calculations have been performed and the results compared with the experimental data the adsorption and the proton exchange of butane. Next, the adsorption and isomerization reaction of 1-butene on H-ZSM-5 is studied with ONIOM(MP2:M06-2X) and ONIOM(MP2: **ω**B97X-D). The transition structures are be checked by frequency calculations to have one mode with an imaginary frequency corresponding to the correct reaction coordinate. All calculations were performed using the G**aussian 09 set of programs**.

ผลการวิจัยและอภิปรายผล

Adsorption and hydrogen exchange reaction of butane on the H-ZSM-5 zeolite model.

Due to the high reactivity of alkenes over acidic zeolite no experimental data for adsorption energy of 1-butene on acidic zeolites is available. For butane, the experimentally measured heat of adsorption energies on H-ZSM-5 zeolite lies in the range of -13.9 to -14.8 kcal/mol. The adsorption of butane in the microporous zeolite occurs via weak interactions between the alkyl group and the Brønsted acid of the zeolite. The distances between the carbon atom of the adsorbed butane and the zeolite proton (C2 ··· Hz) are in the range of 2.39 - 2.51 Å. The calculated adsorption energies of n-butane on H-ZSM-5 with ONIOM(MP2:B3LYP), ONIOM(MP2:cam-B3LYP), ONIOM(MP2:M06-2X) and ONIOM(MP2: ωB97X-D) are spread over the wide range of -7.1, -8.3, -14.4 and -21.4 kcal/mol, respectively. However the ONIOM(MP2:M06-2X) value falls within the experimental range given above.

The Al ··· Hz distance of 2.36 Å compares well with the experimental value of 2.38 – 2.48 Å. The Brønsted O1-Hz bond length in the bare ZSM-5 are about 0.97 Å and do not change much upon adsorption.

The proton exchange takes place at the Brønsted acid of the zeolite (O1-Hz). The transition state of the reaction between butane (C2) and the Brønsted acid site (Hz) where Hz-C2 bond formation and the O2-H2 bond dissociation propagate corresponds to a butonium cation ($C_4H_{11}^+$). This is a six-membered transition structure. The apparent activation energies for this hydrogen exchange reaction are 24.1, 22.0, 15.8 and 10.6 kcal/mol from the ONIOM(MP2:B3LYP), ONIOM(MP2:cam-B3LYP), ONIOM(MP2:M06-2X) and ONIOM(MP2:ωB97X-D) models, respectively. The measured apparent activation energy for the proton exchange of butane on H-ZSM-5 with 19.1 kcal/mol lies between the M06-2X and cam-B3LYP values. The calculated total activation energies (30.2 - 32.0) kcal/mol compare well with the experimental ones of 32.9 - 33.9 kcal/mol.

The 1-butene molecule resides inside the 10T membered ring at the intersection of the H-ZSM-5 zeolite. As mentioned above, only a slight increase of the O1-Hz length by about 0.03 Å is observed upon adsorption, together with a slight elongation of the C-C double bond by about 0.01 Å. The ONIOM(MP2:M06-2X) values of the intermolecular distance between the Brønsted acid and the carbon of the double bond are 2.22 and 2.25 Å for Hz ··· C1 and Hz ··· C2, respectively. The values of the latter with the other functionals between 2.12 and 2.28 Å. The adsorption energies are -11.8, -12.9, -16.5 and -20.3 kcal/mol for ONIOM(MP2:B3LYP), ONIOM(MP2:cam-B3LYP), ONIOM(MP2:M06-2X) and ONIOM(MP2:ωB97X-D), respectively. We can therefore assume that the

adsorption energy of 1-butene is slightly higher than the one of butane. That can easily be rationalized from the π-interaction with the Brønsted acid aite of the zeolite that is not possible for butane.

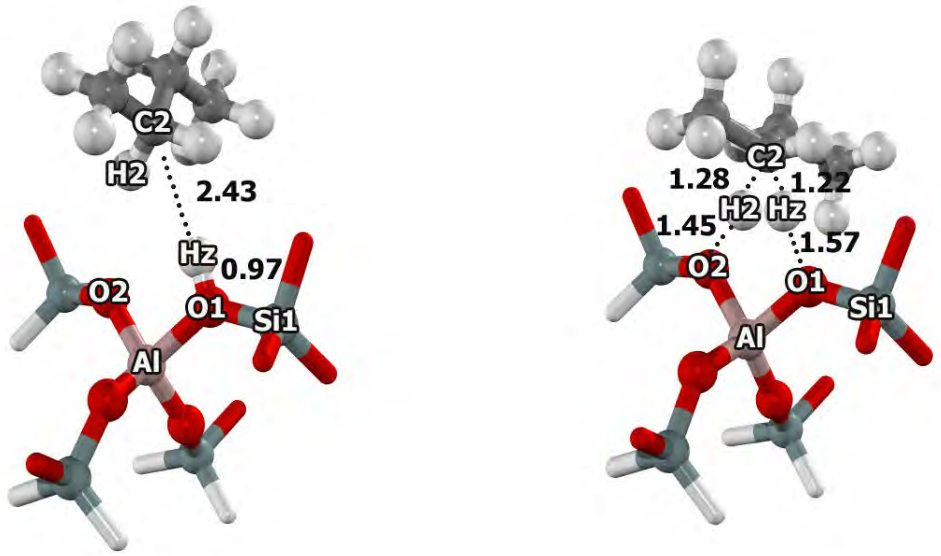

Figure 1. Optimized structures of the proton exchange of n-butane on H-ZSM-5 zeolite with ONIOM (MP2:M06-2X): (a) the adsorption complex of 1-butane and (b) the transition structures (TS). Distances are in Å.

Skeletal Isomerization of 1-butene on the H-ZSM-5 Zeolite Model

The isomerization reaction of 1-butene to iso-butene on the Brønsted acid site of zeolite starts with the adsorption of 1-butene. The reaction proceeds in four steps: 1) The protonation of the adsorbed 1-butene and form the secondary alkoxide intermediate, 2) The methyl shift via the cyclic transition state and formation of the primary alokoxide intermediate, 3) the proton transfer and formation of the tert-carbenium cation and 4) the protonation back to zeolite and desorption of isobutene. The isomerization reaction was studied with the ONIOM(MP2:M06-2X) and ONIOM(MP2:ωB97X-D) model chemistries.

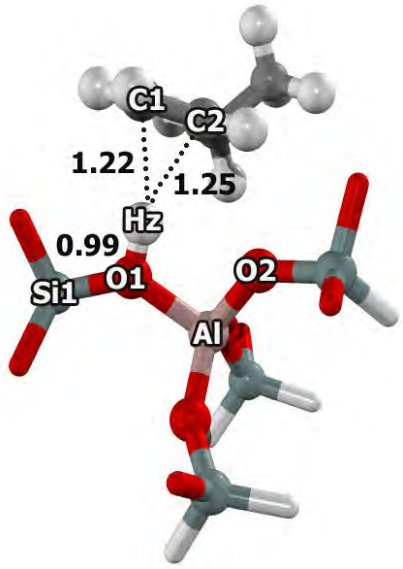

Figure 2. Optimized structures of 1-butene on H-ZSM-5 zeolite obtained with ONIOM (MP2:M06-2X). Distances are in Å.

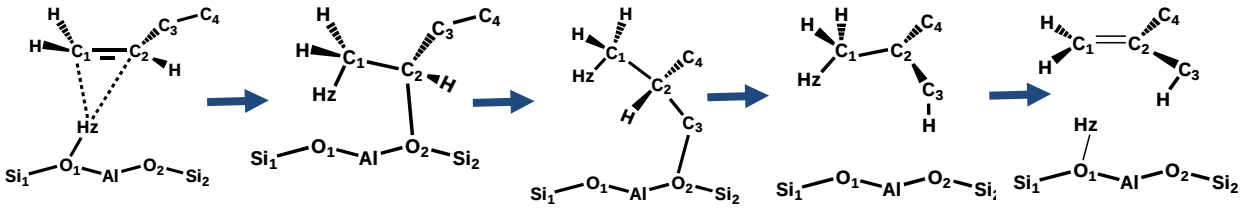

1-butene | Secondary Alkoxide intermediate (IN1) | Primary Alkoxide intermediate (IN2) | Tert-carbenium cation (IN3) | isobutene

Scheme 1

For ONIOM(MP2:M06-2X), after adsorption of the 1-butene molecule, the secondary alkoxide intermediate is formed via the first step of the reaction [TS1]. The O1-Hz bond is broken and the O2-C2 bond is formed. The C1-C2 double bond is elongated to become a single bond. The C1-C2 bond is at 1.40 Å and the C2-O2 bond is at 2.58 Å. The hybridization of C1 is changed from planar (sp^2) to tetrahedral (sp^3). The transition state has one imaginary frequency at -217.4 cm^{-1}, related to the transfer of the proton Hz from the zeolite to the C1 carbon of 1-butene and the formation of the bond between the C2 carbon atom of 1-butene and the O2 atom of the zeolite. The activation energy is about 19.6 kcal/mol, in agreement with the experimental estimates from isotope exchange of ethylene in zeolites (15-20 kcal/mol). The intermediate is the secondary alkoxide of 1-butene (IN1). The strong covalent C2-O2 bond is formed with a bond distance of 1.56 Å while C1-C2 becomes singly bonded. The relative energy is -10.7 kcal/mol.

The next step is the methyl shift via the cyclic transition state (TS2) in which the C3-C4 and O2-C2 bonds are breaking and the C2-C4 and C3-O3 bonds are formed. The imaginary frequency of TS2 is -101.3 cm^{-1}. C2, C3 and C4 form a triangle with bond distances of 1.39, 1.80 and 1.76 Å, respectively. This step requires an activation energy of 22.2 kcal/mol and its apparent activation energy is 11.5 kcal/mol. The product is the primary alkoxide intermediate (IN2). The primary alkoxide intermediate is formed with a relative energy of -16.9 kcal/mol. The fact that IN2 is slightly more stable than IN1 is also reflected in the fact that its C3-O3 bond is shorter (1.52 Å) than the C2-O2 bond in the secondary alkoxide intermediate IN1 (1.53 Å).

The third step is the proton transfer and the formation of the tert-carbenium cation [IN3]. In this step, the covalent C3-O3 bond is breaking and a proton is moving from C2 to C3. Its C2-H2 and C3-O2 bond distances are 1.14 Å and 2.36 Å, respectively. The imaginary frequency at the transition state geometry [TS3] is -482.4 cm^{-1}. In the corresponding mode H2 breaks away from C2 atom to form a bond with C3 atom and simultaneously the C3-O3 bond is broken. This step is rate determining step of the whole reaction. Its apparent activation energy is 17.9 kcal/mol. This value can be compared with an experiment study of the monomolecular conversion of 1-butene to isobutene on H-FER by Domokos et al [ref] where an apparent activation energy of about 14 kcal/mol has been reported. The total activation energy is 34.7 kcal/mol. The tert-carbenium ion (IN3) is the intermediate with a relative energy of -8.5 kcal/mol. In it, the C1-C2, C3-C2 and C2-C4 distances are about 1.44, 1.47 and 1.45 Å, respectively. It is less stable than the alkoxide intermediate and easily transfers to the isobutene.

The last step is the proton shift-back to the zeolite. Its transition state [TS4] shows the breaking of the C1-Hz bond (1.20 Å) and the formation of the O1-Hz bond (1.60 Å). This step requires an activation barrier of only 0.3kcal/mol. The isobutene product has a relative energy -22.4 kcal/mol. Its location in the 10T member channel of zeolite is shown in Figure 6(b). Its C1-C2 π-bond interacts with the zeolite Brønsted acid site. The Hz ··· C1 and Hz ··· C2 distances are at 2.29 and 2.34 Å, respectively. The conversion of 1-butene to iso-butene is an exothermic reaction.

The ONIOM(MP2:ωB97X-D) model chemistry gives similar activation energies of are 19.6, 22.2, 34.7 and 0.3 kcal/mol, respectively. The relative energies of the adsorption for the intermediate and product complex (AD, IN1, IN2, IN3 and PR) are -20.3, -13.6, -19.2, -11.7 and -26.3 kcal/mol, about 20% more binding than the ONIOM(MP2:ωB97X-D) values.

We also analysed the interactions from the inner ONIOM layer alone. The 5T//ONIOM(5T:34T)interactions are similar for both ONIOM(MP2:ωB97X-D) and ONIOM(MP2:M06-2X). The adsorption energy of 1-butene on H-ZSM-5 from the latter model is -10.9 kcal/mol and the apparent activation energies are 15.1, 27.6, 33.2 and 5.4 kcal/mol for the four steps, respectively. These apparent activation energies are higher than the experimental values and the

ones from the complete ONIOM(MP2:M06-2X) (and ONIOM(MP2:ωB97X-D)) model, showing that the framework must be for reliable predictions in cases like the present one where it increases the adsorption energy and stabilizes the transition state structures.

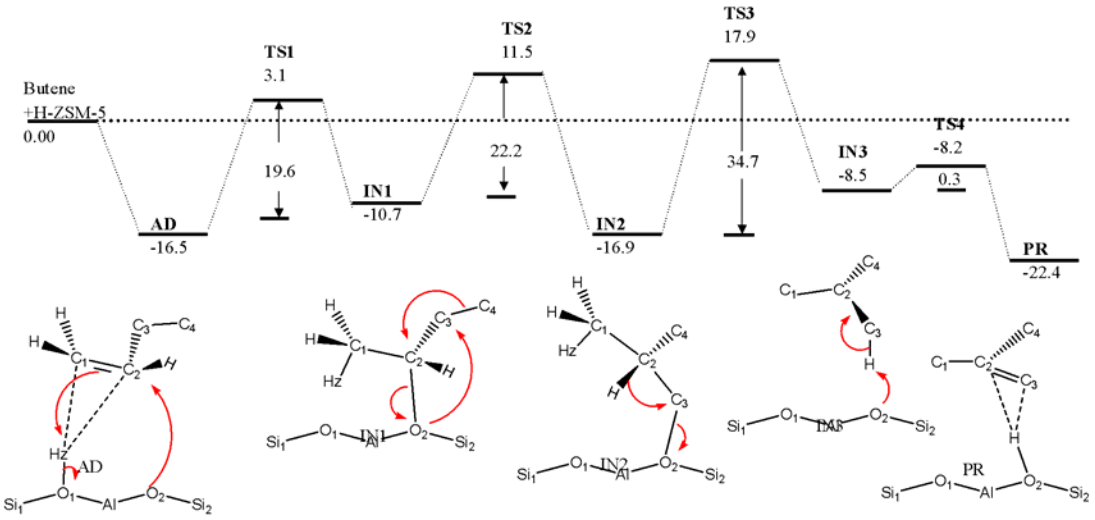

Figure 3. Potential energy diagram of the 1-butene to isobutene on the ONIOM(5T:34T) quantum cluster of H-ZSM-5, calculated with the ONIOM(MP2:M06-2X) approach (kcal/mol).

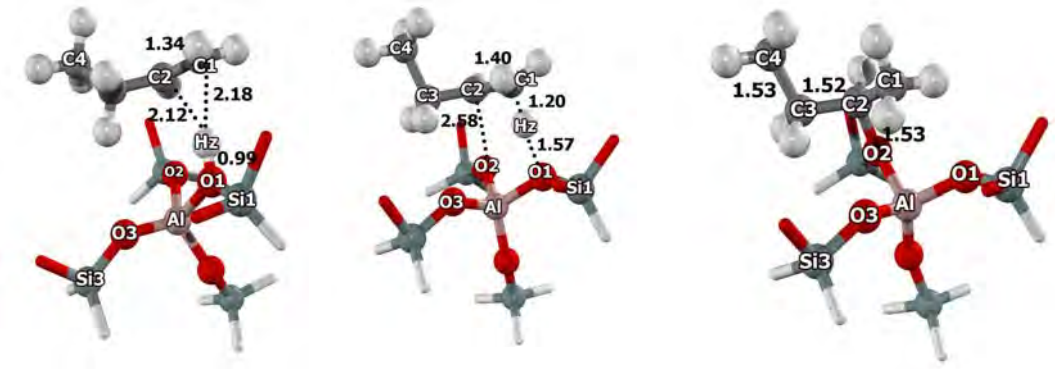

(a) AD1, ΔE= -16.5 kcal/mol (b) TS1, ΔE= 3.1 kcal/mol (c) IN1, ΔE= -10.7 kcal/mol

Figure 4. Optimized structures of 1-butene isomerization to isobutene on H-ZSM-5 zeolite with ONIOM(MP2:M06-2X): (a) the adsorption complex of 1-butene (AD1), (b) the transition structures (TS1), and (c) the secondary alkoxide intermediate (IN1). Distances are in Å.

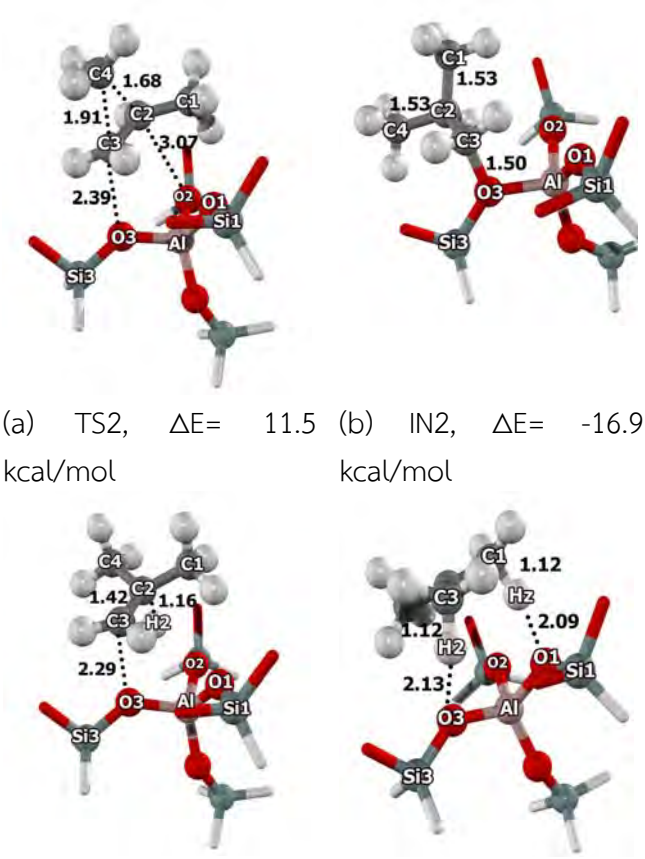

(a) TS2, ΔE= 11.5 kcal/mol

(b) IN2, ΔE= -16.9 kcal/mol

(c) TS3, ΔE= 17.9 kcal/mol

(d) IN3, ΔE= -8.5 kcal/mol

Figure 5. Optimized structures of 1-butene isomerization to isobutene on H-ZSM-5 zeolite with ONIOM(MP2:M06-2X): (a) the transition state (TS2), (b) the primary alkoxide intermediate (IN2), (c) the transition state (TS3), and (d) tert-butyl carbenium cation (IN3). Distances are in Ås.

Propene Oxide Isomerization on the H-FER Zeolite

The confinement effect of the zeolite framework on the adsorption and reaction mechanism of propene oxide has been studied with various methods: quantum cluster, ONIOM (Our own N-layered Integrated molecular Orbital + Molecular mechanics) method. The pore structure of H-FER is represented by models from 5T clusters up to realistic 34T clusters. The models are calculated with the newly developed and much accurate computational methods MP2/6-311+G(2df,2p):M06-2X/6-311+G(2df,2p), with the periodic charge from the infinite zeolite lattice included. To begin, the adsorption of propene oxide, propanal and propanone on H-FER

zeolite are calculated and found to be -25.5, -24.5 and -26.0 kcal/mol, which agree well with experimental data for the propanone interacted with zeolite (-31.1 kcal/mol). The contributions of the confinement effect from the extended framework are 36, 38 and 67 % of adsorption energies for propene oxide, propanal and propanone over H-FER, respectively. The isomerization reaction mechanism of propene oxide is considered to proceed through a stepwise mechanism: (1) the epoxide ring protonation, and, concurrently, the ring-opening, and (2), the 1,2-hydride shift formatting the adsorbed carbonyl compound. Two different types of product, propanal and propanone, were observed. Exothermic reactions were detected with the heat of reaction -20.1 and -29.3 kcal/mol for propene oxide to propanal and propanone, respectively. The transition state complexes are stabilized by the framework. Consequently, it decreases the activation barrier by about 16 – 50%. For the propanal product, the ring opening step is found to be the rate-determining step with an activation barrier of 31.6 kcal/mol, whereas for the propanone product, the hydride shift formatting step is found to be the rate-determining step with a higher activation barrier of 48.9 kcal/mol. The results suggest that the "embedded MP2:M06" is a suitable tool for evaluating the adsorption and reaction mechanism in the nanoconfinement of zeolite.

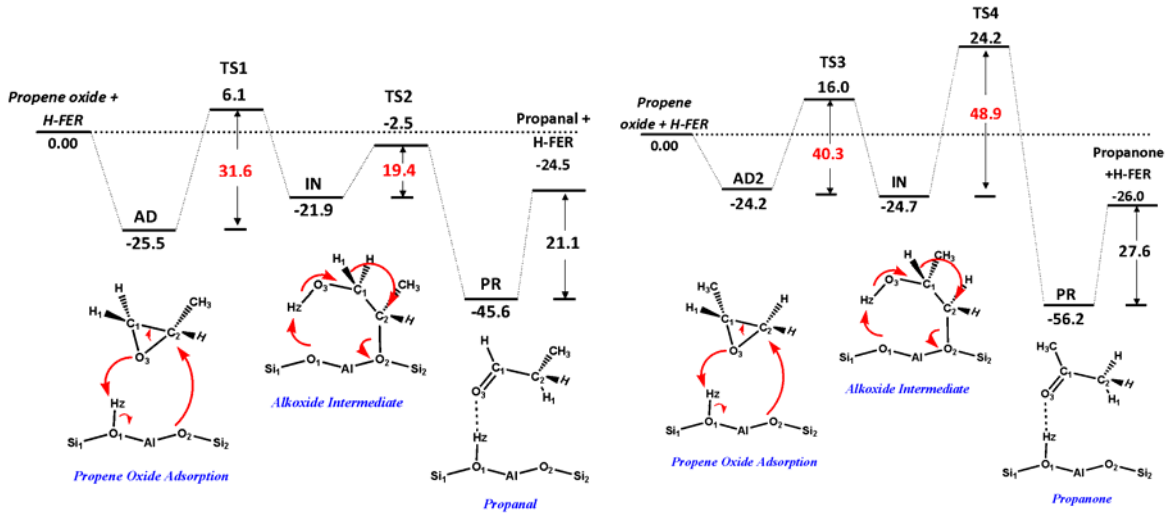

Figure 6. Potential energy diagram of the propene oxide isomerization to (a) propanal and (b) propanone on the 5T:34T ONIOM cluster of H-FER, calculated with the embedded MP2/6-311+G(2df,2p):M06-2X/6-311+G(2df,2p)//MP2/6-31G(d,p):M06-2X/6-31G(d,p) method. (kcal/mol).

ผลงานวิจัยที่ตีพิมพ์ในวารสารวิชาการระดับนานาชาติ

1. Skeletal Isomerization of 1-Butene over Ferrierite Zeolite: A Quantum Chemical Analysis of Structures and Reaction Mechanisms
   Wattanakit, Chularat; Nokbin, Somkiat; **Boekfa, Bundet;** Pantu, Piboon; Limtrakul, Jumras
   Journal of Physical Chemistry C (2012), 116(9), 5654-5663.
2. Glycine Peptide Bond Formation Catalyzed by Faujasite
   Phuakkong, Oranit; Bobuatong, Karan; Pantu, Piboon; **Boekfa, Bundet;** Probst, Michael; Limtrakul, Jumras
   ChemPhysChem (2011), 12(11), 2160-2168.
3. Density functional theory study on catalytic cracking of n-hexane on heteropoly acid: A comparison with acidic zeolite
   Choomwattana, S., Maihom, T., **Boekfa, B.,** Pantu, P., Limtrakul, J.
   Canadian Journal of Chemical Engineering, (2012), 90(4), 865-872.
4. Density functional study of the activity of gold-supported ZSM-5 zeolites for nitrous oxide decomposition
   Maihom, Thana; Wannakao, Sippakorn; **Boekfa, Bundet**: Limtrakul, Jumras
   Chemical Physics Letters (2012), 556, 217-224.

Preprints การประชุม American Chemical Society

1. Aldol Condensation of Acetaldehyde over H-ZSM-5 Zeolite: An advanced DFT approach
   Boekfa, Bundet; Limtrakul, Jumras
   Preprints - American Chemical Society, Division of Energy & Fuels (2012), 58(1)713-716.
2. Selective oxidation of methane to methanol over catalytic Fe-ZSM-5 zeolite: a DFT (M06-L) study
   Boekfa, Bundet; Maihim, Thana; Wannakao, Sippakorn; Limtrakul, Jumras
   Preprints - American Chemical Society, Division of Energy & Fuels (2012), 57(2), 490-494.
3. Isomerization mechanism of m-xylene to p-xylene on H-ITQ-22: A DFT mechanistic study
   Boekfa, Bundet; Limtrakul, Jumras
   Preprints - American Chemical Society, Division of Fuel Chemistry (2012), 57(1), 1048-1051.
4. Reaction mechanism of isomerization of 1-butene to isobutene over multipore H-ITQ-22 zeolite: A DFT study
   Boekfa, Bundet; Treesukol, Piti; Limtrakul, Jumras
   Preprints - American Chemical Society, Division of Petroleum Chemistry (2011), 56(2), 208-211.

THE JOURNAL OF PHYSICAL CHEMISTRY C

Article

pubs.acs.org/JPCC

Skeletal Isomerization of 1-Butene over Ferrierite Zeolite: A Quantum Chemical Analysis of Structures and Reaction Mechanisms

Chularat Wattanakit,[†,‡,§,∥] Somkiat Nokbin,[†,‡,§,∥] Bundet Boekfa,[‡,§,∥,⊥] Piboon Pantu,[†,‡,§,∥] and Jumras Limtrakul*[,†,‡,§,∥]

[†]National Center of Excellence for Petroleum, Petrochemicals and Advanced Materials, Department of Chemistry, Faculty of Science, [‡]Center for Advanced Studies in Nanotechnology and Its Applications in Chemical, Food and Agricultural Industries, [§]NANOTEC Center of Excellence, National Nanotechnology Center, and [∥]Center of Nanotechnology, Kasetsart University Research Development Institute, Kasetsart University, Bangkok 10900, Thailand

[⊥]Department of Chemistry, Faculty of Liberal Arts and Science, Kasetsart University, Kamphaeng Saen Campus, Nakhon Pathom 73140, Thailand

Supporting Information

ABSTRACT: The monomolecular skeletal isomerization of 1-butene to isobutene on H-FER zeolite was theoretically studied by using the ONIOM(MP2/6-311+G(2df,2p):M08-HX/6-311+G-(2df,2p))//ONIOM(MP2/6-31G(d,p):M08-HX/6-31G(d,p)) approach. A full quantum cluster of 37T (T means tetrahedral of Si or Al atoms) was used to represent the confinement effect from the FER zeolite. The model correctly predicted adsorption energies in favor of 1-butene to isobutene, −18.0 and −14.8 kcal/mol, respectively, indicating the unfavorable steric hindrance of the branched isomer with the medium pore H-FER zeolite. The monomolecular mechanism of skeletal isomerization of 1-butene was found to involve transformation of adsorbed 1-butene through secondary linear butoxide, primary isobutoxide, and *tert*-butyl cation intermediates. The rate-determining step is the conversion of isobutoxide to isobutene in which the reaction has to proceed through the primary isobutyl cation transition state. The primary isobutyl cation is stabilized by the interactions with the zeolite framework. Its energy relative to the isolated 1-butene and zeolite cluster is 16.9 kcal/mol, which is comparable to the experimental apparent activation energy of 14 kcal/mol. The shape selectivity due to the "nano-confinement" effect of the zeolite framework on the adsorption, the stabilities of intermediates, as well as the skeletal isomerization reaction mechanism of 1-butene were clearly demonstrated.

1. INTRODUCTION

The skeletal isomerization of linear butenes to isobutene[1] is one of the most interesting topics for both academia and industry because isobutene can be used for the production of important gasoline additives, for example, methyl *tert*-butyl ether (MTBE) and ethyl *tert*-butyl ether (ETBE).[2] Medium pore zeolites, with pore diameters in the range of 4 to 5.5 Å, have been found to be active for skeletal isomerization of linear butenes to isobutene. Among these zeolites, H-FER has been found to be the most efficient and the most selective catalyst for the skeletal isomerization of *n*-butene.[3−5] Three possible mechanisms for skeletal isomerization of butenes in zeolites have been proposed,[6−11] which are monomolecular, bimolecular, and pseudomonomolecular mechanisms. The monomolecular mechanism involves direct protonation of an *n*-butene molecule and isomerization through various unstable carbenium ion transition states and alkoxide intermediates.[7,8] The bimolecular mechanism involves butene dimerization, isomerization, and cracking to produce isobutene and byproducts.[3,9] The pseudomonomolecular mechanism involves an active carbonaceous species in coke deposit that acts as a catalyst for the isomerization of *n*-butene.[10,11] There are a number of reports that suggested that over a fresh FER catalyst, monomolecular and bimolecular mechanisms are both important in accounting for the *n*-butene conversion and selectivity to isobutene. However, it was suggested that isobutene was predominantly produced from the monomolecular mechanism, whereas the bimolecular route was mainly responsible for the byproduct formation.[12−15]

From the theoretical point of view, the monomolecular mechanism is particularly interesting because it involves several theoretically important carbenium ions and alkoxides as reaction intermediates and transition states. The presence of these highly unstable species has been commonly suggested to be key intermediates for many reactions involving conversion of hydrocarbons in zeolite catalysts. (See refs 16−22 for examples.) The FT-IR[23] and NMR[24] revealed that the carbenium ions are not a stable species in the zeolite framework, except for some cyclic carbenium ions that can persist in acidic zeolites.[25] Solid-state NMR revealed that

Received: October 18, 2011
Revised: January 16, 2012
Published: February 8, 2012

alkenes protonation by zeolite Brønsted acid did not result in a free carbenium ion but gave surface alkoxyl species instead.[24] Boronat et al.[16] have proposed that the skeletal isomerization of 1-butene in theta-1 zeolites can follow the monomolecular path. In the proposed mechanism, an adsorbed 1-butene is protonated to form a linear secondary butoxide intermediate. Then, it is converted to a branched primary butoxide through a cyclopropyl transition state. The presence of a free *pri*-butyl carbenium ion can be avoided in this mechanism by having two oxygen atoms on the zeolite framework actively participating in the decomposition of the isobutoxide into isobutene through a cyclic transition state. One oxygen atom helps stabilize the positive charge on the primary carbon, whereas the other oxygen atom abstracts a proton from the tertiary carbon simultaneously to give isobutene adsorbed on the zeolite Brønsted acid. The authors also reported that the relative energies of alkoxide intermediates are strongly affected by the geometry restrictions of the zeolite framework. As the geometry restriction increases, the alkoxides are more destabilized compared with the adsorbed alkene. Recently, Tuma et al.[20] have raised a question as to whether or not tertiary butyl cation can be a true reaction intermediate for transformation of isobutene. The authors have reported that the tertiary butyl cation can be formed by protonation of isobutene. However, it is highly unstable and will rapidly deprotonate giving a proton back to the zeolite. The confinement effects,[26−28] which mainly consist of dispersive van der Waals interactions and the electrostatic potential of the zeolite framework, are expected to have significant effects on the stabilities of the alkoxide reaction intermediates and the carbocation transition states. Therefore, it is of interest to reinvestigate the monomolecular mechanism of skeletal isomerization of 1-butene in the presence of environmental effects of the zeolite framework.

Zeolites are microporous aluminosilicates with a large number of atoms in the unit cell. Large quantum clusters and periodic calculations have been developed to study the confinement of the zeolite framework. MP2 calculations can describe well both van der Waals interactions and electrostatic interactions in zeolite pores. However, MP2 calculations on large quantum clusters or the periodic calculations are too computationally expensive. To overcome such immense computational demand, the ONIOM scheme[29] combined with QM/MM calculation is applied. The ONIOM schemes that typically utilized DFT in combination with semiempirical methods or molecular mechanics force fields for computational efficiency have been shown to be practical for investigation of many reaction mechanisms under the confinement of zeolite pore networks.[30−33] Recently, the ONIOM scheme has been successfully employed with the combination of the sophisticated MP2 method and the efficient newly developed Minnesota density functional,[34] for a more accurate account of the zeolite framework effects on the adsorptions, and hydrogen-exchange reactions in zeolites.[35] Many reaction mechanisms in zeolites have also been successfully studied with the Minnesota density functionals.[36−40] These hybrid meta functionals improve the known deficiencies of conventional DFT[21,41,42] by including dispersion interactions and reducing the self-interaction in the correlation functional.[43] They have been shown to perform well in benchmarks for interactions in zeolite model complexes.[44]

In this Article, we report the skeletal isomerization of 1-butene to isobutene in ferrierite zeolite. The monomolecular mechanism for the skeletal isomerization of 1-butene to isobutene was carried out by means of a full quantum calculation using the ONIOM (MP2:M08-HX) approach.

2. MODEL AND COMPUTATIONAL DETAILS

The H-FER zeolite is used for the study due to the activity and selectivity of this catalyst for the isomerization reaction. To cover the confinement effect from the zeolite framework, we used the 37T quantum cluster ($AlSi_{36}O_{49}H_{51}$) (see Figure 1b),

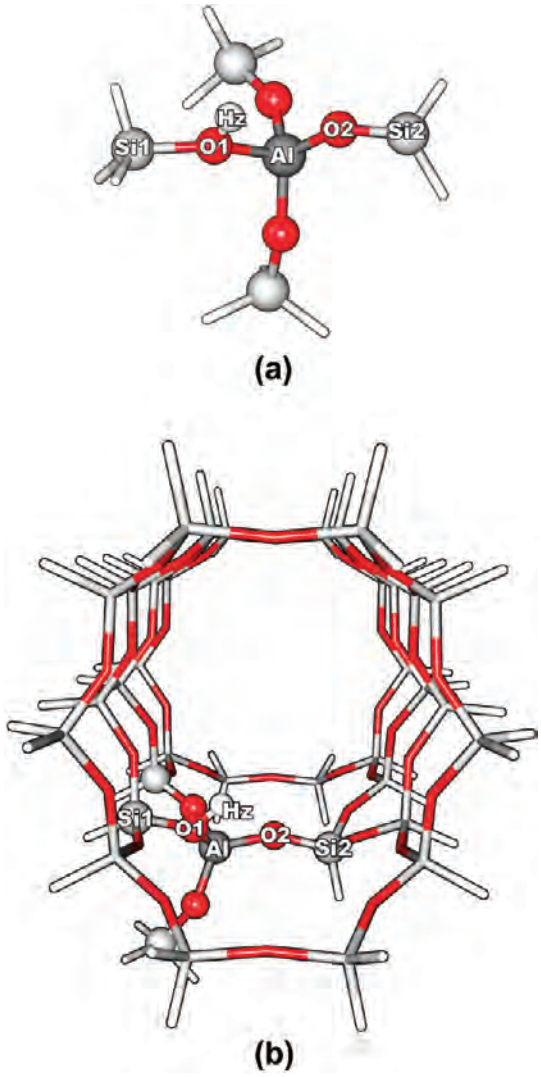

Figure 1. Different models used in the skeletal isomerization of 1-butene to isobutene in H-FER: (a) 5T quantum cluster and (b) 5T/37T ONIOM2 model.

which covered a 2-D pore system consisting of 10-ring (4.2 Å × 5.4 Å) channels intersected by 8-ring (3.5 Å × 4.8 Å) channels[45] (Figure S1 in Supporting Information), in this study. At the active site of the 37T model, a silicon atom at the T(2) position was replaced by an aluminum atom[46] and to neutralize the system the H atom was added to one of the neighboring oxygen atoms at the most energetically favorable position, which is the O(7) position[47−50] rather than the O(1) position, resulting in the generation of the Brønsted acid site of the ferrierite zeolite (H-FER), as illustrated in Figure 1. We note here that the O(7) and O(1) positions will be written as "O1" and "O2", respectively, for convenience in all Figures and Tables in this Article. In the models employed, the dangling

dx.doi.org/10.1021/jp209991y | J. Phys. Chem. C 2012, 116, 5654−5663

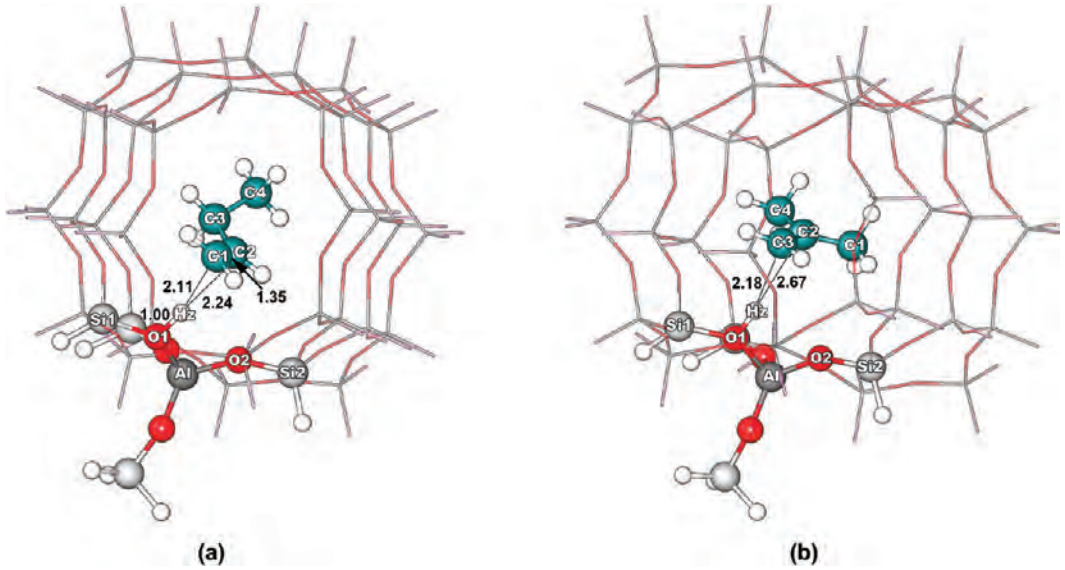

Figure 2. Optimized structures of adsorption complexes over 37T H-FER: (a) 1-butene (reactant, **I**) and (b) isobutene (product, **IX**). Geometrical parameters are in angstroms.

bonds of surface oxygen atoms are terminated by the H atom at the distance 1.47 Å from the Si, yielding the Si−H bonds which are aligned along the corresponding Si−O bonds of the structure of the ferrierite zeolite.

The ONIOM scheme is applied on the 37T quantum cluster. The 5T quantum cluster, where the Brønsted acid site is located, is assigned to be the inner layer, and the extended 37T quantum cluster is the outer layer. Only the active region ($AlSi_4O_4H$) and the probe molecule are allowed to relax, whereas the rest is kept fixed with the crystallographic structure. The 5T inner layer, where the isomerization reaction occurs, is calculated with the sophisticated MP2 method, and the M08-HX functional[43] was applied for the 37T outer layer to account for the framework effect on the local geometry, especially for the van der Waals interaction that plays a significant role in the hydrocarbon interaction with the zeolite. The 6-31G(d,p) basis set was used for all atom types. Structure optimizations were carried out using the Gaussian 03 program[51] incorporated with the Minnesota Density Functionals by Zhao and Truhlar.

The BSSE correction may not lead to an improvement of the transition-state energies.[52] To better estimate reaction energies and activation energies, we performed single-point calculations with the 6-311+G(2df,2p) basis set. The zero-point vibration corrections for the 5T model have been calculated. They are in a range of 0.5 to 1.2 kcal/mol for adsorption and activation energies (results are shown in Table S8 in the Supporting Information) and, therefore, can be omitted in practice.

3. RESULTS AND DISCUSSION

The monomolecular mechanism of skeletal isomerization of 1-butene in H-FER was theoretically investigated. To realize the environment of H-FER zeolite, the ONIOM(MP2/6-311+G-(2df,2p):M08-HX/6-311+G(2df,2p)//ONIOM(MP2/6-31G-(d,p):M08-HX/6-31G(d,p)) method was used to represent a section of the 10T straight channel of H-FER that can be considered as a nanoreactor where the reaction can take place inside. The 37T model is subdivided into two parts: the inner layer is a 5T quantum cluster calculated at MP2/6-311+G-(2df,2p) level of theory, and the outer layer is the 37T quantum cluster calculated with M08-HX/6-311+G(2df,2p) for computational efficiency.

3.1. Adsorption of 1-Butene and Isobutene over H-FER. 1-butene and isobutene both physically adsorb on the Brønsted acid site of zeolite via a π-interaction between the acidic proton (Hz) and the C═C double bond. Figure 2 and Table S1 in the Supporting Information show the selected geometric parameters of 1-butene and isobutene adsorption complexes in the ONIOM(5T:37T) H-FER. The π-interaction does not significantly change the structures of the zeolite and adsorbed molecules compared with the corresponding isolated structures. The adsorbed 1-butene molecule locates in the 10T straight channel of the H-FER where the reaction can subsequently take place. The O1−Hz bond distance of the acidic zeolite slightly elongates from 0.97 to 1.00 Å, and the corresponding O1−Al−O2 angle slightly increases by 2.3° (from 90.8 to 93.1°), whereas Al−O1−Si1 angle decreases by 2.6°. The Brønsted proton of the acid site is closer to the C1 atom (C1···Hz = 2.11 Å) than to the C2 atom (C2···Hz = 2.24 Å) of the 1-butene molecule because the terminal carbon is less steric. The C1═C2 double-bond distance does not significantly change by the weak π-interaction. The adsorbed isobutene also shows features of the π-adsorption complex similar to the adsorbed 1-butene. Because of more steric hindrance on the C2 atom of isobutene, the π-interactions are very asymmetric. The C2···Hz distance is much longer than the C3···Hz distance. (The distances are 2.67 and 2.18 Å, respectively.)

The adsorption energies are computed to be −18.0 and −14.8 kcal/mol for 1-butene and isobutene on H-FER, respectively. The experimental adsorption energies for alkenes on acidic zeolites are not available because of the complexity involving the facile isomerization and oligomerization of alkenes over the zeolite surface. We, thus, have to compare with the heat of adsorption for *n*-butane in ferrierite zeolite, which is reported to be −14.1[53] and −15.1[54] kcal/mol. It is expected that the adsorption energy of 1-butene must be stronger than that of *n*-butane. Therefore, our calculated result of −18.0 kcal/mol appears to be reasonable. It was reported that in medium pores of H-ZSM-5[55] and H-TON[53] zeolites,

dx.doi.org/10.1021/jp209991y | J. Phys. Chem. C 2012, 116, 5654−5663

Scheme 1. Monomolecular Mechanism for the Skeletal Isomerization of 1-Butene to Isobutene

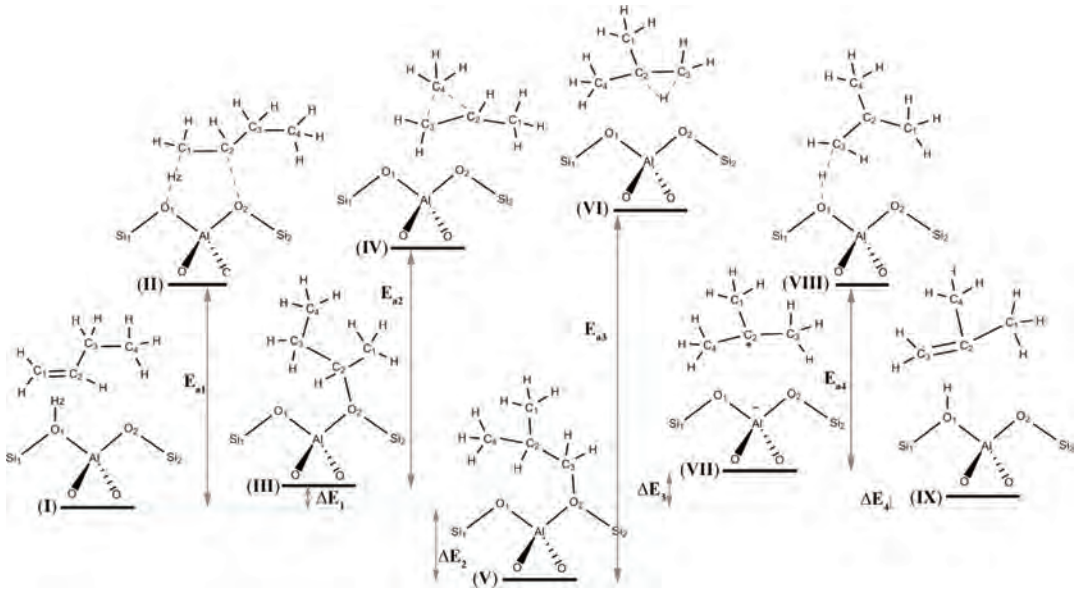

the adsorption energies of isobutane were less than that of *n*-butane due to the steric repulsion of the zeolite walls to the branched isobutane molecule. The adsorption energies of *n*-butane and isobutane in H-ZSM-5 zeolite were reported to be −13.4 and −11.9 kcal/mol, respectively,[55] and the adsorption energies of *n*-butane and isobutane in the H-TON zeolite were reported to be −14.3 and −11.3 kcal/mol, respectively.[53] Because the H-FER pore (4.2 × 5.4 Å) is smaller than the H-ZSM-5 pore (5.1 × 5.5 Å), the steric repulsion of the isobutene with zeolite walls would be more pronounced in H-FER. Therefore, our computed adsorption energy of isobutene of −14.8 kcal/mol, which is less than that of 1-butene by 3.2 kcal/mol, appears to be reasonable.

3.2. Monomolecular Skeletal Isomerization of 1-Butene over H-FER. The monomolecular skeletal isomerization mechanism consists of four elementary steps (shown in Scheme 1), which are described as follows: protonation of adsorbed 1-butene (**I**) to produce 2-butoxide intermediate (**III**), transformation of the 2-butoxide intermediate into isobutoxide intermediate (**V**) through a cyclo-propyl carbenium ion transition state (**IV**), then formation of the *tert*-butyl cation (**VII**) via 1,2 hydride shift, and deprotonation of the *tert*-butyl cation to form an adsorbed isobutene (**IX**) on zeolite. Figures 3 and 4 and Tables S2 and S3 in the Supporting Information show the selected optimized geometrical parameters of the intermediate species and the transition-state structures. All transition structures are confirmed by the frequency calculations, and the vibrational movements corresponding to the imaginary frequency at the transition states are shown in Figure 5.

The complete energy profile of skeletal isomerization of 1-butene is shown in Figure 6 and Table 1. In the first step, the adsorbed 1-butene (**I**) is protonated by the acidic proton of the zeolite. The acidic proton is preferably protonated to the C1 atom of 1-butene because it is less steric (more accessible) and, more importantly, its transition state will be a secondary carbenium ion, which is much more stable than a primary carbenium ion if the C2 atom was protonated. The optimized structure of the transition state **II** is shown in Figure 4a. The Brønsted O1-Hz bond distance is elongated to 1.72 Å, and the C1-Hz bond is being formed (C1···Hz = 1.19 Å). The distance from the C2 atom to the O2 atom of the zeolite is 2.79 Å, indicating that there is no covalent bond between the protonated butene and the zeolite. The Mulliken population analysis for the partial atomic charge on the butyl fragment is +0.819*e*, and most of the positive charge is located on the C2 position. The results indicate that the transition state is a secondary butyl carbenium ion. The activation energy (E_{a1}) for this step is calculated to be 19.5 kcal/mol. At the end of this step, a strong covalent bond is formed between the C2 atom of the butyl carbenium ion and the O2 atom of the zeolite framework resulting in 2-butoxide on the zeolite surface (**III**). The C2−O2 alkoxide bond distance is 1.56 Å. The 2-butoxide is less stable than the initial π-adsorption complex by 3.0 kcal/mol.

In the second step, the 2-butoxide is converted into the isobutoxide intermediate via a cyclic transition state (**IV**). At the transition state, the C2−O2 alkoxide bond is cleaved, and, simultaneously, the methyl group that connects to the C3 carbon atom is moving toward the C2 carbon atom. The C4, C3, and C2 carbon atoms, thus, form a triangular shape that is the characteristic of protonated cyclopropyl cation. The bond distances of C4···C2 and C4···C3 are 1.81 and 1.77 Å, respectively, and C2···C3 bond distance changes from 1.51 to 1.38 Å. The Mulliken population analysis indicates a partial charge of +0.913*e* on the cyclopropyl cation transition state in which the C3 position carries the most positive charge. The calculated activation energy (E_{a2}) for this step is 20.8 kcal/mol. The transition state is, then, decomposed by breaking the C4−C3 bond and forming a new C4−C2 bond to form isobutoxide (**V**), which is covalently bonded to the O2 atom on the zeolite framework. The alkoxide C−O bond distance of isobutoxide is 1.53 Å, which is slightly shorter than the C−O bond distance for the 2-butoxide by 0.03 Å. The primary isobutoxide species is more stable than the secondary 2-butoxide species by 4.2 kcal/mol and somewhat more stable than the physically adsorbed 1-butene by 1.2 kcal/mol.

The transformation of the surface isobutoxide to isobutene initiates by the breaking of the strong covalent bond between C3 and O2 atoms to form a highly unstable primary isobutyl

dx.doi.org/10.1021/jp209991y | J. Phys. Chem. C 2012, 116, 5654−5663

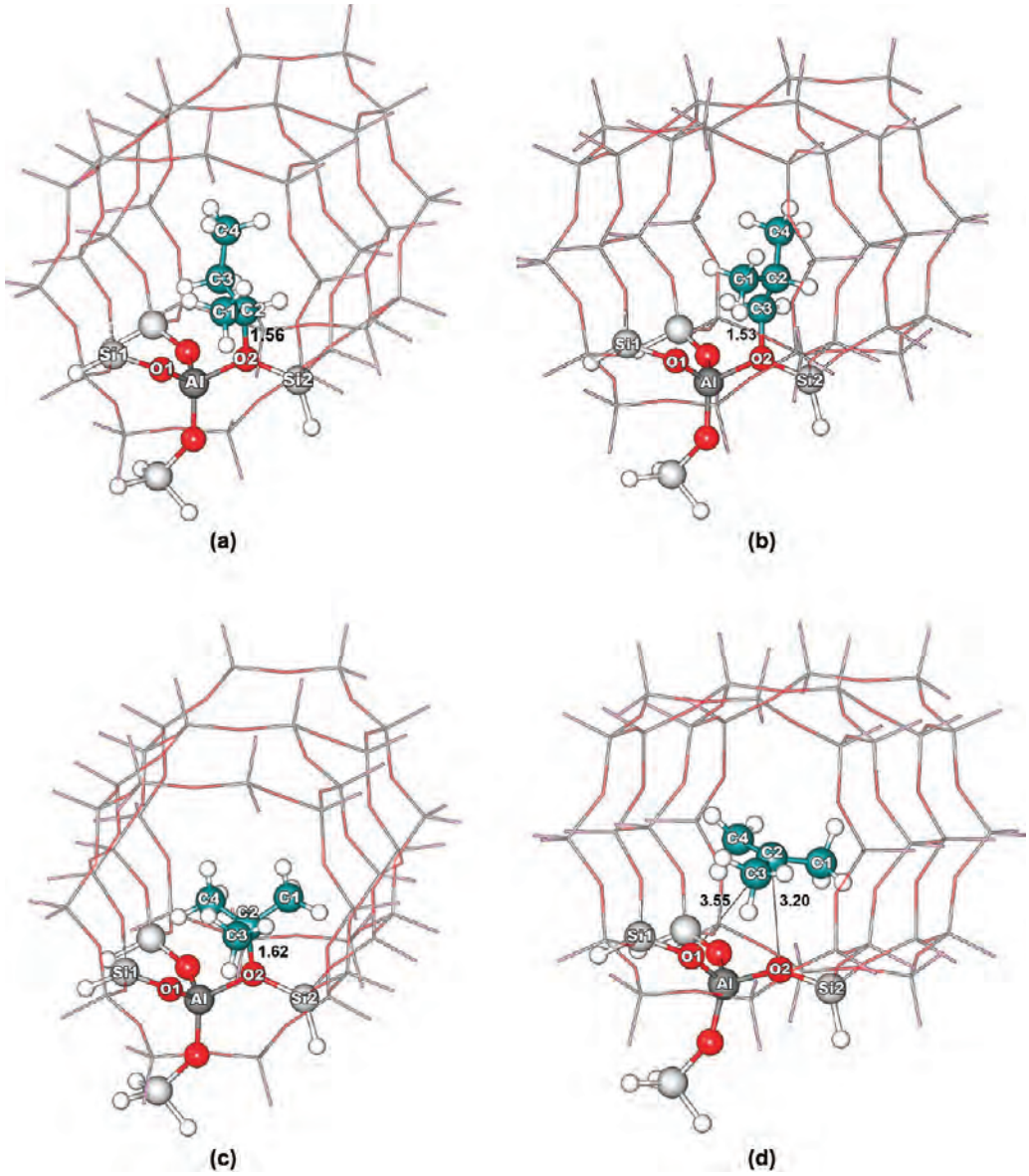

Figure 3. Optimized structures of (a) 2-butoxide (**III**), (b) isobutoxide (**V**), (c) *tert*-butoxide (**VII′**), and (d) *tert*-butyl cation (**VII**) over the 37T H-FER model. Geometrical parameters are in angstroms.

cation (**VI**). This step requires very high activation energy of 36.1 kcal/mol to reach the corresponding transition state. The optimized transition-state structure is shown in Figure 4c. At the transition, the isobutyl cation has a partial charge of +0.853*e* in which the terminal C3 position has the most positive charge, indicating that it is indeed the primary isobutyl cation. At this point, the hydride shift from the C2 to C3 carbon atom is still in an early stage. The C2−H bond distance is at 1.14 Å, whereas the C3−H bond distance is at 1.73 Å. From the vibrational analysis of the transition state (shown in Figure 5), there is one imaginary frequency corresponding to the movement of the H atom from the C2 to C3 carbon atom. There is a large distance of 2.55 Å separating the proton (H) and O2 oxygen atom of the active site, which suggests that the proton should not be directly deprotonated back to the zeolite but should be shifted to the positively charged primary carbon to form either a tertiary butyl cation or tertiary butoxide. Although *tert*-butyl cation and tertiary butoxide have not yet been experimentally found in zeolite, theoretical studies have predicted that they could be present as reactive intermediates in zeolites.[16−22] In this study, we are able to find an optimized structure (shown in Figure 3d) of the *tert*-butyl cation as a reaction intermediate in this zeolite system. The *tert*-butyl cation exhibits an almost planar structure with the equivalent C−C bond lengths of 1.45 Å. The closest distance from the tertiary C2 carbon atom to the zeolite O2 oxygen atom is 3.20 Å. The *tert*-butyl cation is stabilized in the zeolite pore by the electrostatic interactions as well as the hydrogen bonds among the cation methyl group and the zeolite oxygen atoms. For example, more than three hydrogen bonds between H and O of the framework were observed below 2.5 Å, and almost all bonds were observed below 3.0 Å (Figure 7). It is more stable than the primary cation transition state by 22.9 kcal/mol, but it is less stable than its preceding intermediate, isobutoxide, by 13.2 kcal/mol. Because of the high steric hindrance among the three methyl groups on the *tert*-butyl cation intermediate and the local structure of the active site of H-FER, the *tert*-butyl species could not easily access the oxygen atom at the active site to

dx.doi.org/10.1021/jp209991y | *J. Phys. Chem. C* 2012, 116, 5654−5663

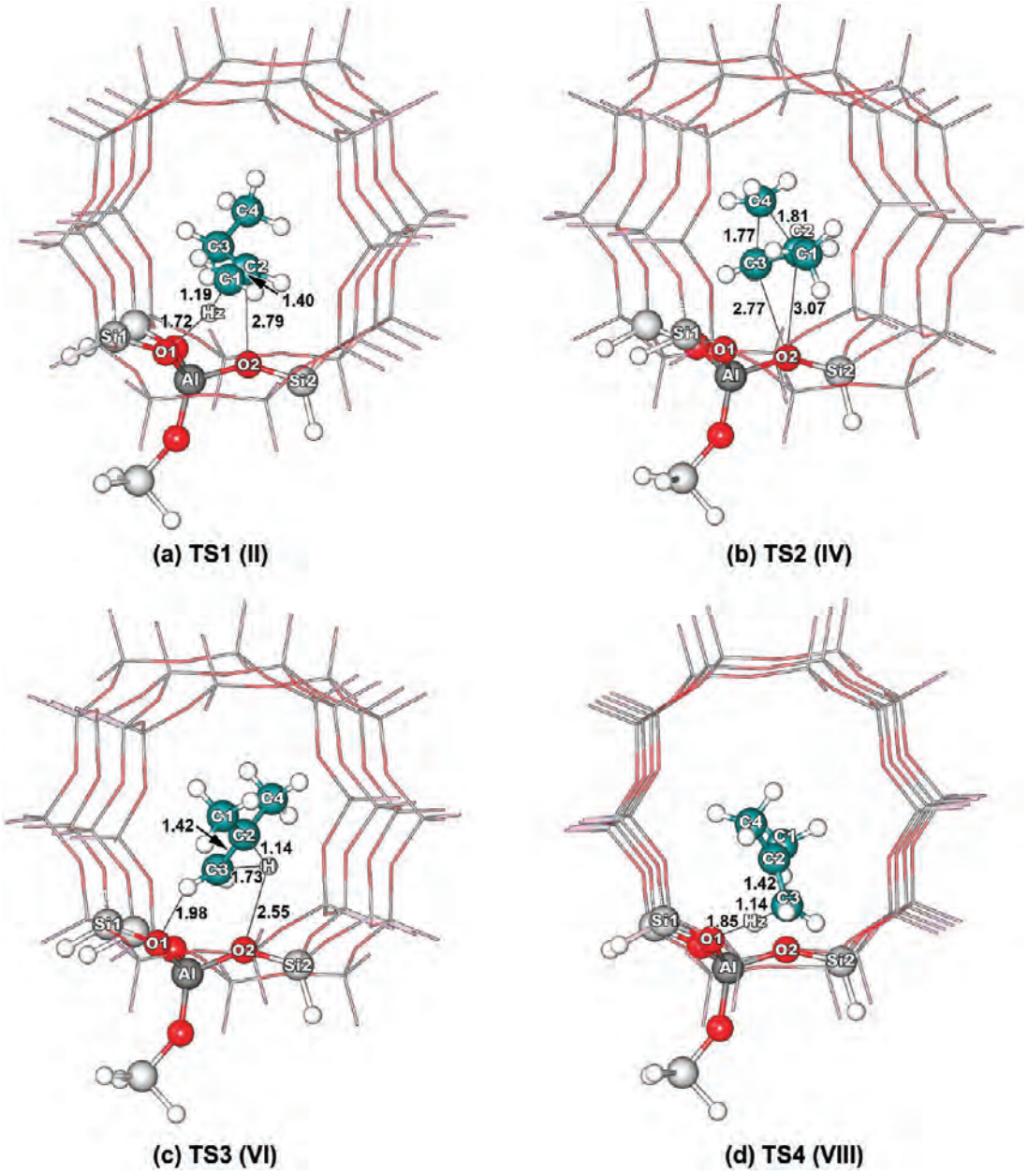

Figure 4. Optimized structures of transition states. Geometrical parameters are in angstroms.

form a covalent bond and become a surface alkoxide species. In this system, the *tert*-butyl alkoxide is found to be less stable than the *tert*-butyl cation by 4.6 kcal/mol. Therefore, in this study, we disregard the *tert*-butyl alkoxide as a reaction intermediate.

The *tert*-butyl carbenium ion is then rapidly deprotonated to the zeolite, resulting in the formation of the adsorbed isobutene complex over the zeolite Brønsted acid site. The activation energy for the *tert*-butyl carbenium ion deprotonation to form the physically adsorbed isobutene is only 2.8 kcal/mol, and the reaction energy for this step is exothermic by 12.8 kcal/mol. These results compared well with the activation energy of 3.3 kcal/mol and reaction energy of −14.4 kcal/mol for the deprotonation of *tert*-butyl cation in H-FER reported by Tuma et al.[22] calculated from a complex scheme of hybrid MP2:DFT calculations that gave an estimated MP2 energy at the complete basis set limit.

From the energy profile of the reaction mechanism, it can be observed that the first two steps are facile and reversible. The relative energies of the three reaction intermediates (1-butene π-adsorption complex, 2-butoxide, and isobutoxide) are within a few kilocalories per mole of each other. The relative energies of the transition states compared with the isolated 1-butene and H-FER are 1.5 kcal/mol for the first step and 5.8 kcal/mol for the second step. The third step is clearly the rate-determining step. An activation energy of 36.1 kcal/mol is required to remove the strong covalent bond between the isobutoxide and the zeolite surface to form the unstable primary isobutyl cation transition state. The relative stability of this transition state compared with the isolated 1-butene and zeolite would correspond to the apparent activation energy observed experimentally. Domokos et al.[14] studied skeletal isomerization of linear butenes and isobutene over H-FER and found that isobutene was formed by the monomolecular mechanism and

dx.doi.org/10.1021/jp209991y | J. Phys. Chem. C 2012, 116, 5654−5663

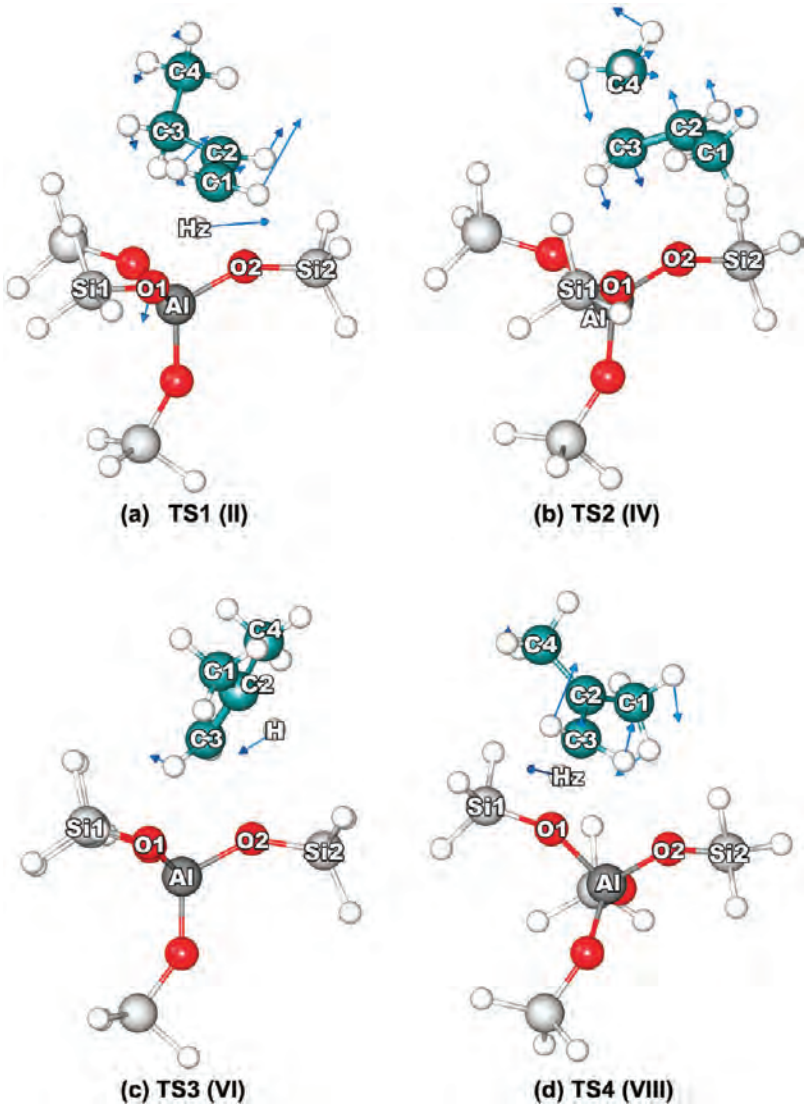

Figure 5. Vibrational movements corresponding to the imaginary frequency at the transition states.

reported the apparent activation energy for the rate of isobutene production to be ~14 kcal/mol. Our computed apparent activation energy for this mechanism is 16.9 kcal/mol, which agrees well with the experimental report.

3.3. Effects of the Zeolite Framework on the Monomolecular Skeletal Isomerization. To illustrate the zeolite framework effects on the relative stabilities of reactive species and energetic of the reaction, we compare the energy profile of the reaction mechanism computed with the explicit zeolite framework (37T model) to one without the zeolite framework (5T model). A small zeolite active site model (5T) was chosen for this purpose with the optimization procedure at MP2/6-31G(d,p) level of theory. The adsorption energies of 1-butene and isobutene on this model, carried out at MP2/6-311+G(2df,2p) level of theory, were calculated to be −10.3 and −10.7 kcal/mol, respectively (Supporting Information). Obviously, without the zeolite framework, the calculated adsorption energies are underestimated. The 5T model cannot represent the shape selectivity of medium pore zeolite against the bulkier isobutene. The shape selectivity of H-FER cannot be represented if the extended framework is not included in the calculations.

The first two steps of the reaction mechanisms on the 5T cluster are found to be similar to the 37T model. However, on the 5T model, the computed activation energies are very high, 27.2 and 37.8 kcal/mol for the protonation and branching step, respectively. The transition states in the 5T model are not stabilized, obviously due to lack of electrostatic interaction with the framework. The relative stability of TS1 and TS2 compared with the isolated 1-butene and zeolite cluster are 16.9 and 26.4 kcal/mol, respectively. The 37T model shows a markedly different picture. With the extended framework included in the model, the first two steps are facile with intrinsic activation energies of 19.5 and 20.8 kcal/mol for the first and second steps, respectively. The transition states are stabilized by electrostatic interactions with the framework. Their relative energies are 1.5 and 5.8 kcal/mol, for the first and second transition states, respectively. These results indicate that the zeolite framework can greatly decrease the activation energy because the transition state, which is typically more ionic than its preceding intermediate, experiences stronger stabilizing interactions with the zeolite framework.

The third step of the mechanism is completely different in the 5T and 37T models. In the 5T model, the primary

dx.doi.org/10.1021/jp209991y | J. Phys. Chem. C 2012, 116, 5654−5663

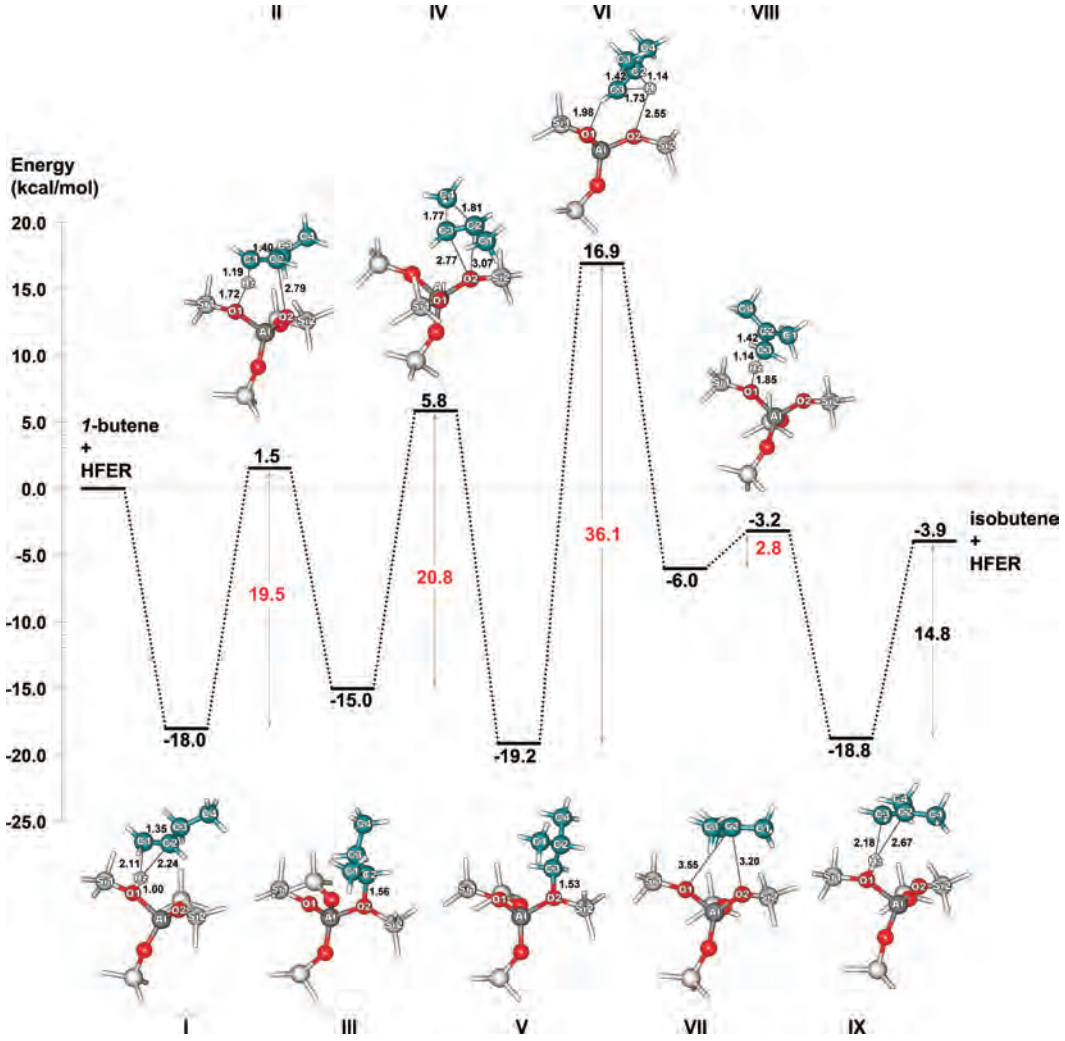

Figure 6. Reaction energy profile of 1-butene skeletal isomerization over 37T H-FER zeolite model obtained from ONIOM(MP2/6-311+G(2df,2p):M08-HX/6-311+G(2df,2p))//ONIOM(MP2/6-31G(d,p):M08-HX/6-31G(d,p)) calculation. Geometrical parameters and energies are in angstroms and kilocalories per mole, respectively.

isobutoxide can be decomposed to form isobutene in a single step in which the alkoxide bond is dissociated and, simultaneously, a proton on the C2 tertiary carbon atom is deprotonated back to the zeolite O1 oxygen atom. In this step, oxygen O1 and O2 atoms on the framework are both participating. The negative charge on the O2 atom stabilizes the positive charge on the C3 atom, whereas the O1 atom abstracts a hydrogen atom from the C2 of the butyl transition state. The computed activation energy is 37.2 kcal/mol, which is less than that of the previous step. Thus, the 5T model indicates that the branching step is the rate-determining step. Our predicted mechanism on the 5T cluster model is very similar to the mechanism previously reported by Boronat et al.,[16] in which they also employed a small cluster model.

However, such mechanism that can proceed on the small 5T cluster model is prohibited when the restriction of the zeolite pore is taken into consideration. When using the 37T model, the transition-state structure (TS3) that was found in the 5T model could not be optimized. For the decomposition of the isobutoxide, the C3−O2 covalent bond has to be completely dissociated, leading to the primary isobutyl carbenium ion transition state, which is stabilized by the interactions with the zeolite framework. At the transition state, the hydrogen atom on the C2 tertiary carbon atom cannot be transferred to the oxygen atom on the zeolite framework because of the large distance separating these two atoms. The hydrogen atom is, instead, transferred to the positive charged C3 carbon atom to form the tertiary butyl carbenium ion as a reactive intermediate, which is rapidly decomposed to form isobutene. These results demonstrated that in this case, where the molecular sizes of reactive species are comparable to the zeolite pore dimension, the zeolite framework exhibits very strong influences on the structures and stability of reactive intermediates and transition states so that a new pathway that is only possible to carry out under strong confinement of the zeolite framework can be observed.

4. CONCLUSIONS

The monomolecular mechanism of skeletal isomerization of 1-butene over ferrierite zeolite has been theoretically investigated with the full quantum ONIOM(MP2/6-311+G(2df,2p):M08-HX/6-311+G(2df,2p))//ONIOM(MP2/6-31G(d,p):M08-HX/6-31G(d,p)) approach. The model reasonably predicted adsorption energies of 1-butene and isobutene to be −18.0 and −14.8 kcal/mol, respectively, indicating the unfavorable steric hindrance of the branched isomer with the H-FER pore. The

dx.doi.org/10.1021/jp209991y | J. Phys. Chem. C 2012, 116, 5654−5663

Table 1. Calculated Activation (E_a), Relative Energies of Intermediate Species (ΔE), and Apparent Activation Energies (E_{ap}) in Kilocalories Per Mole

	5T[a]	37T[b]
E_{a1} (II-I)	27.2	19.5
ΔE_1 (III-I)	−1.1	3.0
E_{a2} (IV-III)	37.8	20.8
ΔE_2 (V-I)	−3.7	−1.2
E_{a3} (VI-V)		36.1
ΔE_3 (VII-I)		12.0
E_{a3}' (VI′-V)	37.2	
ΔE_3(IX-I)	−3.3	
E_{a4} (VIII-VII)		2.8
ΔE_4 (IX-I)		−0.8
E_{ap2} (IV-I)	36.7	23.8
E_{ap3} (VI-I)		34.9

[a]Corresponding to the energy profile in Scheme S1 in the Supporting Information obtained by the optimization of 5T H-FER model at MP2/6-311+G(2df,2p)//MP2/6-31G(d,p) level of theory. [b]Corresponding to the energy profile in Scheme 1 obtained by the optimization of 37T model using ONIOM(MP2/6-311+G(2df,2p):M08-HX/6-311+G(2df,2p))//ONIOM(MP2/6-31G(d,p):M08-HX/6-31G(d,p)) approach.

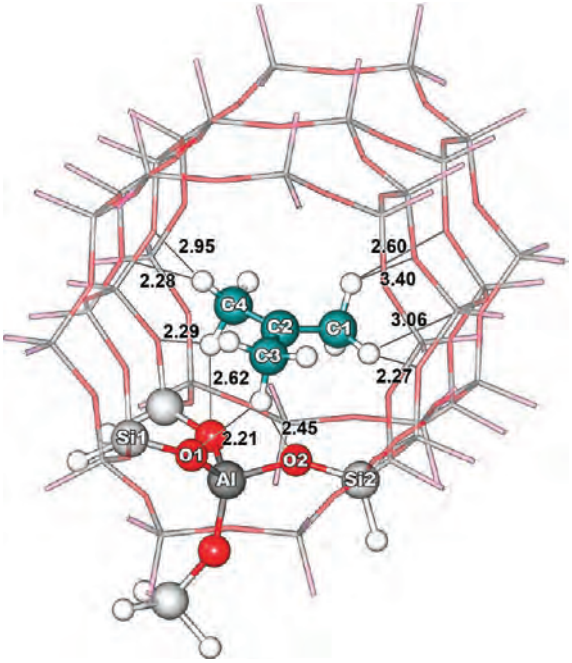

Figure 7. Illustration of the hydrogen bonds among the cation methyl group and the zeolite oxygen of *tert*-butyl cation stabilized in the zeolite pore.

rate-determining step is found to be the decomposition of the surface isobutoxide intermediate through the highly unstable primary isobutyl carbenium ion transition state with an activation energy of 36.1 kcal/mol. The confined space of the H-FER framework prevents the direct deprotonation of the primary isobutyl carbenium ion transition state to the zeolite framework. The intramolecular 1,2-hydride shift thus occurs to form a relatively more stable tertiary butyl carbenium ion that is rapidly decomposed to isobutene. The shape selectivity due to the "nano-confinement" effect of the zeolite framework strongly affects the adsorption, the stabilities of alkoxide species and carbenium ion, as well as the skeletal isomerization mechanism of 1-butene.

■ ASSOCIATED CONTENT

Supporting Information

The unit cell of ferrierite (H-FER), the optimized geometrical parameters, as well as interaction energies for 1-butene skeletal isomerization over the large model 37T and small 5T active site model are shown. The complete reaction energy profile of 1-butene skeletal isomerization over the 5T H-FER zeolite model obtained from the MP2/6-31G(d,p) method is also given. This material is available free of charge via the Internet at http://pubs.acs.org.

■ AUTHOR INFORMATION

Corresponding Author

*Fax: +66 2562 5555, ext. 2176. E-mail jumras.l@ku.ac.th.

Notes

The authors declare no competing financial interest.

■ ACKNOWLEDGMENTS

This work was partially supported by grants from The National Research University (NRU), Kasetsart University, the National Science and Technology Development Agency (2009 NSTDA Chair Professor funded by the Crown Property Bureau under the Management of the National Science and Technology Development Agency and NANOTEC Center of Excellence funded by the National Nanotechnology Center), Kasetsart University Research and Development Institute (KURDI), the Thailand Research Fund (TRF), and the Commission of Higher Education, Ministry of Education under Postgraduate Education and Research Programs in Petroleum and Petrochemicals and Advanced Materials. C.W. wishes to thank the Thailand Research Fund (TRF) for a Royal Golden Jubilee Ph.D. fellowship (3.C.KU/50/A.2). Donald G. Truhlar and Yan Zhao are thanked for their support with the M08-HX functional.

■ REFERENCES

(1) Butler, A. C.; Nicolaides, C. P. *Catal. Today* **1994**, *18*, 443−471.
(2) Collignon, F.; Mariani, M.; Moreno, S.; Remy, M.; Poncelet, G. *J. Catal.* **1997**, *166*, 53−66.
(3) Mooiweer, H. H.; Jong, K. P. d.; Kraushaar-Czarnetzki, B.; Stork, W. H. J.; Krutzen, B. C. H. *Stud. Surf. Sci. Catal.* **1994**, *84*, 2327−2334.
(4) Houžvička, J.; Hansildaar, S.; Ponec, V. *J. Catal.* **1997**, *167*, 273−278.
(5) Oyoung, C. L.; Pellet, R. J.; Casey, D. G.; Ugolini, J. R.; Sawicki, R. A. *J. Catal.* **1995**, *151*, 467−469.
(6) Houžvička, J.; Ponec, V. *Catal. Rev.: Sci. Eng.* **1997**, *39*, 319−344.
(7) Xu, W.-Q.; Yin, Y.-G.; Suib, S. L.; Edwards, J. C.; Oyoung, C.-L. *J. Phys. Chem.* **1995**, *99*, 9443−9451.
(8) Mériaudeau, P.; Tuan, V. A.; Le, N. H.; Szabo, G. *J. Catal.* **1997**, *169*, 397−399.
(9) Cheng, Z. X.; Ponec, V. *J. Catal.* **1994**, *148*, 607−616.
(10) Petkovic, L. M.; Larsen, G. *J. Catal.* **2000**, *191*, 1−11.
(11) Guisnet, M.; Andy, P.; Gnep, N. S.; Travers, C.; Benazzi, E. *J. Chem. Soc., Chem. Commun.* **1995**, 1685−1686.
(12) Meriaudeau, P.; Bacaud, R.; Hung, L. N.; Vu, A. T. *J. Mol. Catal. A: Chem.* **1996**, *110*, L177−L179.
(13) Houžvička, J.; Ponec, V. *Ind. Eng. Chem. Res.* **1997**, *36*, 1424−1430.
(14) Domokos, L.; Lefferts, L.; Seshan, K.; Lercher, J. A. *J. Catal.* **2001**, *197*, 68−80.

(15) Kangas, M.; Salmi, T.; Murzin, D. Y. *Ind. Eng. Chem. Res.* **2008**, *47*, 5413−5426.
(16) Boronat, M.; Viruela, P.; Corma, A. *Phys. Chem. Chem. Phys.* **2001**, *3*, 3235−3239.
(17) Boronat, M.; Corma, A. *Appl. Catal., A* **2008**, *336*, 2−10.
(18) Boronat, M.; Viruela, P. M.; Corma, A. *J. Am. Chem. Soc.* **2004**, *126*, 3300−3309.
(19) Rozanska, X.; van Santen, R. A.; Demuth, T.; Hutschka, F.; Hafner, J. *J. Phys. Chem. B* **2003**, *107*, 1309−1315.
(20) Tuma, C.; Sauer, J. *Angew. Chem., Int. Ed.* **2005**, *44*, 4769−4771.
(21) Tuma, C.; Sauer, J. *Phys. Chem. Chem. Phys.* **2006**, *8*, 3955−3965.
(22) Tuma, C.; Kerber, T.; Sauer, J. *Angew. Chem., Int. Ed.* **2010**, *49*, 4678−4680.
(23) Farneth, W. E.; Gorte, R. J. *Chem. Rev. (Washington, D. C.)* **1995**, *95*, 615−635.
(24) Haw, J. F.; Nicholas, J. B.; Xu, T.; Beck, L. W.; Ferguson, D. B. *Acc. Chem. Res.* **1996**, *29*, 259−267.
(25) Haw, J. F. *Phys. Chem. Chem. Phys.* **2002**, *4*, 5431−5441.
(26) Derouane, E. G.; Andre, J. M.; Lucas, A. A. *J. Catal.* **1988**, *110*, 58−73.
(27) Derouane, E. G. *J. Mol. Catal. A: Chem.* **1998**, *134*, 29−45.
(28) Zicovich-Wilson, C. M.; Corma, A.; Viruela, P. *J. Phys. Chem.* **1994**, *98*, 10863−10870.
(29) Dapprich, S.; Komáromi, I.; Byun, K. S.; Morokuma, K.; Frisch, M. J. *J. Mol. Struct.: THEOCHEM* **1999**, *461−462*, 1−21.
(30) Boronat, M.; Martínez-Sánchez, C.; Law, D.; Corma, A. *J. Am. Chem. Soc.* **2008**, *130*, 16316−16323.
(31) Joshi, Y. V.; Thomson, K. T. *J. Phys. Chem. C* **2008**, *112*, 12825−12833.
(32) Zheng, A.; Liu, S.-B.; Deng, F. *Microporous Mesoporous Mater.* **2009**, *121*, 158−165.
(33) Zheng, A.; Deng, F.; Liu, S.-B. *Catal. Today* **2011**, *164*, 40−45.
(34) Zhao, Y.; Truhlar, D. G. *Theor. Chem. Acc.* **2008**, *120*, 215−241.
(35) Boekfa, B.; Choomwattana, S.; Khongpracha, P.; Limtrakul, J. *Langmuir* **2009**, *25*, 12990−12999.
(36) Maihom, T.; Boekfa, B.; Sirijaraensre, J.; Nanok, T.; Probst, M.; Limtrakul, J. *J. Phys. Chem. C* **2009**, *113*, 6654−6662.
(37) Boekfa, B.; Pantu, P.; Probst, M.; Limtrakul, J. *J. Phys. Chem. C* **2010**, *114*, 15061−15067.
(38) Maihom, T.; Pantu, P.; Tachakritikul, C.; Probst, M.; Limtrakul, J. *J. Phys. Chem. C* **2010**, *114*, 7850−7856.
(39) Kongpatpanich, K.; Nanok, T.; Boekfa, B.; Probst, M.; Limtrakul, J. *Phys. Chem. Chem. Phys.* **2011**, *13*, 6462−6470.
(40) Namuangruk, S.; Meeprasert, J.; Khemthong, P.; Faungnawakij, K. *J. Phys. Chem. C* **2011**, *115*, 11649−11656.
(41) Civalleri, B.; Zicovich-Wilson, C. M.; Valenzano, L.; Ugliengo, P. *CrystEngComm* **2008**, *10*, 1693.
(42) Svelle, S.; Tuma, C.; Rozanska, X.; Kerber, T.; Sauer, J. *J. Am. Chem. Soc.* **2009**, *131*, 816−825.
(43) Zhao, Y.; Truhlar, D. G. *J. Chem. Theory Comput.* **2008**, *4*, 1849−1868.
(44) Zhao, Y.; Truhlar, D. G. *J. Phys. Chem. C* **2008**, *112*, 6860−6868.
(45) Vaughan, P. A. *Acta Crystallogr.* **1966**, *21*, 983−990.
(46) Nieminen, V.; Sierka, M.; Murzin, D. Y.; Sauer, J. *J. Catal.* **2005**, *231*, 393−404.
(47) Jousse, F.; Leherte, L.; Vercauteren, D. P. *Mol. Simul.* **1996**, *17*, 175−196.
(48) Blanco, F.; Urbina-Villalba, G.; Agudelo, M. M. R. D. *Mol. Simul.* **1995**, *14*, 165−176.
(49) Nachtigall, P.; Bludsky, O.; Grajciar, L.; Nachtigallova, D.; Delgado, M. R.; Arean, C. O. *Phys. Chem. Chem. Phys.* **2009**, *11*, 791−802.
(50) Grajciar, L.; Arean, C. O.; Pulido, A.; Nachtigall, P. *Phys. Chem. Chem. Phys.* **2010**, *12*, 1497−1506.
(51) Frisch, M. J.; Trucks, G. W.; Schlegel, H. B.; Scuseria, G. E.; Robb, M. A.; Cheeseman, J. R.; Montgomery, J. A., Jr.; Vreven, T.; Kudin, K. N.; Burant, J. C.; Millam, J. M.; Iyengar, S. S.; Tomasi, J.; Barone, V.; Mennucci, B.; Cossi, M.; Scalmani, G.; Rega, N.; Petersson, G. A.; Nakatsuji, H.; Hada, M.; Ehara, M.; Toyota, K.; Fukuda, R.; Hasegawa, J.; Ishida, M.; Nakajima, T.; Honda, Y.; Kitao, O.; Nakai, H.; Klene, M.; Li, X.; Knox, J. E.; Hratchian, H. P.; Cross, J. B.; Adamo, C.; Jaramillo, J.; Gomperts, R.; Stratmann, R. E.; Yazyev, O.; Austin, A. J.; Cammi, R.; Pomelli, C.; Ochterski, J. W.; Ayala, P. Y.; Morokuma, K.; Voth, G. A.; Salvador, P.; Dannenberg, J. J.; Zakrzewski, V. G.; Dapprich, S.; Daniels, A. D.; Strain, M. C.; Farkas, O.; Malick, D. K.; Rabuck, A. D.; Raghavachari, K.; Foresman, J. B.; Ortiz, J. V.; Cui, Q.; Baboul, A. G.; Clifford, S.; Cioslowski, J.; Stefanov, B. B.; Liu, G.; Liashenko, A.; Piskorz, P.; Komaromi, I.; Martin, R. L.; Fox, D. J.; Keith, T.; Al-Laham, M. A.; Peng, C. Y.; Nanayakkara, A.; Challacombe, M.; Gill, P. M. W.; Johnson, B.; Chen, W.; Wong, M. W.; Gonzalez, C.; Pople, J. A. *Gaussian 03*; revision B.05 ed.; Gaussian, Inc.: Pittsburgh, PA, 2003.
(52) Lendvay, G.; Mayer, I. *Chem. Phys. Lett.* **1998**, *297*, 365−373.
(53) Eder, F.; Lercher, J. A. *J. Phys. Chem. B* **1997**, *101*, 1273−1278.
(54) Yoda, E.; Kondo, J. N.; Domen, K. *J. Phys. Chem. B* **2005**, *109*, 1464−1472.
(55) Zhang, J.; Zhao, Z.; Duan, A.; Jiang, G.; Liu, J.; Zhang, D. *Energy Fuels* **2008**, *23*, 617−623.

CHEMPHYSCHEM

DOI: 10.1002/cphc.201100047

Glycine Peptide Bond Formation Catalyzed by Faujasite**

Oranit Phuakkong,[a, b, c] Karan Bobuatong,[a, b, c] Piboon Pantu,[a, b, c] Bundet Boekfa,[b, c, d] Michael Probst,[e] and Jumras Limtrakul*[a, b, c]

The catalysis of peptide bond formation between two glycine molecules on H-FAU zeolite was computationally studied by the M08-HX density functional. Two reaction pathways, the concerted and the stepwise mechanism, starting from three differently adsorbed reactants, amino-bound, carboxyl-bound, and hydroxyl-bound, are studied. Adsorption energies, activation energies, and reaction energies, as well as the corresponding intrinsic rate constants were calculated. A comparison of the computed energetics of the various reaction paths for glycine indicates that the catalyzed reaction proceeds preferentially via the concerted reaction mechanism of the hydroxyl-bound configuration. This involves an eight-membered ring of the transition structure instead of the four-membered ring of the others. The step from the amino-bound configuration to glycylglycine is the rate-determining step of the concerted mechanism. It has an estimated activation energy of 51.2 kcal mol^{-1}. Although the catalytic reaction can also occur via the stepwise reaction mechanism, this path is not favored.

1. Introduction

Peptide bond formation is an essential step in the synthesis of proteins and peptides. Understanding this process allows the control of construction and organization of these polymers with useful applications in medical, biological, and food sciences.[1] Its reaction mechanism has attracted much attention over the last five decades. It is relevant to the synthesis of peptides from amino acids or their esters under prebiotic conditions[2] and numerous attempts from the experimental and computational side were performed to examine the basic steps of peptide bond formation.[3] Of even more practical importance is that many current works deal with designing peptides as parts of biocompatible units and take advantage of their self-assembly features. Peptides are also increasingly used as sensing devices.[1a–c,4]

For the acid/base-catalyzed aminolysis of alkyl esters, the mechanism of peptide bond formation has been studied experimentally in aqueous solution by Jencks et al.[3c–e] The basic step is the nucleophilic attack of the lone electron pair of the amino group onto the carbon atom of the carboxyl group followed by proton transfer from the amino group to one of the oxygen atoms of the carboxyl group. In the proposed concerted and/or stepwise reaction mechanisms, a possible formation of a relatively stable zwitterionic intermediate is considered. The relative stability of this adduct depends on the acid–base properties of the solvent, and its lifetime can be an important factor in the whole reaction mechanism.

Despite the intensive experimental works mentioned above and various studies using silica,[5] clays[5,6], and aluminas[5,7] as catalysts for the peptide formation, mechanistic discussions are rare and no detailed molecular picture is available for these processes. Nevertheless, some mechanisms have been suggested in the past to interpret the experimental evidence of the formation of small oligopeptides, albeit at the level of very simple schemes by Zamaraev et al.,[6a] for adsorption of glycine on zeolites and kaolinite and by Basiuk et al. for silica and alumina.[7a] Recently, zeolites have found potential applications in amino acid separation,[8] immobilized peptide synthesis,[9] and biomedical sensors.[10]

Theoretically, the mechanism of the uncatalyzed amide bond formation has been investigated by Oie et al. and Jensen et al.,[3g,h] who have shown that stepwise and concerted mechanisms may compete since both involve comparable activation energies. The latter authors also performed a study for the glycine + glycine reaction, and the main conclusion was that the model system glycine + glycine appears to be a good representative of a dipeptide system. Moreover, the mechanisms of amide bond formation in various catalytic systems have been

[a] O. Phuakkong, K. Bobuatong, Prof. Dr. P. Pantu, Prof. Dr. J. Limtrakul
Laboratory for Computational and Applied Chemistry, Department of Chemistry, Faculty of Science and Center of Nanotechnology
Kasetsart University Research and Development Institute
Kasetsart University, Bangkok 10900 (Thailand)
Fax: (+66) 2-562-5555 ext 2159
E-mail: Jumras.l@ku.ac.th

[b] O. Phuakkong, K. Bobuatong, Prof. Dr. P. Pantu, Dr. B. Boekfa, Prof. Dr. J. Limtrakul
Center for Advanced Studies in Nanotechnology and Its Applications in Chemical, Food and Agricultural Industries
Kasetsart University, Bangkok 10900 (Thailand)

[c] O. Phuakkong, K. Bobuatong, Prof. Dr. P. Pantu, Dr. B. Boekfa, Prof. Dr. J. Limtrakul
NANOTEC Center of Excellence, National Nanotechnology Center
Kasetsart University, Bangkok 10900 (Thailand)

[d] Dr. B. Boekfa
Chemistry Department, Faculty of Liberal Arts and Science
Kasetsart University Kamphaeng Saen Campus
Nakhon Pathom 73140 (Thailand)

[e] Prof. Dr. M. Probst
Institute of Ion Physics and Applied Physics
University of Innsbruck, 6020 Innsbruck (Austria)

[**] A Density Functional Theory Study

Supporting information for this article is available on the WWW under http://dx.doi.org/10.1002/cphc.201100047.

theoretically investigated. Rimalo et al. examined the role of Lewis and Brønsted catalysts on peptide formation using HF and AlF_3,[11] anorthite and sanidine[12] as the catalytic models, respectively. It has been found that the synergy of those catalysts dramatically lowers the activation barrier for the amide bond formation, a fact relevant in the prebiotic synthesis of peptides on the surface of oxide minerals that are rich in Lewis/Brønsted sites.

Brønsted acid sites are usually well characterized in the interior of zeolites. To our knowledge, their catalytic role in the peptide bond formation process has never been addressed together with a realistic representation of the zeolite. Therefore, we investigated the reaction mechanisms and kinetics of the zeolite-catalyzed peptide bond formation between two glycine molecules as the simplest model of such a reaction.

Quantum chemical calculations are reliable theoretical tools for studying chemical reactions which cannot be readily characterized by experimental techniques. Moreover, it is possible to compute valuable information about the nature of the transition states and the stable intermediate states as well as details of thermodynamics, kinetics of reaction, and spectroscopic properties such as the frequencies of vibration[13] of the system. Thus, direct insight into the reaction mechanism is possible, provided that the data are checked against available experimental results.

Zeolites usually possess hundreds of atoms per unit cell which makes the use of sophisticated methods, such as periodic ab initio calculations, computationally too expensive. The recent development of hybrid methods, such as the embedded cluster or combined quantum mechanics/molecular mechanics (QM/MM) methods,[13,14] has brought accurate results on large systems within reach.[14h,15] This was, for example, demonstrated in a study of the interaction of glycine with H-ZSM-5 zeolite.[15f] Complementary to this development, density functionals like the M06 set[16] can be applied to account for a more accurate treatment of the interactions in these systems, as has, for example, been done when studying the reactions of hydrocarbons inside zeolites.[14e,i,17] Herein we proceed along similar lines but apply a newer density functional and discuss its performance.

The aims of the present work are: 1) to investigate the peptide bond formation on zeolite and 2) to study the effect of the zeolite framework on the reaction. Two possible reaction mechanisms are investigated, a concerted and a stepwise one. The results of this study may be helpful for understanding the fundamentals of peptide formation of amino acid catalyzed by zeolite.

2. Results and Discussion

It was assumed that the reaction can either occur via a concerted reaction mechanism (Figure S1 in the Supporting Information) or by a stepwise reaction mechanism through the formation of the diolic intermediate (Figure S2 in the Supporting Information).

2.1. Concerted Reaction Mechanism

The peptide bond formation of two glycine molecules catalyzed by faujasite zeolite (Figure 1) via a concerted reaction mechanism is shown in Figure S1 in the Supporting Information. Depending on the site of initial adsorption, three possible energy profiles are presented for the concerted reaction in Figure 2a. The reaction is catalyzed by the Brønsted acidic proton acting as a proton donor to the oxygen atom of the amino group (amino-bound, Figure 3a), the carboxyl group (carboxyl-bound, Figure 4a), and the hydroxyl group (hydroxyl-bound, Figure 5a) of the glycine molecule, respectively. All of them are involved in the nucleophilic attack of the amino group on the

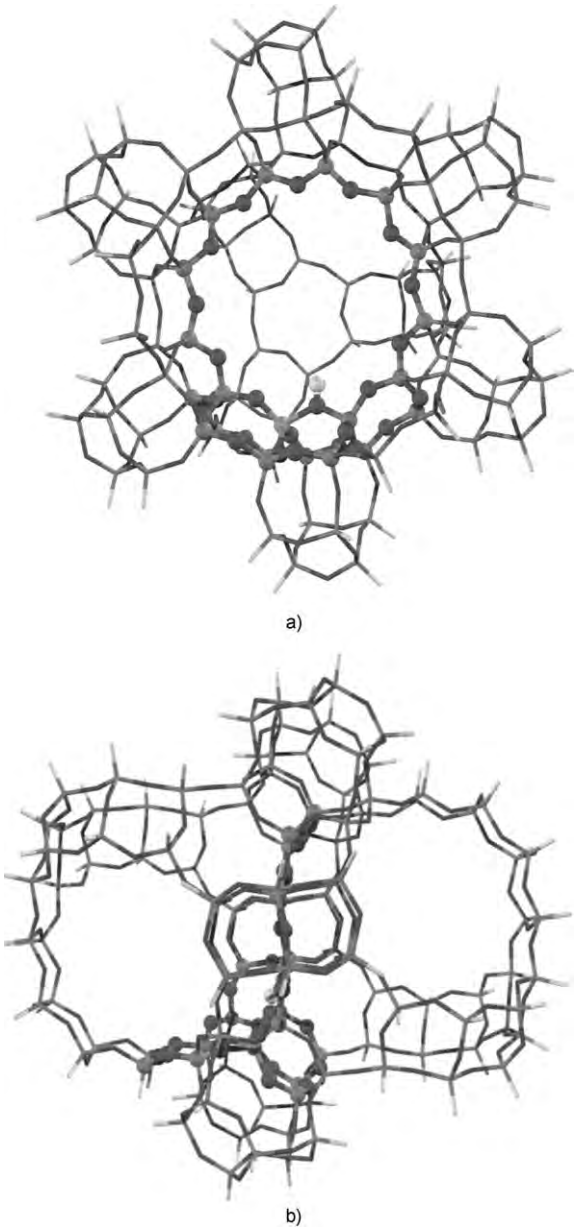

Figure 1. The 120T cluster models of H-FAU. Atoms belonging to the 21T quantum cluster are drawn as balls and sticks. a) Front view showing the 12-membered-ring window connecting the two supercages. b) Side view showing the two supercages connected to the 120T quantum cluster.

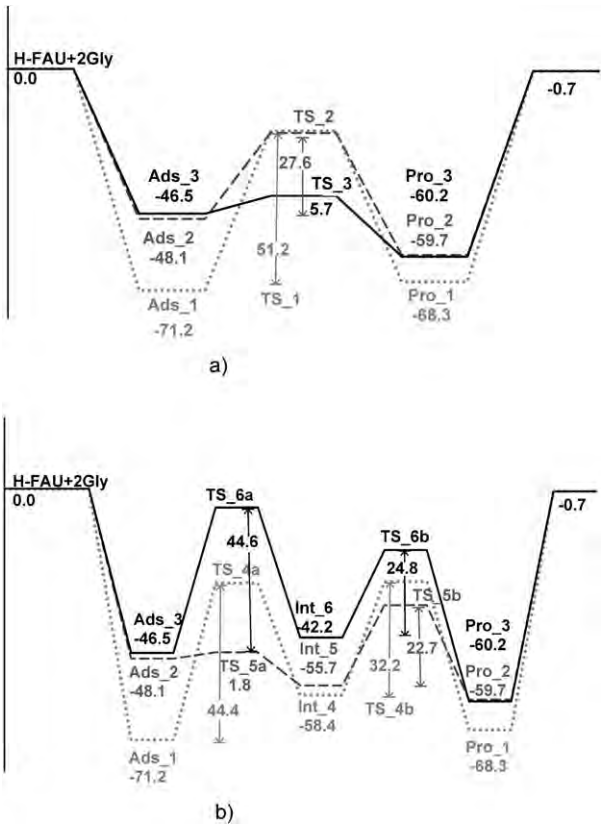

Figure 2. Energy profile (kcal mol^{-1}) of the peptide bond formation from different configurations of two glycine molecules interacting with H-FAU zeolite model 120T//21T calculated at the M08-HX/6-31G(d,p) level. Amino-bound configuration (•••••), carboxyl-bound configuration (– – –), and hydroxyl-bound configuration (——): a) concerted reaction mechanism; b) stepwise reaction mechanism.

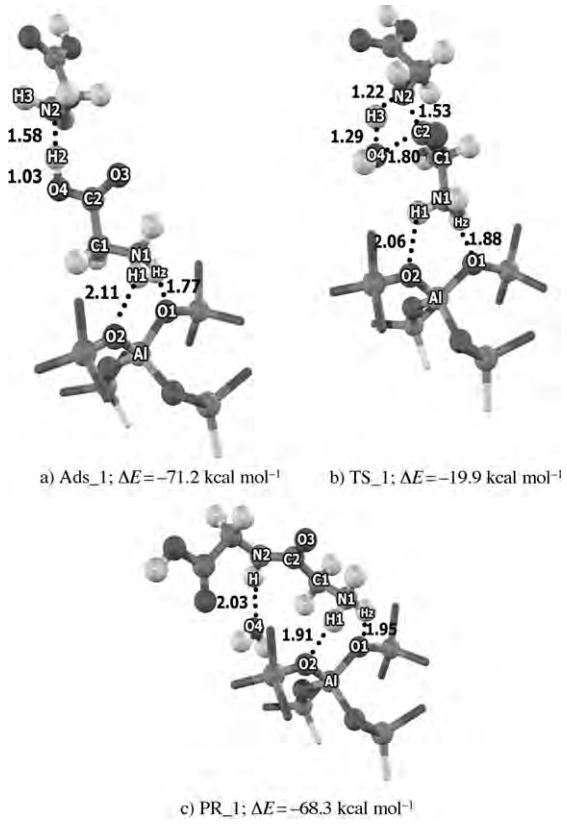

Figure 3. Optimized geometries of adsorption complexes, transition states, and products. a) Adsorption complex of the amino-bound configuration in the concerted reaction mechanism, Ads_1. b) Transition structure of the amino-bound configuration in the concerted reaction mechanism, TS_1. c) Adsorption complex of the products glycylglycine and water in the amino-bound configuration in the concerted reaction mechanism, Pro_1.

carboxyl carbon atom and the indirect transfer of a hydrogen atom from the nucleophilic amino group to a hydroxyl of another glycine molecule, which results in adsorbed glycylglycine and an adsorbed water molecule which is desorbed in the final step.

2.1.1. Interactions of Two Glycine Molecules in Different Configurations with H-FAU Zeolite

The calculated adsorption energies of two glycine molecules in different configurations on H-FAU zeolites are shown in the energy profile (Figure 2a) and in Table S1 in the Supporting Information, together with selected geometrical parameters.

The reaction proceeds as follows: First, two glycine molecules adsorb on the Brønsted acidic proton of the active zeolite site. This can occur via the amino group (amino-bound, Ads_1, Figure 3a), the carboxyl group (carboxyl-bound, Ads_2, Figure 4a) or the hydroxyl group (hydroxyl-bound, Ads_3, Figure 5a). In the first two configurations the adsorption (amino-bound and carboxyl-bound) of glycine is accompanied by a barrierless proton transfer from the active site to its C=O and $-NH_2$ groups. This causes the second hydroxyl group of glycine and the $-NH_3^+$ group to interact through two strong hydrogen bonds; the computed adsorption energies are −71.2 and −48.1 kcal mol^{-1}, respectively. In the hydroxyl-bound configuration glycine is adsorbed at the active site by hydrogen bonding between –OH of glycine and the Brønsted acidic proton. Its adsorption energy is −46.5 kcal mol^{-1}. It is difficult to directly compare calculated adsorption energies of glycine in zeolites with experimental results, and, to the best of our knowledge, there are no experimental data available on the glycine adsorption energy. The result for the amino-bound configuration can be compared with experimental data for ammonia which is protonated in zeolite with adsorption energies in the range of 24.9–25.6 kcal mol^{-1}.[18] Glycine is a more basic substance than NH_3. Moreover, the other glycine molecule is involved in the adsorption of the first one via hydrogen bonding between $-NH_3$ and the hydrogen atom of the carboxylic group of the first glycine, enhancing the adsorption energy of this configuration. Therefore, the adsorption energy of the amino-bound configuration over H-FAU should exceed that for ammonia, which agrees well with the known adsorption trend of this zeolite. The result shows that these adsorption energies are determined by both chemical (heat of protonation) and physical (confinement) factors. The latter, which arise from van der Waals interactions, cannot be ignored.

The first configuration is amino-bound (Ads_1, Figure 3a). Selected geometrical parameters of this configuration are pre-

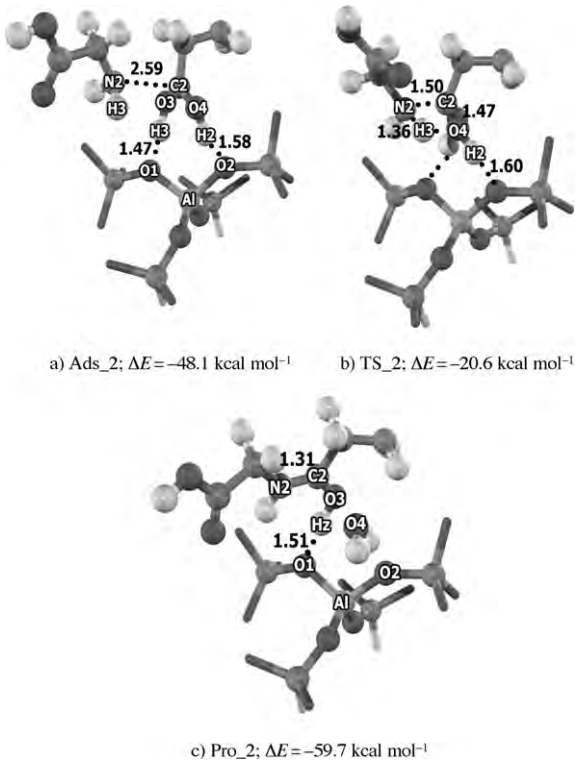

a) Ads_2; $\Delta E = -48.1$ kcal mol^{-1} b) TS_2; $\Delta E = -20.6$ kcal mol^{-1}

c) Pro_2; $\Delta E = -59.7$ kcal mol^{-1}

Figure 4. Optimized geometries of adsorption complexes, transition states, and products. a) Adsorption complex of the carboxyl-bound configuration in the concerted reaction mechanism, Ads_2. b) Transition structure of the carboxyl-bound configuration in the concerted reaction mechanism, TS_2. c) Adsorption complex of products glycylglycine and water of carboxyl-bound configuration in the concerted reaction mechanism, Pro_2.

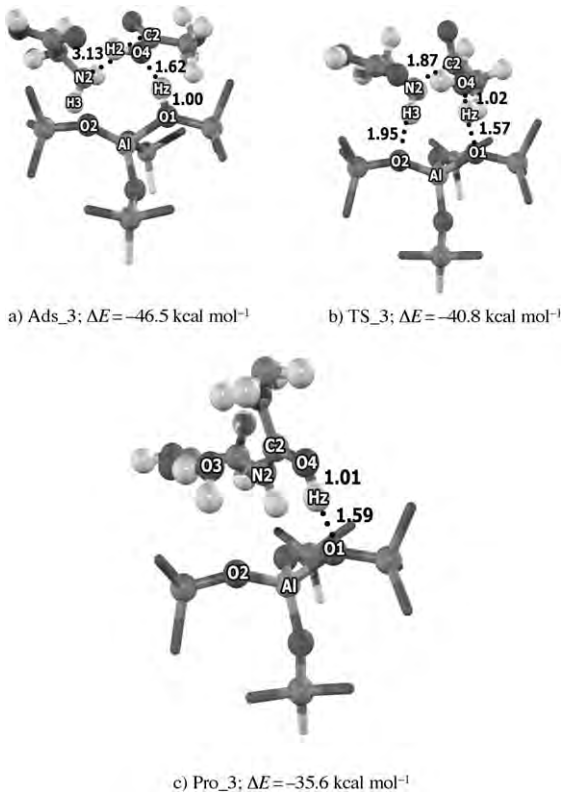

a) Ads_3; $\Delta E = -46.5$ kcal mol^{-1} b) TS_3; $\Delta E = -40.8$ kcal mol^{-1}

c) Pro_3; $\Delta E = -35.6$ kcal mol^{-1}

Figure 5. Optimized geometries of adsorption complexes, transition states, and products. a) Adsorption complex of the hydroxyl-bound configuration in the concerted reaction mechanism, Ads_3. b) Transition structure of the hydroxyl-bound configuration in the concerted reaction mechanism, TS_3. c) Adsorption complex of the products glycylglycine and water of the hydroxyl-bound configuration in the concerted reaction mechanism, Pro_3.

sented in Table S1 in the Supporting Information. The Brønsted acid of the zeolite O1–Hz bond is broken while the N1–Hz bond is formed. The O1···Hz distance in the amino configuration is about 1.77 Å. Both distances of N1–H1 and N1–Hz are virtually the same, indicating that there is a complete transfer of Brønsted acid. The second glycine is adsorbed by the hydrogen bond with a distance between H2···N2 of about 1.58 Å. The two hydrogen-bound adducts of glycine and zeolite (N1–Hz···O1 and N1–H1···O2) generate an "ion-pair-like structure" resulting in the highest adsorption energy of -71.2 kcal mol^{-1}.

For the carboxyl-bound configuration (Ads_2, Figure 4a), the adsorption of glycine involves a barrierless proton transfer from the active site to C=O. The O1–Hz bond distance of the Brønsted acidic proton is increased from 0.97 to 1.47 Å as compared to isolated H-FAU, indicating the weakening of the C=O bond. The C=O bond of glycine is elongated from 1.20 Å to 1.27 Å as compared to the isolated glycine molecule. The partial charge of the C atom changes from $+0.8$ in isolated glycine to $+0.9$ (Table 1). This shows that the catalyst facilitates the nucleophilic attack by the lone pair of the amine. Since the C2···N2 distance between the nitrogen atom of the $-NH_2$ group and this carbon atom (2.59 Å) is shorter than in the hydroxyl-bound configuration (3.13 Å) this co-adsorption complex is also stronger.

In the hydroxyl-bound configuration (Ads_3, Figure 5a) the hydrogen atom (H2) of the hydroxyl group of the first glycine points outward to interact with the oxygen atom (O5) of the carboxyl group of another glycine, with an O5···H2 distance of 1.58 Å and an O4–H2–O5 angle of 174.3°. The C2–O3 bond distance and the positive charge on the C atom at the reaction center are slightly increased with respect to the isolated glycine molecule. In summary, the carboxyl-bound configuration is more perturbed by the Brønsted acidic proton of H-FAU zeolite, explaining why the hydroxyl-bound configuration is the least stable one of the three configurations.

2.1.2. Peptide Bond Formation

The reaction pathways of the concerted mechanism for the three different configurations are shown in Figure S1 with selected geometries given in Table S1 of the Supporting Information. At the transition state of the amino-bound (TS_1, Figure 3b) and carboxyl-bound (TS_2, Figure 4b) configurations the concerted mechanism proceeds via four-center transition structures. This step is the nucleophilic attack of the lone electron pair of the amino group onto the carbon atom of the carboxyl group while simultaneously the proton transfer from the amino group to one of the oxygen atoms of the hydroxyl group takes place. The activation barriers in this step were cal-

Table 1. Activation barriers, ΔE_{ac} [kcal mol^{-1}], intrinsic rate constants for concerted and stepwise reaction mechanism, k, of peptide bond formation from two glycine molecules over H-FAU at 298 K [s^{-1}] and atomic charges, q(C), on the carbon atom of the carboxyl group of glycine at the reaction center (charges are in e).

	Concerted			Stepwise					
	Amino	Carboxyl	Hydroxyl	Amino		Carboxyl		Hydroxyl	
	TS_1	TS_2	TS_3	TS_4a	TS_4b	TS_5a	TS_5b	TS_6a	TS_6b
ΔE_{ac}	51.2	27.6	5.7	44.4	32.2	1.8	22.7	44.6	24.8
k	1.48×10^{-26}	6.37×10^{-9}	4.21×10^{3}	6.15×10^{-22}	1.95×10^{-9}	6.30×10^{10}	1.81×10^{-3}	2.35×10^{-20}	7.67×10^{-5}
q(C)	0.73	0.76	0.80	0.76	0.74	0.92	0.76	0.76	0.74

culated to be 51.2 and 27.6 kcal mol^{-1}, respectively, at which the adsorbed glycylglycine and a water molecule are formed.

In the transition state of the amino-bound configuration (TS_1, Figure 3b), C2 and N2 atoms form the peptide bond (C2···N2 distance: 1.53 Å) and the transfer of H3 from N2 to the oxygen atom of the hydroxyl group ends with an O4–H3 distance of 1.22 Å. The activation barrier of the amino-bound configuration, 51.2 kcal mol^{-1}, is similar to 47.7–52.7 kcal mol^{-1} for the uncatalyzed reaction of two glycine molecules obtained by MP2 calculations.[3h] This means that protonation of the amino group by the Brønsted acidic proton does not significantly enhance the electrophilicity of the C=O group. In summary, the high barrier is a consequence of the most stable adsorption configuration together with the strained four-center ring at the transition state.

The carboxyl-bound configuration is about 23.1 kcal mol^{-1} higher in adsorption energy. Since the transition state energy is similar, this brings the activation barrier down to 27.6 kcal mol^{-1} (Table 1). The transition structure is also a four-membered ring.

The hydroxyl-bound configuration is the least stable one and its transition state is also the lowest (TS_3, Figure 5b). The total activation barrier is therefore only 5.7 kcal mol^{-1}. The reason for such a low barrier is the presence of an eight-membered ring in the transition structure in which a double proton transfer occurs: one Brønsted acidic proton from the H-FAU zeolite toward the glycine OH group and the other one from NH_3 back to the H-FAU zeolite in order to regenerate the active site. The C–O2 distance is elongated from 1.37 Å to 2.05 Å and the peptide bond is generated by the C–N bond formation when the C···N distance decreases from 3.20 Å to 1.61 Å.

From the energetic data we calculated the intrinsic rate constants, k, to be 1.48×10^{-26}, 6.37×10^{-9}, and 4.21×10^{3} s^{-1} for the amino-bound, the carboxyl-bound, and the hydroxyl-bound configurations, respectively.

The peptide bond formation is endothermic with a reaction energy of 2.9 kcal mol^{-1} for the amino-bound configuration and exothermic with a reaction energy of 11.6 kcal mol^{-1} for the carboxyl-bound and 13.7 kcal mol^{-1} for the hydroxyl-bound configurations. The latter one is different from the first two because of the back donation of the proton from glycine to O4 instead of O3, which is the most stable position of the proton in H-FAU zeolite.[19] The endothermicity compares well with the value of 2.0–10.0 kcal mol^{-1} from a theoretical study of the uncatalyzed reaction reported by Jensen et al.[3h]

2.2. Stepwise Reaction Mechanism

Alternatively, the peptide bond formation of two glycine molecules can proceed via a stepwise mechanism [Eqs. (1)–(4)]:

$$2\,\text{Glycine} + \text{H-FAU} \rightarrow 2\,\text{Glycine}-\text{H-FAU} \quad (1)$$

$$2\,\text{Glycine}-\text{H-FAU} \rightarrow \text{Diol}-\text{H-FAU} \quad (2)$$

$$\text{Diol}-\text{H-FAU} \rightarrow \text{Glycylglycine}-\text{H}_2\text{O}-\text{H-FAU} \quad (3)$$

$$\text{Glycylglycine}-\text{H}_2\text{O}-\text{H-FAU} \rightarrow \text{Glycylglycine} + \text{H}_2\text{O} + \text{H-FAU} \quad (4)$$

First, step (1) is the adsorption of two glycine molecules on the active site of the H-FAU. Then, in step (2), the nucleophilic attack of the amino group on the carboxyl carbon atom coincides with the intramolecular hydrogen transfer in order to form a diolic intermediate. Step (3) involves the diolic intermediate and the intramolecular rearrangement to form glycylglycine and the water molecule adsorbed over H-FAU which is desorbed in the final step (4).

The energy profile of the reaction mechanisms from three starting orientations of the first glycine adsorption is shown in Figure 2b and selected geometric parameters are listed in Table S3 in the Supporting Information.

2.2.1. Interactions of Two Glycine Molecules in Different Configurations with H-FAU Zeolite

The same three configurations for the adsorbtion of two glycine molecules adsorbing on the active site are possible. Adsorption in the amino-bound (AD_1, Figure 3a), carboxyl-bound (AD_2, Figure 4a), and hydroxyl-bound (AD_3, Figure 5a) configuration is identical to the concerted mechanism discussed above. The adsorption energies are −71.2, −48.1, and −46.5 kcal mol^{-1} for the amino-bound, carboxyl-bound, and hydroxyl-bound glycine interaction, respectively.

2.2.2. Peptide Bond Formation

Starting from the amino-bound configurations, the peptide bond is generated simultaneously with hydrogen transfer in the four-membered transition structure (TS_4a, Figure 6a). The amino hydrogen atom from the second glycine is moved to the carboxyl oxygen atom on the first glycine as the C2–N2 bond is formed. At the first transition state, the C2···N2 dis-

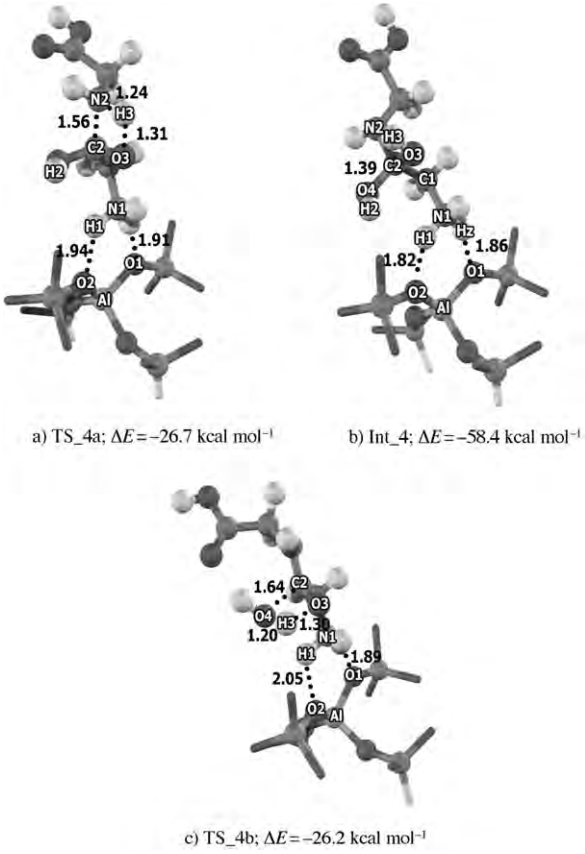

Figure 6. Optimized geometries of adsorption complexes, transition states, and products. a) First transition structure of the amino-bound configuration in the stepwise reaction mechanism, TS_4a. b) Intermediate of the amino-bound configuration in the stepwise reaction mechanism, Int_4. c) Second transition structure of the amino-bound configuration in the stepwise reaction mechanism, TS_4b.

For the carboxyl-bound configuration, the peptide formation involves only a nucleophilic attack of the amine nitrogen to the carboxyl carbon (TS_5a, Figure 7a). An activation energy of

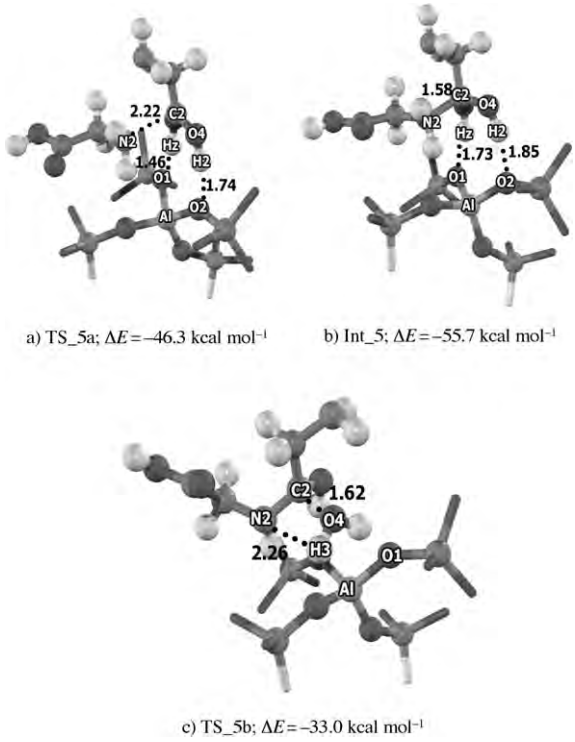

Figure 7. Optimized geometries of adsorption complexes, transition states, and products. a) First transition structure of the carboxyl-bound configuration in the stepwise reaction mechanism, TS_5a. b) Intermediate of the carboxyl-bound configuration in the stepwise reaction mechanism, Int_5. c) Second transition structure of the carboxyl-bound configuration in the stepwise reaction mechanism, TS_5b.

tance is 1.56 Å and N2–H3 is elongated to 1.24 Å. The activation barrier (44.4 kcal mol^{-1}) is smaller than for the hydrogen transfer in the concerted reaction mechanism (51.2 kcal mol^{-1}) from the amino group to the more basic oxygen atom of the carboxyl group and is preferred over the transfer to the less basic hydroxyl group. The diolic intermediate (Int_4, Figure 6b), with a tetrahedral sp^3 configuration on the carbon atom at the peptide bond, is produced and adsorbed over the deprotonated active site. Its energy is −58.4 kcal mol^{-1}.

At the second transition state (TS_4b, Figure 6c), water is eliminated from the planar four-membered ring transition structure and a distorted tetrahedral configuration at the carbon atom of the peptide bond of the diolic intermediate rearrangement is formed. Its activation energy is 32.2 kcal mol^{-1}. At the C2 atom previously linked to the N2 atom, H_2O is formed through hydrogen transfer from one hydroxyl group to the leaving one. The hydroxyl cleavage is accompanied by an extension of the C2–O4 distance from 1.39 Å to 1.64 Å and a contraction of the C–N bond from 1.43 Å to 1.39 Å. The water molecule is co-adsorbed between the framework and the newly formed glycylglycine (Pro_1). The relative energy of the product is −68.3 kcal mol^{-1}.

1.8 kcal mol^{-1} is required. The intermolecular C2···N2 distance is shortened to 2.22 Å while the reacting molecules move further from the active site by 1.46 Å. In the intermediate (Int_5, Figure 7b) the C2–N2 bond length is 1.58 Å and its energy is −55.7 kcal mol^{-1}. The intermediate consequently loses a water molecule through hydrogen abstraction from the amino group to the leaving group with an energy barrier of 22.7 kcal mol^{-1}. In the four-membered transition structure (TS_5b, Figure 7c) the N2–H3 bond length is extended to 2.26 Å and the O3–H4 distance is contracted to 0.96 Å. The departure of the hydroxyl group is promoted by a C2–O4 bond length of 1.62 Å. The final step is then again the co-adsorption of protonated glycylglycine (Pro_2) and water molecules over the zeolitic framework. The relative energy for this step is −59.7 kcal mol^{-1}.

Concerning the hydroxyl-bound configuration, no transfer of the zeolitic proton is involved in the first transition state (TS_6a, Figure 8a). The diolic intermediate (Int_6, Figure 8b) is generated via the four-membered transition state. The conversion, like for the amino-bound configuration discussed above, consists of the proton transfer and the formation of the intermolecular C2···N2 bond. The protonic H3 from the second glycine N2 moves towards O3 of the first glycine molecule as

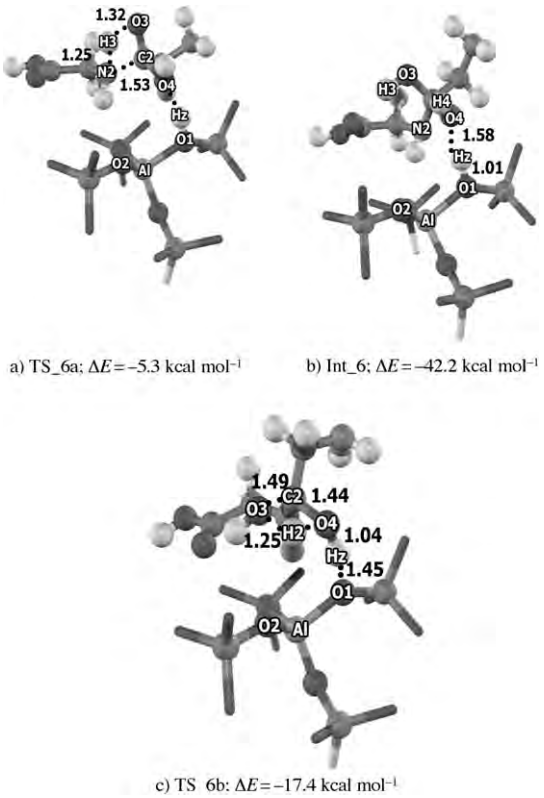

Figure 8. Optimized geometries of adsorption complexes, transition states, and products. a) First transition structure of the hydroxyl-bound configuration in the stepwise reaction mechanism, TS_6a. b) Intermediate of the hydroxyl-bound configuration in the stepwise reaction mechanism, Int_6. c) Second transition structure of the hydroxyl-bound configuration in the stepwise reaction mechanism, TS_6b.

shown in the distances of N2–H3 and O3–H3 of 1.25 Å and 1.32 Å, respectively. The C–O3 bond length is extended to 1.33 Å as O3 receives the proton H3. The intermolecular distance of C2–N2 is shortened from 3.13 Å to 1.53 Å. As the O1–Hz length is 1.01 Å and O4–Hz is 1.51 Å, the Brønsted proton is moving slightly closer to O2 of the first glycine and the reacting molecules are stabilized by adsorbing closer to the framework with a distance of 2.28 Å. At the adsorption complex of this configuration, the positive charge of the C atom at the reaction center (0.83) is in between the ones of the amino-bound and the carboxyl-bound configurations (0.82 and 0.890, respectively). The formed diolic intermediate has an adsorption energy of -42.15 kcal mol^{-1}. The four-membered transition structure (TS_6b, Figure 8c) is similar to the other configurations. The zeolitic proton is then transferred to the reacting molecule. The protonic H2 is abstracted from the leaving OH group and the transition structure adsorbs 2 Å closer to the framework. The process needs an activation energy of 24.8 kcal mol^{-1} yielding as products protonated glycylglycine (Pro_3, Figure 5d) and water located over the active region of the zeolite.

The barriers at the first transition state, 44.4, 1.8, and 44.6 kcal mol^{-1}, result in intrinsic rate constants, of 6.15×10^{-22}, 6.30×10^{10}, and 2.35×10^{-20} s^{-1} for the amino-bound, carboxyl-bound, and hydroxyl-bound configurations, respectively. The activation barriers of the second transition state for the three configurations (32.2, 22.7, and 24.8 kcal mol^{-1}, respectively) lead to intrinsic rate constants of 1.95×10^{-9}, 1.81×10^{-3}, and 7.67×10^{-5} s^{-1}, respectively.

For the stepwise reaction mechanism, the peptide bond formation is an exothermic reaction with a reaction energy of 0.7 kcal mol^{-1}. The energies required for desorption of the water molecule are 20.6, 14.2, and 15.0 kcal mol^{-1} for the amino-bound, carboxyl-bound, and the hydroxyl-bound configuration, respectively.

The complete energy profiles for the peptide formation mechanisms of glycine on H-FAU are shown in Figure 2. The three types of adsorptions, amino-bound, carboxyl-bound, and hydroxyl-bound have, for 2 glycine molecules, energies of -71.2, -48.4, and -46.5 kcal mol^{-1}, respectively. The reaction is exothermic. In the concerted mechanism, the activation energies are 51.2, 27.6, and 5.7 kcal mol^{-1} for amino-bound, carboxyl-bound, and hydroxyl-bound, respectively. In the stepwise mechanism the activation energies are 44.4 and 32.2 kcal mol^{-1} for amino-bound, 1.8 and 22.7 kcal mol^{-1} for carboxyl-bound and 44.6 and 24.8 kcal mol^{-1} for hydroxyl-bound configurations. The reaction via the amino-bound adsorbate in the concerted mechanism is the energetically preferred one.

3. Conclusions

The catalysis of peptide bond formation of two glycine molecules on H-FAU zeolite has been studied with density functional theory at the M08-HX level. There are three possible adsorption orientations for the first adsorbed glycine molecule which lead to different reaction pathways, these are, amino-bound, carboxyl-bound, and hydroxyl-bound configurations. For each of them, the concerted and the stepwise reaction mechanisms have been investigated.

In the concerted reaction, both the C–N bond formation and the release of water by N–H and C–O bond cleavages take place simultaneously. The catalytic activity of H-FAU zeolite influences the transition states for each reaction. The interaction to the Brønsted acidic proton increases the charge deficiency on the carbon atom of the carboxyl group and thus facilitates the nucleophilic attack by the lone electron pair of the amine.

The peptide bond is then generated by the dehydration of glycine taking place in a single step without a prior zwitterionic intermediate. The order of the activation barriers is amino-bound (51.2 kcal mol^{-1}) > carboxyl-bound (27.6 kcal mol^{-1}) > hydroxyl-bound (5.7 kcal mol^{-1}). The barrier height is significantly reduced by the presence of an eight-membered ring in the transition structure instead of the four-membered ring.

For the stepwise reaction mechanism, the reaction takes place through a stable diolic intermediate. Already in the first step, the C–N bond is formed through nucleophilic attack of the nitrogen on a carbon atom and simultaneous hydrogen transfer from ammonia to a carboxyl oxygen atom, except for the carboxyl-bound configuration, where a nucleophilic attack of the amine nitrogen on the carboxyl carbon was found.

In the second step, a water molecule is released by C–O and O–H bond cleavages. In contrast to the first mechanism, in which a hydrogen atom is transferred to hydroxyl oxygen from the ammonia, the stepwise reaction mechanism involves transfer of hydrogen to the carboxyl oxygen.

The concerted reaction mechanism should therefore dominate the overall reaction with an estimated activation barrier of 51.2 kcal mol^{-1}, starting from the amino-bound configuration. The overall reaction is predicted to be slightly endothermic.

Computational Methods

The cluster models of H-FAU are taken from the lattice structure of faujasite zeolite.[20] The active region consists of a 21T cluster, which is considered to be the smallest unit required to represent the acidic site of zeolite and the reactive molecules. In the 21T cluster, one of the silicon atoms in the faujasite zeolite is substituted by an aluminum atom, and a proton is added to one of the bridging oxygen atoms bonded directly to the aluminum atom, conventionally called the O1 position.[19,20] During the structure optimization, only the 5T part of the active site region [(≡SiO)$_2$(H)Al(OSi≡)$_2$] and the adsorbates are allowed to relax while the rest of the active region is fixed at the crystallographic coordinates. To represent the confinement effect of the zeolite pore structure, the extended structure of a 120T cluster (Figure 1) which includes two supercages is used in single point calculations. It is assumed that these models for the H-FAU zeolites are large enough to cover all the important framework effects that act on both the active site and on the adsorbates. Attempts have been made to demonstrate that the geometry constraints imposed in this work do not influence the results and the reliability of the M08-HX functional was compared with MP2 calculations. Some test calculations on glycine over the H-FAU zeolite have been performed relaxing 5T and 8T atoms (see Table S4 in the Supporting Information). All calculations were performed by means of the M08-HX density functional[21] and the 6-31G(d,p) basis set. For the transition structures, frequency calculations were performed in order to check whether the imaginary frequency mode corresponds to the reaction coordinate.

Atomic charges were computed from the natural population analysis (NPA). All calculations were performed using the Gaussian 03 code with the Minnesota density functionals module 3.1 by Zhao and Truhlar incorporated.[16a,22]

In order to analyze the kinetics of the reaction, classical transition state theory was used to derive the intrinsic rate constants k. They were calculated within the harmonic oscillator–rigid rotor approximation [Eq. (5)]:

$$k(T) = \frac{K_B T}{h} e^{-\Delta^{\neq} G^0/RT} \quad (5)$$

where k_B, T, h, $\Delta^{\neq}G^0$, and R are the Boltzmann constant, the temperature of the system (taken to be 298 K), Planck's constant, Gibbs free energy of activation, and the gas constant, respectively.

Acknowledgements

This work was supported in part by grants from the National Science and Technology Development Agency (2009 NSTDA Chair Professor funded by the Crown Property Bureau under the management of the National Science and Technology Development Agency and NANOTEC Center of Excellence funded by the National Nanotechnology Center), Kasetsart University Research and Development Institute (KURDI), the Thailand Research Fund (TRF), and the Commission on Higher Education, Ministry of Education (the "National Research University Project of Thailand (NRU)" and the "National Center of Excellence for Petroleum, Petrochemical and Advanced Materials (NCE-PPAM)"). Support from the Graduate School Kasetsart University and from the RFBR-FWF projects 09-03-91001-a and I200-N19 is also acknowledged. The authors are grateful to Donald G. Truhlar and Yan Zhao for their support with the M08-HX functional. We thank P. Khongpracha for helpful suggestions.

Keywords: density functional calculations · dipeptide · glycine · reaction mechanisms · zeolites

[1] a) J. Liu, Z. Cao, Y. Lu, *Chem. Rev.* **2009**, *109*, 1948 – 1998; b) Y. Ura, J. M. Beierle, L. J. Leman, L. E. Orgel, M. R. Ghadiri, *Science* **2009**, *325*, 73 – 77; c) K. J. Waldron, N. J. Robinson, *Nat. Rev. Microbiol.* **2009**, *7*, 25 – 35; d) I. Ben-Gera, G. Zimmermann, *Nature* **1964**, *202*, 1007 – 1008.

[2] a) L. E. Orgel, *Trends Biochem. Sci.* **1998**, *23*, 491 – 495; b) P. Davies, *Sci. Prog.* **2001**, *84*, 17 – 29; c) P. Davies, *Sci. Prog.* **2001**, *84*, 1 – 16.

[3] a) J. D. Bernal, *The Physical Basis of Life*, Routledge and Kegan Paul, London, **1951**; b) B. K. G. Theng, *The Chemistry of Clay-Organic Reactions*, Wiley, New York, **1974**; c) M. J. Gresser, W. P. Jencks, *J. Am. Chem. Soc.* **1977**, *99*, 6963 – 6970; d) C. C. Yang, W. P. Jencks, *J. Am. Chem. Soc.* **1988**, *110*, 2972 – 2973; e) M. M. Cox, W. P. Jencks, *J. Am. Chem. Soc.* **1981**, *103*, 572 – 580; f) A. C. Satterthwait, W. P. Jencks, *J. Am. Chem. Soc.* **1974**, *96*, 7018 – 7031; g) T. Oie, G. H. Loew, S. K. Burt, J. S. Binkley, R. D. MacElroy, *J. Am. Chem. Soc.* **1982**, *104*, 6169 – 6174; h) J. H. Jensen, K. K. Baldridge, M. S. Gordon, *J. Phys. Chem.* **1992**, *96*, 8340 – 8351.

[4] H. Yang, S.-Y. Fung, M. Pritzker, P. Chen, *Langmuir* **2009**, *25*, 7773 – 7777.

[5] J. Bujdak, B. M. Rode, *React. Kinet. Catal. Lett.* **1997**, *62*, 281 – 286.

[6] a) K. I. Zamaraev, V. N. Romannikov, R. I. Salganik, W. A. Wlassoff, V. V. Khramtsov, *Origins Life Evol. Biosphere* **1997**, *27*, 325 – 337; b) M. Meng, L. Stievano, J.-F. Lambert, *Langmuir* **2004**, *20*, 914 – 923; c) N. Lahav, D. White, S. Chang, *Science* **1978**, *201*, 67 – 69; d) M. Rao, D. G. Odom, J. Oro, *J. Mol. Evol.* **1980**, *15*, 317 – 331; e) A. J. A. Aquino, D. Tunega, M. H. Gerzabek, H. Lischka, *J. Phys. Chem. B* **2004**, *108*, 10120 – 10130.

[7] a) V. A. Basiuk, T. Y. Gromovoy, V. G. Golovaty, A. M. Glukhoi, *Origins Life Evol. Biosphere* **1991**, *20*, 483 – 498; b) J. Bujdák, B. M. Rode, *J. Mol. Evol.* **1997**, *45*, 457 – 466; c) J. Bujdak, B. M. Rode, *J. Mol. Catal. A* **1999**, *144*, 129 – 136; d) A. Rimola, L. Rodriguez-Santiago, P. Ugliengo, M. Sodupe, *J. Phys. Chem. B* **2007**, *111*, 5740 – 5747.

[8] a) J. E. Krohn, M. Tsapatsis, *Langmuir* **2005**, *21*, 8743 – 8750; b) J. E. Krohn, M. Tsapatsis, *Langmuir* **2006**, *22*, 9350 – 9356; c) F. Xu, Y. Wang, X. Wang, Y. Zhang, Y. Tang, P. Yang, *Adv. Mater.* **2003**, *15*, 1751 – 1753; d) S. Munsch, M. Hartmann, S. Ernst, *Chem. Commun.* **2001**, 1978 – 1979.

[9] G.-W. Xing, X.-W. Li, G.-L. Tian, Y.-H. Ye, *Tetrahedron* **2000**, *56*, 3517 – 3522.

[10] a) Y. Cui, Q. Wei, H. Park, C. M. Lieber, *Science* **2001**, *293*, 1289 – 1292; b) J. Kong, N. R. Franklin, C. Zhou, M. G. Chapline, S. Peng, K. Cho, H. Dailt, *Science* **2000**, *287*, 622 – 625.

[11] A. Rimola, S. Tosoni, M. Sodupe, P. Ugliengo, *Chem. Phys. Lett.* **2005**, *408*, 295 – 301.

[12] A. Rimola, M. Sodupe, P. Ugliengo, *J. Am. Chem. Soc.* **2007**, *129*, 8333 – 8344.

[13] R. Z. Khaliullin, A. T. Bell, V. B. Kazansky, *J. Phys. Chem. A* **2001**, *105*, 10454 – 10461.

[14] a) P. E. Sinclair, A. de Vries, P. Sherwood, C. R. A. Catlow, R. A. van Santen, *J. Chem. Soc. Faraday Trans.* **1998**, *94*, 3401 – 3408; b) M. Brändle, J. Sauer, *J. Am. Chem. Soc.* **1998**, *120*, 1556 – 1570; c) S. P. Greatbanks, I. H. Hillier, N. A. Burton, P. Sherwood, *J. Chem. Phys.* **1996**, *105*, 3770 – 3776; d) J. Limtrakul, T. Nanok, S. Jungsuttiwong, P. Khongpracha, T. N. Truong, *Chem. Phys. Lett.* **2001**, *349*, 161 – 166; e) T. Maihom, B. Boekfa, J. Sirijaraensre, T. Nanok, M. Probst, J. Limtrakul, *J. Phys. Chem. C* **2009**,

113, 6654 – 6662; f) T. Maihom, S. Namuangruk, T. Nanok, J. Limtrakul, *J. Phys. Chem. C* **2008**, *112*, 12914 – 12920; g) P. Treesukol, K. Srisuk, J. Limtrakul, T. N. Truong, *J. Phys. Chem. B* **2005**, *109*, 11940 – 11945; h) P. Pantu, S. Pabchanda, J. Limtrakul, *ChemPhysChem* **2004**, *5*, 1901 – 1906; i) B. Boekfa, S. Choomwattana, P. Khongpracha, J. Limtrakul, *Langmuir* **2009**, *25*, 12990 – 12999.

[15] a) S. Yuan, J. Wang, Y.-B. Duan, Y.-W. Li, H. Jiao, *J. Mol. Catal. A* **2006**, *256*, 130 – 137; b) A. Waclaw, K. Nowinska, W. Schwieger, *Appl. Catal. A* **2004**, *270*, 151 – 156; c) S. Kasuriya, S. Namuangruk, P. Treesukol, M. Tirtowidjojo, J. Limtrakul, *J. Catal.* **2003**, *219*, 320 – 328; d) K. Bobuatong, J. Limtrakul, *Appl. Catal. A* **2003**, *253*, 49 – 64; e) S. Namuangruk, P. Pantu, J. Limtrakul, *J. Catal.* **2004**, *225*, 523 – 530; f) B. Boekfa, P. Pantu, J. Limtrakul, *J. Mol. Struct.* **2008**, *889*, 81 – 88; g) C. Tuma, J. Sauer, *Phys. Chem. Chem. Phys.* **2006**, *8*, 3955 – 3965.

[16] a) Y. Zhao, D. G. Truhlar, *Theor. Chem. Acc.* **2008**, *120*, 215 – 241; b) Y. Zhao, D. G. Truhlar, *J. Phys. Chem. C* **2008**, *112*, 6860 – 6868.

[17] a) C. Kumsapaya, K. Bobuatong, P. Khongpracha, Y. Tantirungrotechai, J. Limtrakul, *J. Phys. Chem. C* **2009**, *113*, 16128 – 16137; b) B. Boekfa, P. Pantu, M. Probst, J. Limtrakul, *J. Phys. Chem. C* **2010**, *114*, 15061 – 15067; c) S. Wannakao, B. Boekfa, P. Khongpracha, M. Probst, J. Limtrakul, *ChemPhysChem* **2010**, *11*, 3432 – 3438.

[18] H. G. Karge, V. Dondur, J. Weitkamp, *J. Phys. Chem.* **1991**, *95*, 283 – 288.

[19] J.-R. Hill, C. M. Freeman, B. Delley, *J. Phys. Chem. A* **1999**, *103*, 3772 – 3777.

[20] D. H. Olson, E. Dempsey, *J. Catal.* **1969**, *13*, 221 – 231.

[21] a) Y. Zhao, D. G. Truhlar, *J. Chem. Theory Comput.* **2008**, *4*, 1849 – 1868; b) Y. Zhao, D. G. Truhlar, *J. Chem. Theory Comput.* **2011**, *7*, 669 – 676.

[22] *Gaussian 03* (*Revision B.05*), M. J. Frisch, G. W. Trucks, H. B. Schlegel, G. E. Scuseria, M. A. Robb, J. R. Cheeseman, J. A. Montgomery, Jr., T. Vreven, K. N. Kudin, J. C. Burant, J. M. Millam, S. S. Iyengar, J. Tomasi, V. Barone, B. Mennucci, M. Cossi, G. Scalmani, N. Rega, G. A. Petersson, H. Nakatsuji, M. Hada, M. Ehara, K. Toyota, R. Fukuda, J. Hasegawa, M. Ishida, T. Nakajima, Y. Honda, O. Kitao, H. Nakai, M. Klene, X. Li, J. E. Knox, H. P. Hratchian, J. B. Cross, C. Adamo, J. Jaramillo, R. Gomperts, R. E. Stratmann, O. Yazyev, A. J. Austin, R. Cammi, C. Pomelli, J. W. Ochterski, P. Y. Ayala, K. Morokuma, G. A. Voth, P. Salvador, J. J. Dannenberg, V. G. Zakrzewski, S. Dapprich, A. D. Daniels, M. C. Strain, O. Farkas, D. K. Malick, A. D. Rabuck, K. Raghavachari, J. B. Foresman, J. V. Ortiz, Q. Cui, A. G. Baboul, S. Clifford, J. Cioslowski, B. B. Stefanov, G. Liu, A. Liashenko, P. Piskorz, I. Komaromi, R. L. Martin, D. J. Fox, T. Keith, M. A. Al-Laham, C. Y. Peng, A. Nanayakkara, M. Challacombe, P. M. W. Gill, B. Johnson, W. Chen, M. W. Wong, C. Gonzalez, J. A. Pople, Gaussian, Inc., Pittsburgh, PA, **2003**.

Received: January 18, 2011
Published online on June 22, 2011

Density Functional Theory Study on Catalytic Cracking of *n*-Hexane on Heteropoly Acid: a Comparison With Acidic Zeolite

Saowapak Choomwattana,[1,2,3] Thana Maihom,[1,2,3] Bundet Boekfa,[2,3,4] Piboon Pantu[1,2,3] and Jumras Limtrakul[1,2,3]*

1. *Department of Chemistry, Faculty of Science, National Center of Excellence for Petroleum, Petrochemicals and Advanced Materials, Center of Nanotechnology, Kasetsart University Research Development Institute, Kasetsart University, Bangkok 10900, Thailand*
2. *Center for Advanced Studies in Nanotechnology and Its Applications in Chemical, Food and Agricultural Industries, Kasetsart University, Bangkok 10900, Thailand*
3. *NANOTEC Center of Excellence, National Nanotechnology Center, Kasetsart University, Bangkok 10900, Thailand*
4. *Chemistry Department, Faculty of Liberal Arts and Science, Kasetsart University Kamphaeng Saen Campus, Nakhon Pathom 73140, Thailand*

We have performed a direct comparison of *n*-hexane cracking catalysed by a zeolite (H-ZSM-5) and a heteropoly acid (phosphotungstic acid, HPW). This comparison was examined by employing density functional theory, including dispersion energy, M06-L, for the purpose of understanding these two catalysts for this industrially important reaction. The predicted adsorption energies of hexane are −21.4 and −6.8 kcal/mol for H-ZSM-5 and HPW, respectively. The protolytic cracking mechanism is proposed to proceed via the first step of the C–C activation and is found to be the rate-determining step with activation energies of 42.8 and 41.4 kcal/mol for H-ZSM-5 and HPW, respectively. We also discuss the advantages and disadvantages of both catalysts for hydrocarbon cracking and give a perspective of utilising cutting-edge molecular design for a tailor-made hybrid catalyst.

Keywords: density functional theory, hydrocarbon cracking, heteropoly acid, zeolite

INTRODUCTION

Sustainable 'green' chemistry is nowadays of increasing interest along with raising environmental awareness. There have been attempts to find a new catalyst family to replace corrosive and toxic conventional acid catalysts. Zeolites and heteropoly acids (HPA) are well known solid catalysts. Both have very strong Brønsted acidities whose acid strengths were determined to be nearly superacid. Zeolites, especially Y and ZSM-5, are widely used in cracking processes and many other petrochemical processes due to their advantages of high catalytic activity and their molecular shape selectivity. Heteropoly acids, have recently been considered as a solid acid alternative because these materials not only have a high acidity (even higher than zeolite) but also redox properties which may lead to broader applications.

For petrochemical purposes, hydrocarbon cracking is a widely accepted case study providing the possibility for comparing experimental results with theory and promising insight into the molecular mechanism of more complicated reactions. Zeolite is, without doubt, capable of cracking hydrocarbons. For instance, cracking reactions over ZSM-5, Beta and Faujasite zeolites occur at a temperature of 623–773 K (Kotrel et al., 1999). HPA is, on the other hand, less well known for application in hydrocarbon cracking reactions due to its poor stability and lack of monodispersity.

Additional Supporting Information may be found in the online version of this article.

*Author to whom correspondence may be addressed.
E-mail address: jumras.l@ku.ac.th

Can. J. Chem. Eng. 90:865–872, 2012

DOI 10.1002/cjce.21619
Published online 22 December 2011 in Wiley Online Library (wileyonlinelibrary.com).

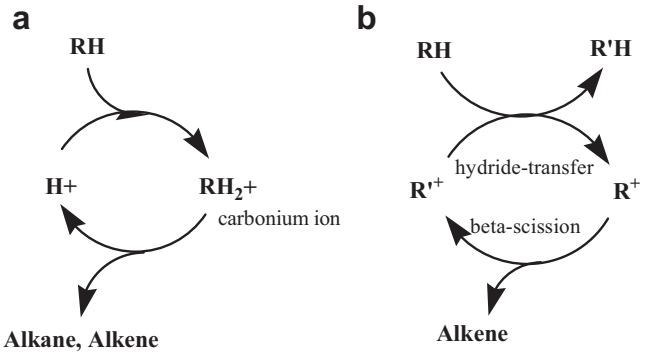

Scheme. 1. Monomolecular (a) and bimolecular (b) mechanisms.

An example of this is the experimental work on the stability and catalytic property of phosphotungstic acid (HPW) on the *n*-hexane cracking reaction (Jalil et al., 2003). It was reported that, in a fixed bed reactor and a nitrogen–hexane mixture feed at atmospheric pressure, the catalyst was active at 473 K for only 8 min before it expired completely. The drawbacks are possibly surmountable, as many attempts, such as applying catalyst support and stabiliser, (Betz et al., 2011; Bhorodwaj and Dutta, 2011; Fiuza et al., 2011) have been made to improve the catalyst.

From the molecular approach, bimolecular and monomolecular mechanisms (see Scheme 1) were proposed to explain the catalytic cracking of hydrocarbons over Brønsted acid sites of solid catalysts, especially acidic zeolites (Corma and Orchilles, 2000; Kotrel et al., 2000). The bimolecular mechanism involves the activation of an alkane molecule by hydride-transfer to an adsorbed carbenium ion on the catalyst surface followed by isomerisation and β-scission. This mechanism prevails under the condition of high partial pressure of hydrocarbons and low reaction temperature. Monomolecular cracking is believed to be overriding under low pressure and high temperature conditions (Haag and Dessau, 1984; Kotrel et al., 2000). In this mechanism, a carbonium-like ionic intermediate, which is a key reacting intermediate species, is formed by the direct protonation of Brønsted acid to the C–C bond. It subsequently leads to the scission of the C–C bond to produce alkane and alkene products. Recently, we reported in our calculation that the protonation step is found to be the rate-determining step (Maihom et al., 2010). Therefore, this work focuses on the study of the protonation step of the alkane cracking to compare the catalyst effectiveness.

Attempts have been made to develop computational methodology that can precisely predict physical and chemical properties of the catalyst itself and the catalysed reactions. Most density functional methods have been unable to include dispersion forces (Wesolowski et al., 1997) which is so important for investigating the adsorption and reactions in confined nanoporous materials such as zeolites, where van der Waals contributions are essentially dominant. Zhao and Truhlar (2008a,b) have developed a new meta-hybrid, a combination of meta generalised gradient approximations (GGA) with Hartree–Fock exchange, called M06 series, that has shown promising performance for calculating the binding energies of adsorbates covalently and non-covalently interacting with the zeolite acid site. The results were comparable to the sophisticated ab initio MP2 (second-order Møller–Plesset perturbation theory) calculations but at much more affordable computer times. M06-L has been reported to be a highly accurate functional for transition metals (Zhao and Truhlar, 2008a; Wannakao et al., 2010). In addition, the functional is also efficient for calculations on large systems of zeolites (Kumsapaya et al., 2009). Therefore, it is practical to use this functional to represent the systems of zeolite and HPW.

In the present work, we have employed the M06-L which includes dispersion energy to theoretically investigate the first step of *n*-hexane cracking catalysed by acidic ZSM-5 zeolite and a heteropoly acid (HPA). Hexane is chosen as a reactant in this work because it is widely used experimentally as a benchmark in cracking reactions to study the catalyst acidity (Bourdillon et al., 1990; Lercher et al., 2008). The direct comparison of the protolytic cracking of *n*-hexane on zeolites and heteropoly acid has been performed for the first time to provide insight into the catalytic activity of these two catalysts for industrially important cracking reactions. The geometrical parameters of optimised structures and relative energies of adsorption complexes and transition states are discussed.

MODELS AND METHODS

Nanocluster models of ZSM-5 zeolite and heteropoly acid (α-Keggin HPW) were generated from their lattice structures reported by van Koningsveld et al. (1987), and Soares-Santos et al. (2008), respectively. The ZSM-5 zeolite was represented by a 34T H-ZSM-5 cluster model (illustrated in Figure 1), which covers the intersection at the interconnection between the straight channel and the zigzag channel. One of the silicon atoms at the T12 site is replaced with an Al atom to generate the bridging hydroxyl group known as the Brønsted acid site of zeolite. In our previous studies (Boekfa et al., 2009; Maihom et al., 2009, 2010), the 34T H-ZSM-5 model had been used for studying the adsorption and reactions of *n*-hexane cracking, hydrogen exchange on unsaturated aliphatic, aromatic and heterocyclic compounds and gave reasonable results for adsorption and activation energies, compared with experimental values. For the phosphotungstic acid, the cluster model (Figure 2) whose molecular formula is $H_3PW_{12}O_{40}$, can be considered as a $W_{12}O_{36}$ cage (which is composed of a 12 edge-sharing WO_6 metal-oxygen octahedral) enveloping a phosphate (PO_4^{3-}) anion (Figure 2b). Similar to zeolites, the acidic proton, for the charge neutralisation, of HPW heteropoly acid resides on the framework oxygen atoms. We adopted the model from the work of Yang et al. (2005) which proposed a rational model based on experimental works (Ueda et al., 2001).

For the zeolite system, only the 5 T cluster of the active site region [$\equiv(SiO)_2(H)Al(OSi)_2\equiv$] and the adsorbate molecule are allowed to relax, while the remaining atoms are fixed at the crystallographic coordinates. For the HPW system, all atoms are allowed to relax during the optimisations. The M06-L density functional was used in all calculations. The basis set of 6-31G(d,p) was employed for Al, Si, O, P, and H atoms. As for the W atom, the effective core potential (ECP) of Stuttgart and Bonn was employed (Dolg et al., 1993) to replace the core electrons with an effective potential, and treated only valence electrons in the calculation. All calculations were performed with the Gaussian 03 code (Frisch et al., 2004) modified to incorporate the Minnesota Density Functionals module 3.1 by Zhao and Truhlar (2008a,b).

RESULTS AND DISCUSSION

Structure and Acidity of the H-ZSM-5 and HPW Structures

H-ZSM-5 and HPW both have very strong Brønsted acid sites that are accessible for acid-catalysed reactions. In a review of Mizuno and Misono (1998), it was stated that heteropoly acids such as

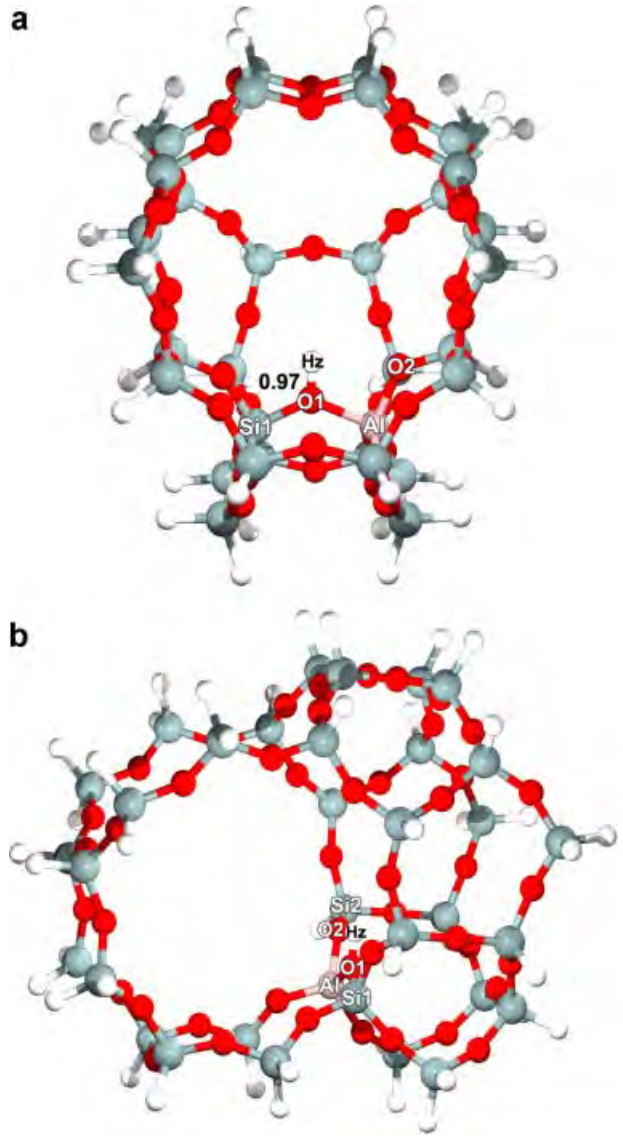

Figure 1. 34T cluster model of H-ZSM-5 zeolite: (a) front view with the acidic bond distance and (b) side view. [Color figure can be seen in the online version of this article, available at http://onlinelibrary.wiley.com/journal/10.1002/(ISSN)1939-019X]

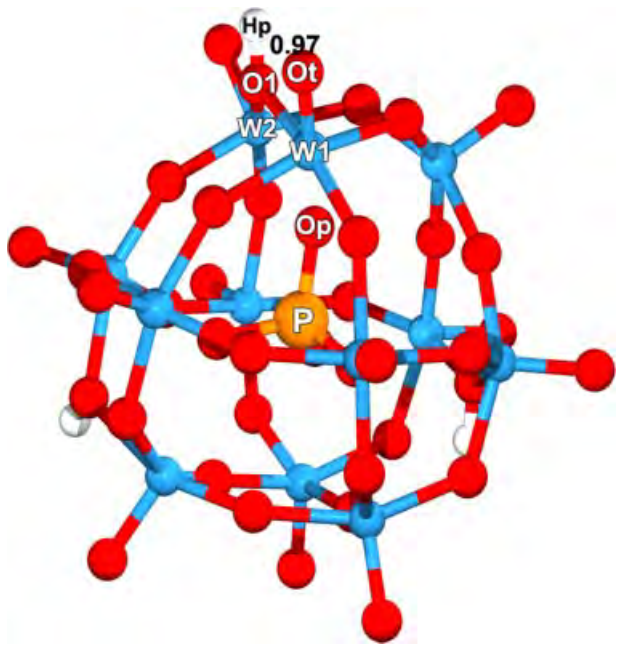

Figure 2. Cluster model of α-Keggin HPW heteropoly acid. [Color figure can be seen in the online version of this article, available at http://onlinelibrary.wiley.com/journal/10.1002/(ISSN)1939-019X]

HPW in the solid state are pure Brønsted acids and stronger acids than the conventional solid acids such as SiO_2–Al_2O_3, H_3PO_4/SiO_2, and HX and HY zeolites. The relative strength of Brønsted acidities can be analysed from the deprotonation energy, which is considered to be the energy required for removing the acidic proton from the catalyst structures calculated with the following equation:

$$\text{Deprotonationenergy} = \text{E(Catalyst-H)} - \text{E(Catalyst)} \quad (1)$$

where E(Catalyst-H) and E(Catalyst) are the energies of the deprotonated and the neutral cluster zeolites. Our calculations have shown that the deprotonation energy of H-ZSM-5 is higher than that of HPW (299.7 and 263.1 kcal/mol, respectively) indicating that HPW is a stronger acid than H-ZSM-5. The O–H acidic bond length in both catalysts is the same (0.97 Å, shown in Tables 1 and 2), but the partial atomic charge on the acidic proton

Table 1. Optimised geometrical parameters of the species involved in the protonation step of *n*-hexane cracking on H-ZSM-5 zeolite

Parameter	Isolated cluster	Hexane adsorption (Ads_ZSM-5)	Transition state (TS_ZSM-5)	Intermediate (Int_ZSM-5)
Distances (Å)				
O1–Hz	0.97	0.97	1.71	1.97
Al–O1	1.83	1.83	1.73	1.72
Al–O2	1.68	1.68	1.71	1.71
Hz–C3	—	2.95	1.34	1.26
Hz–C4	—	3.18	1.33	1.26
C3–C4	1.52	1.52	1.70	1.86
C3–O1	—	3.91	2.89	3.00
C3–O2	—	3.68	2.93	2.92
C4–O1	—	4.10	2.82	2.88
C4–O2	—	4.37	3.16	3.18
Angles (°)				
O2–Al–O1	90.4	90.6	93.3	93.6
Si1–O1–Al	131.1	130.3	129.0	129.7
C3–Hz–C4	—	28.4	79.4	95.2

Table 2. Optimised geometrical parameters of the species involved in the protonation step of *n*-hexane cracking on heteropoly acid (HPW)

Parameter	Isolated cluster	Hexane adsorption (Ads_HPW)	Transition state (TS_HPW)	Intermediate (Int_HPW)
Distances (Å)				
O1–H1	0.97	0.97	1.61	2.25
W1–O1	2.12	2.12	2.00	1.96
W2–O1	2.11	2.10	1.97	1.93
H1–C3	—	2.45	1.39	1.26
H1–C4	—	2.38	1.28	1.23
C3–C4	1.52	1.52	1.72	2.26
C3–Ot	—	4.04	3.74	3.48
C4–Ot	—	3.65	3.35	3.87
Angles (°)				
W1–O1–W2	122.1	122.3	124.7	127.3
C3–H1–C4	—	36.7	79.9	130.0

(H1) derived from the conventional method, Mulliken population analysis (Mulliken, 1955), is observably different. The HPW has a slightly larger positive charge on the acidic proton than H-ZSM-5 (0.413*e* and 0.404*e*, respectively).

Structure and Energetics of *n*-Hexane Adsorption

The optimised adsorption structures of *n*-hexane on H-ZSM-5 and HPW are shown in Figures 3 and 4, respectively. Selected geometrical parameters for all adsorption complexes are listed in Tables 1 and 2. A single *n*-hexane molecule is weakly adsorbed on the zeolite and HPW through the interaction between two central methylene carbon atoms (C3–C4) and the Brønsted acid site (O1–H1). This adsorbed structure corresponds to the cracking reaction mechanism. Upon the adsorption, there is no significant change in the structures of the catalyst and the adsorbed *n*-hexane, when comparing to the isolated components (Tables 1 and 2). Nevertheless, the intermolecular distances between the alkane and the catalytic acid of the catalysts are different. The average interatomic distances between the acidic hydrogen atom (H1) and the C3 and C4 atoms of the adsorbed *n*-hexane molecule are 2.89 Å for H-ZSM-5 and 2.42 Å for HPW. The adsorption energies with respect to the isolated molecule for H-ZSM-5 and HPW systems are −21.4 and −6.8 kcal/mol, respectively. The former calculated adsorption energy is in good agreement with the experimental estimate of −19.6 kcal/mol (Eder et al., 1997). This indicates that the M06-L functional can well represent interactions in the zeolite model and is expected to provide reasonable results for HPW as

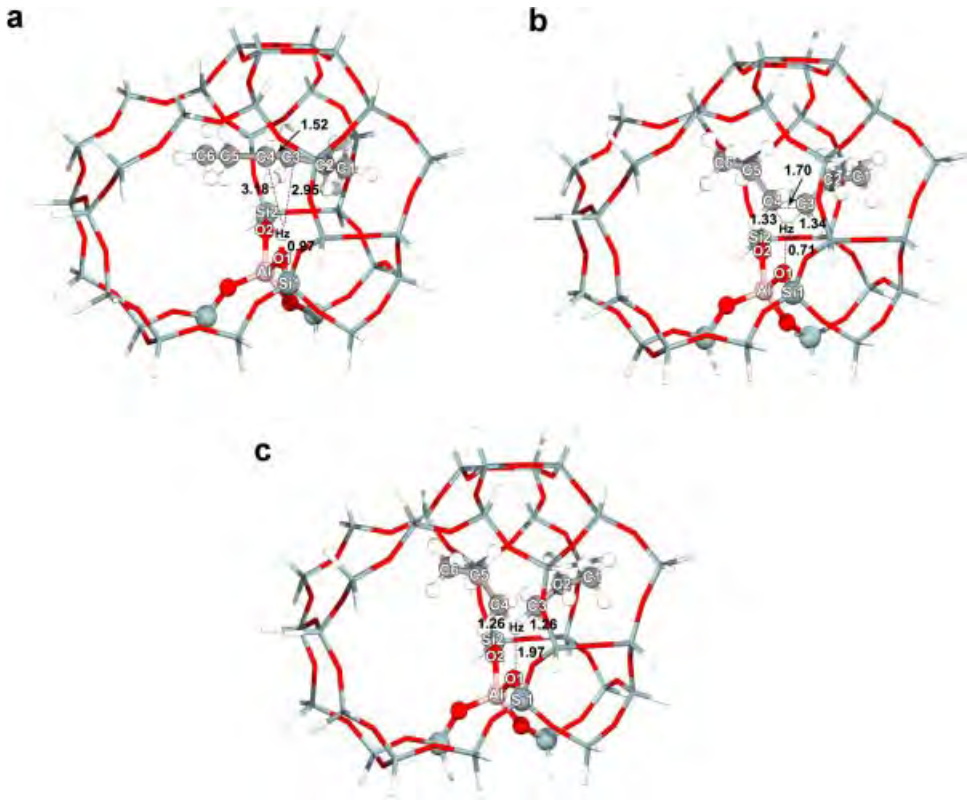

Figure 3. Optimised structures of (a) *n*-hexane adsorption (b) transition state and (c) 3-C-hexonium intermediate involved in the protolytic cracking of *n*-hexane over H-ZSM-5. [Color figure can be seen in the online version of this article, available at http://onlinelibrary.wiley.com/journal/10.1002/(ISSN)1939-019X]

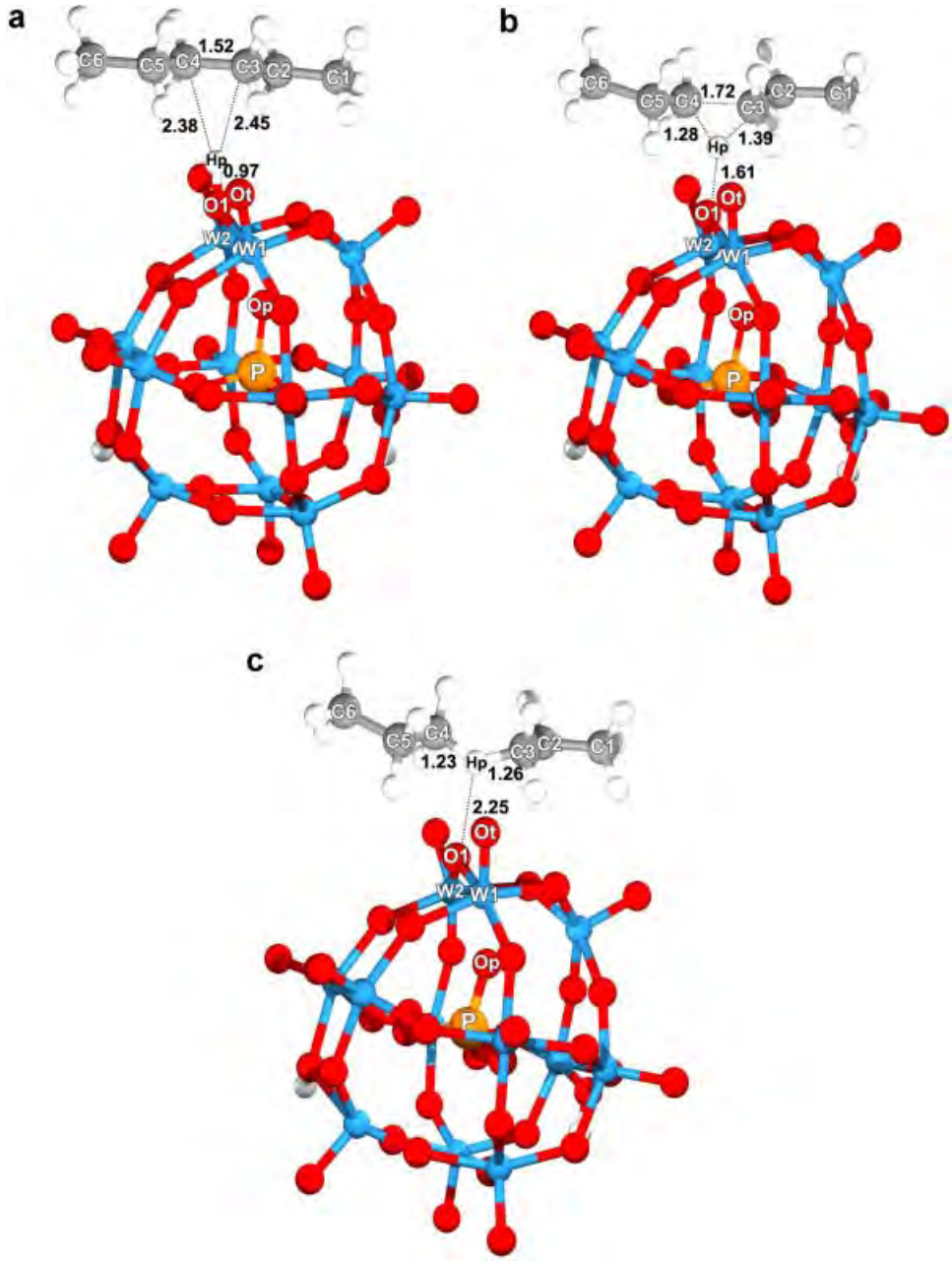

Figure 4. Optimised structures of (a) *n*-hexane adsorption (b) transition state and (c) 3-C-hexonium intermediate involved in the protolytic cracking of *n*-hexane over HPW. [Color figure can be seen in the online version of this article, available at http://onlinelibrary.wiley.com/journal/10.1002/(ISSN)1939-019X]

well. It is noted that the distances between the adsorbed *n*-hexane and the acidic proton in HPW are significantly shorter than in H-ZSM-5 but the adsorption energy in HPW is much lower than in H-ZSM-5. This result indicates that the major contribution to the adsorption energy is not the weak interaction between the C–C bond and the acid site but the van der Waals interactions with the zeolite walls which is obviously lacking in the case of HPW.

STRUCTURES AND ENERGETICS OF PROTOLYTIC CRACKING OF *n*-HEXANE

The adsorbed *n*-hexane molecule can be cracked into products by a two-step protolytic cracking, consisting of the protonation of *n*-hexane to produce the unstable 3-C-hexonium intermediate and, subsequently, is readily decomposed to produce propane and propene products. In this work, we concentrate on the protonation step because this is the rate-determining step of the cracking reaction (Narbeshuber et al., 1995; Xu et al., 2006; Boronat and Corma, 2008; and Maihom et al., 2010).

Selected geometrical parameters for this reaction step are shown in Tables 1 and 2 and optimised structures are shown in Figures 3 and 4 for reactions in H-ZSM-5 and HPW, respectively (see the Supporting Information for Schemes of this reaction step). The energy profiles are shown in Figure 5. At the transition state, the H1 proton is protonated to the C3–C4 bond of adsorbed *n*-hexane. In the H-ZSM-5, the Brønsted proton (H1) is moving toward the C3–C4 bond and causes the bond distance to increase to 1.70 Å. Similarly, the transition state structure was also found in HPW (Table 2). The existence of a true transition state has been confirmed by frequency calculations resulting in one

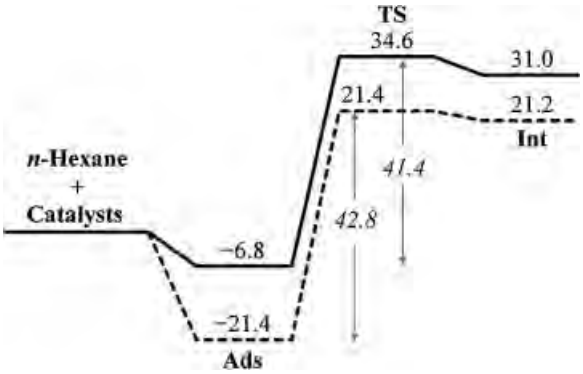

Figure 5. Energy profile for *n*-hexane protolytic cracking catalysed by H-ZSM-5 zeolite (dashed line) and HPW heteropoly acid (solid line) comparing to the isolated systems.

imaginary frequency related to the movement of the acidic proton of zeolite (H1) to the *n*-hexane C3–C4 bond and the breaking of the C3–C4 bond. The activation energies for *n*-hexane protonation in H-ZSM-5 and HPW systems are 42.8 and 41.4 kcal/mol, respectively.

The transition state is followed by the formation of 3-C-hexonium intermediates (see Figures 3c and 4c) which are adsorbed on the surface of catalysts by the attractive columbic interaction with the anionic zeolite or HPW cluster. The distance between the hexonium cation and the anionic cluster was measured between the hydrogen atom (H1) of the 3-C-hexonium and the oxygen atom (O1) of the anionic cluster to be 1.97 and 2.25 Å for H-ZSM-5 and HPW, respectively. The structures of the adsorbed 3-C-hexonium intermediate are considered to be a C3–H1–C4 bridge and formed quite symmetrically. In H-ZSM-5, the C3–H1 and C4–H1 bond distances are nearly equal (Table 1). The C3–C4 bond distance is 1.86 Å and the C3–H1–C4 angle is 95.2°. Slight structure differences are found in HPW. The C3–H1–C4 bridge angle is wider at 130.0° and, as a result, the C3–C4 bond distance is longer at 2.26 Å. The formation of the adsorbed 3-C-hexonium intermediate is highly endothermic with reaction energies of 21.2 and 31.0 kcal/mol, in H-ZSM-5 and HPW, respectively. The adsorbed 3-C-hexonium intermediate is slightly more stable than its transition state by only 0.3 and 3 kcal/mol for H-ZSM-5 and HPW, respectively. Boronat and Corma (2008) have also reported that the 3-C-hexonium is an intermediate for protolytic cracking of alkane on acidic zeolites. In our previous calculations (Maihom et al., 2010), we reported that the decomposition of the 3-C-hexonium intermediate required an activation energy of 9.9 kcal/mol, which is significantly less than the activation for the preceding protonation step.

Figure 5 shows the energy profiles for H-ZSM-5 zeolite and HPW acid superimposed on each other. Although the HPW is a stronger acid than H-ZSM-5, the relative energies of the adsorbed *n*-hexane, transition state and reactive 3-C-hexonium intermediate in the HPW are significantly less stable than in the H-ZSM-5. These results are due to the confinement effect arising mostly from the attractive van der Waals interactions between adsorbed species and the zeolite walls. As a result, the apparent activation energy, considered being the energy difference between the isolate and the transition state, in H-ZSM-5 is lower than in the HPW. The intrinsic activation energy for the *n*-hexane protonation in H-ZSM-5 is, however, higher than in HPW (42.8 and 41.4 kcal/mol for H-ZSM-5 and HPW, respectively) reflecting the higher acidity of HPW. Therefore, the stability of the adsorption is the key factor to determine the height of the activation barrier and the catalytic activity for protolytic cracking.

The results have shown that HPW is more active for the protonation and activation of *n*-hexane than H-ZSM-5. The disadvantage of heteropoly acids is the lack of confinement effect which is uniquely found in zeolite pores that stabilise the transition state and reactivate the intermediate and, hence, facilitate the reaction to proceed through lower apparent activation energy. This weakness can be overcome by embedding heteropoly acids into porous materials. There are a number of publications reporting about the hybrid materials of heteropoly compounds (in either protonated or anionic form) and metal-organic frameworks (MOFs) (Dang et al., 2010; Juan-Alcaniz et al., 2010; Ma et al., 2010). Utilising the molecular design approach, one can vary the type of heteropoly acid and the composition combination of the MOFs to achieve materials with a desired catalytic property of the acid and the tailored environment (i.e., size and shape of the pore and functionality) of the framework.

CONCLUSION

The protolytic cracking of *n*-hexane over H-ZSM-5 and α-Keggin HPW has been investigated by utilising the quantum cluster calculations at the M06-L/6-31G(d,p) level of theory. The key transition state of the protolytic cracking, in which the direct protonation of a C–C single bond occurs, was located and analysed. Both catalysts can activate the saturated hydrocarbon molecule but the different activities of these two catalysts are mainly due to the confinement effect which is uniquely present in the zeolite pores. The confinement effect stabilises the adsorbed reactivity species and, thus, helps to reduce the apparent activation barrier. The present study shows the advantages and disadvantages of both catalysts. While the zeolite provides both confinement effect and shape selectivity, it lacks variety, thus, resulting in it being difficult to modify to suit any new applications. Alternatively, heteropoly acid has no confinement effect and such specific selectivity, but it is tunable by varying the elemental composition and the geometry. The combination of heteropoly acid into hybrid materials is not only better for stability and dispersion, but also promising for breakthrough applications.

ACKNOWLEDGEMENTS

This work was supported in part by grants from the National Science and Technology Development Agency (2009 NSTDA Chair Professor funded by the Crown Property Bureau under the management of the National Science and Technology Development Agency and NANOTEC Center of Excellence funded by the National Nanotechnology Center), the Thai National Grid Center (TNGC) under the Software Industry Promotion Agency (SIPA), the Thailand Research Fund (TRF) (to J.L.), the Kasetsart University Research and Development Institute (KURDI), Graduate School Kasetsart University and the Commission of Higher Education, Ministry of Education ('the National Research University Project of Thailand (NRU)' and 'Postgraduate Education and Research Programs in Petroleum and Petrochemicals, and Advanced Materials'). The program 'Strategic Scholarships for Frontier Research Network for the Joint Ph.D. Program Thai Doctoral degree (CHE-PhD-SW)' from the Office of the Higher Education Commission, Thailand (to S.C. and T.M.) is also acknowledged. The authors are grateful to Donald G. Truhlar and Yan Zhao for providing them with the code for the M06-L functional.

REFERENCES

Betz, D., P. Altmann, M. Cokoja, W. A. Herrmann and F. E. Kuhn, "Recent Advances in Oxidation Catalysis Using Ionic Liquids as Solvents," Coord. Chem. Rev. **255**, 1518–1540 (2011).

Bhorodwaj, S. K. and D. K. Dutta, "Activated Clay Supported Heteropoly Acid Catalysts for Esterification of Acetic Acid with Butanol," Appl. Clay Sci. **53**, 347–352 (2011).

Boekfa, B., S. Choomwattana, P. Khongpracha and J. Limtrakul, "Effects of the Zeolite Framework on the Adsorptions and Hydrogen-Exchange Reactions of Unsaturated Aliphatic, Aromatic, and Heterocyclic Compounds in ZSM-5 Zeolite: A Combination of Perturbation Theory (MP2) and a Newly Developed Density Functional Theory (M06-2X) in ONIOM Scheme," Langmuir **25**(22), 12990–12999 (2009).

Boronat, M. and A. Corma, "Are Carbenium and Carbonium Ions Reaction Intermediates in Zeolite-Catalysed Reactions?" Appl. Catal. A: Gen. **336**, 2–10 (2008).

Bourdillon, G., C. Gueguen and M. Guisnet, "Characterisation of Acid Catalysts by Means of Model Reactions: I. Acid Strength Necessary for the Catalysis of Various Hydrocarbon Reactions," Appl. Catal. **61**, 123–139 (1990).

Corma, A. and A. V. Orchilles, "Current Views on the Mechanism of Catalytic Cracking," Micropor. Mesopor. Mater. **35–36**, 21–30 (2000).

Dang, D.-B., Y. Bai, C. He, J. Wang, C.-Y. Duan and J.-Y. Niu, "Structural and Catalytic Performance of a Polyoxometalate-Based Metal−Organic Framework Having a Lanthanide Nanocage as a Secondary Building Block," Inorg. Chem. **49**, 1280–1282 (2010).

Dolg, M., H. Stoll, H. Preuss and R. M. Pitzer, "Relativistic and Correlation Effects for Element 105 (Hahnium, Ha): A Comparative Study of M and MO (M=Nb, Ta, Ha) Using Energy-Adjusted Ab Initio Pseudopotentials," J. Phys. Chem. **97**, 5852–5859 (1993).

Eder, F., M. Stockenhuber and J. A. Lercher, "Brønsted Acid Site and Pore Controlled Siting of Alkane Sorption in Acidic Molecular Sieves," J. Phys. Chem. B **101**, 5414–5419 (1997).

Fiuza, R. A., I. V. Santos, R. P. Fiuza, N. M. José and J. S. Boaventura, "Characterisation of Electrolyte Polyester Membranes for Application in PEM Fuel Cells," Macromol. Symp. **299-300**, 234–240 (2011).

Frisch, M. J., G. W. Trucks, H. B. Schlegel, G. E. Scuseria, M. A. Robb, J. R. Cheeseman, J. A. Montgomery, Jr., T. Vreven, K. N. Kudin, J. C. Burant, J. M. Millam, S. S. Iyengar, J. Tomasi, V. Barone, B. Mennucci, M. Cossi, G. Scalmani, N. Rega, G. A. Petersson, H. Nakatsuji, M. Hada, M. Ehara, K. Toyota, R. Fukuda, J. Hasegawa, M. Ishida, T. Nakajima, Y. Honda, O. Kitao, H. Nakai, M. Klene, X. Li, J. E. Knox, H. P. Hratchian, J. B. Cross, V. Bakken, C. Adamo, J. Jaramillo, R. Gomperts, R. E. Stratmann, O. Yazyev, A. J. Austin, R. Cammi, C. Pomelli, J. W. Ochterski, P. Y. Ayala, K. Morokuma, G. A. Voth, P. Salvador, J. J. Dannenberg, V. G. Zakrzewski, S. Dapprich, A. D. Daniels, M. C. Strain, O. Farkas, D. K. Malick, A. D. Rabuck, K. Raghavachari, J. B. Foresman, J. V. Ortiz, Q. Cui, A. G. Baboul, S. Clifford, J. Cioslowski, B. B. Stefanov, G. Liu, A. Liashenko, P. Piskorz, I. Komaromi, R. L. Martin, D. J. Fox, T. Keith, M. A. Al-Laham, C. Y. Peng, A. Nanayakkara, M. Challacombe, P. M. W. Gill, B. Johnson, W. Chen, M. W. Wong, C. Gonzalez and J. A. Pople, "Gaussian 03, Revision C.02," Gaussian, Inc., Wallingford, CT (2004).

Haag, W. O. and R. M. Dessau, "Duality of Mechanism for Acid-Catalysed Paraffin Cracking," in "Proc. 8th Intl. Cong. Catal.," Dechema, Frankfurt-am-Main, Germany, ON (1984), pp. 305–316.

Jalil, A., M. Faiz, N. Tabet, N. M. Hamdan and Z. Hussain, "A Study of the Stability of Tungstophosphoric Acid, $H_3PW_{12}O_{40}$, Using Synchrotron XPS, XANES, Hexane Cracking, XRD, and IR Spectroscopy," J. Catal. **217**, 292–297 (2003).

Juan-Alcaniz, J., E. V. Ramos-Fernandez, U. Lafont, J. Gascon and F. Kapteijn, "Building MOF Bottles Around Phosphotungstic Acid Ships: One-Pot Synthesis of Bi-Functional Polyoxometalate-MIL-101 Catalysts," J. Catal. **269**, 229–241 (2010).

Kotrel, S., H. Knözinger and B. C. Gates, "The Haag–Dessau Mechanism of Protolytic Cracking of Alkanes," Micropor. Mesopor. Mater. **35−36**, 11–20 (2000).

Kotrel, S., M. P. Rosynek and J. H. Lunsford, "Intrinsic Catalytic Cracking Activity of Hexane over H−ZSM-5, H−β and H−Y Zeolites," J. Phys. Chem. B **103**, 818–824 (1999).

Kumsapaya, C., K. Bobuatong, P. Khongpracha, Y. Tantirungrotechai and J. Limtrakul, "Mechanistic Investigation on 1,5- to 2,6-Dimethylnaphthalene Isomerisation Catalysed by Acidic β Zeolite: ONIOM Study with an M06-L Functional," J. Phys. Chem. C **113**, 16128–16137 (2009).

Lercher, J. A., A. Jentys and A. Brait, "Catalytic Test Reactions for Probing the Acidity and Basicity of Zeolites," Mol. Sieves Sci. Technol. **6**, 153–212 (2008).

Ma, F.-J., S.-X. Liu, D.-D. Liang, G.-J. Ren, C.-D. Zhang, F. Wei and Z.-M. Su, "Hydrogen Adsorption in Polyoxometalate Hybrid Compounds Based on Porous Metal−Organic Frameworks," Eur. J. Inorg. Chem. **24**, 3756–3761 (2010).

Maihom, T., B. Boekfa, J. Sirijaraensre, T. Nanok, M. Probst and J. Limtrakul, "Reaction Mechanisms of the Methylation of Ethene with Methanol and Dimethyl Ether over H-ZSM-5: An ONIOM Study," J. Phys. Chem. C **113**, 6654–6662 (2009).

Maihom, T., P. Pantu, C. Tachakritikul, M. Probst and J. Limtrakul, "Effect of the Zeolite Nanocavity on the Reaction Mechanism of *n*-Hexane Cracking: A Density Functional Theory Study," J. Phys. Chem. C **114**, 7850–7856 (2010).

Mizuno, N. and M. Misono, "Heterogeneous Catalysis," Chem. Rev. **98**, 199–218 (1998).

Mulliken, R. S., "Electronic Population Analysis on LCAO-MO Molecular Wave Functions. I," J. Chem. Phys **23**, 1833–1840 (1955).

Narbeshuber, T. F., H. Vinek and J. A. Lercher, "Monomolecular Conversion of Light Alkanes over H-ZSM-5," J. Catal. **157**, 388–395 (1995).

Soares-Santos, P. C., R. L. Cunha-Silva, F. L. Sousa, L. Mafra, J. Rocha, A. M. V. Cavaleiro, T. Trindade, F. A. A. Paz, J. Klinowski and H. I. S. Nogueira, "Two Novel Supramolecular Organic–Inorganic Adducts Containing dibenzo-30-crown-10 and $H_3PM_{12}O_{40}$ (M=W or Mo)," J. Mol. Struct. **888**, 99–106 (2008).

Ueda, T., T. Tatsumi, T. Eguchi and N. Nakamura, "Structure and Properties of Acidic Protons in Anhydrous Dodecatungstophosphoric Acid, $H_3PW_{12}O_{40}$, As Studied by Solid-State ^1H, ^2H NMR, and $^1H-^{31}P$ Sedor NMR," J. Phys. Chem. B **105**, 5391–5396 (2001).

van Koningsveld, H., H. van Bekkum and J. C. Jansen, "On the Location and Disorder of the Tetrapropylammonium (TPA) Ion in Zeolite ZSM-5 with Improved Framework Accuracy," Acta. Crystallogr. B **43**, 127–132 (1987).

Wannakao, S., B. Boekfa, P. Khongpracha, M. Probst and J. Limtrakul, "Oxidative Dehydrogenation of Propane over a VO_2-Exchanged MCM-22 Zeolite: A DFT Study," Chem. Phys. Chem. **11**, 3432–3438 (2010).

Wesolowski, T. A., O. Parisel, Y. Ellinger and J. Weber, "A Comparative Study of Weak van der Waals Complexes using Density Functional Theory: The Importance of an Accurate Exchange-Correlation Density at High Density Gradients," J. Phys. Chem. A **101**(42), 7818–7825 (1997).

Yang, J., M. J. Janik, D. Ma, A. Zheng, M. Zhang, M. Neurock, R. J. Davis, C. Ye and F. Deng, "Location, Acid Strength, and Mobility of the Acidic Protons in Keggin 12-$H_3PW_{12}O_{40}$: A Combined Solid-State NMR Spectroscopy and DFT Quantum Chemical Calculation Study," J. Am. Chem. Soc. **127**, 18274–18280 (2005).

Xu, B., C. Sievers, S. B. Hong, R. Prins and J. A. van Bokhoven, "Catalytic Activity of Brønsted Acid Sites in Zeolites: Intrinsic Activity, Rate-Limiting Step, and Influence of the Local Structure of the Acid Sites," J. Catal. **244**, 163–168 (2006).

Zhao, Y. and D. G. Truhlar, "Density Functionals with Broad Applicability in Chemistry," Acc. Chem. Res. **41**, 157–167 (2008a).

Zhao, Y. and D. G. Truhlar, "Benchmark Data for Interactions in Zeolite Model Complexes and Their Use for Assessment and Validation of Electronic Structure Methods," J. Phys. Chem. C **112**, 6860–6868 (2008b).

Manuscript received August 11, 2011; revised manuscript received October 6, 2011; accepted for publication October 19, 2011.

Chemical Physics Letters 556 (2013) 217–224

Contents lists available at SciVerse ScienceDirect

Chemical Physics Letters

journal homepage: www.elsevier.com/locate/cplett

Density functional study of the activity of gold-supported ZSM-5 zeolites for nitrous oxide decomposition

Thana Maihom [a,b,c], Sippakorn Wannakao [a,b,c], Bundet Boekfa [d], Jumras Limtrakul [a,b,c,*]

[a] Laboratory for Computational and Applied Chemistry, Department of Chemistry, Faculty of Science and Center of Nanotechnology, Kasetsart University Research and Development Institute, Kasetsart University, Bangkok 10900, Thailand
[b] NANOTEC Center for the Design of Nanoscale Materials for Green Nanotechnology, Kasetsart University, Bangkok 10900, Thailand
[c] Center for Advanced Studies in Nanotechnology and its Applications in Chemical, Food, and Agricultural Industries, Kasetsart University, Bangkok 10900, Thailand
[d] Kasetsart University Kamphaeng Saen Campus, Chemistry Department, Faculty of Liberal Arts and Science, Nakhon Pathom 73140, Thailand

ARTICLE INFO

Article history:
Received 31 July 2012
In final form 20 November 2012
Available online 29 November 2012

ABSTRACT

Decomposition of the toxic gas N_2O over gold supported ZSM-5 zeolite has been investigated by using the M06-L functional. The activation energy for the Au/H-ZSM-5 is 15.2 kcal/mol lower than on the Au/ZSM-5, which is 26.7 kcal/mol. The results suggest that the Au/H-ZSM-5 zeolite is more active than Au/ZSM-5 zeolite. Our findings also indicate that the charge state of Au plays an important role for controlling N_2O decomposition and the supported zeolite facilitates charge transfer between metal and N_2O which is a key process for the reaction.

1. Introduction

Effective reduction of toxic gases into environmentally friendly products is one of the challenging strategies to develop clean, 'green' and sustainable technology for industry at an affordable cost. Nitrous oxide (N_2O), from industrial processes and motor vehicle exhausts, is well known as an environmental pollutant because it is a strong greenhouse effect gas and also plays an important role in the destruction of the stratospheric ozone layer. With increasing concern over environmental problems, the reduction of N_2O has become not only an extremely important priority but also attractive in the field of environmental research. The catalytic decomposition is one of the most promising ways to remove the N_2O. It is a simple method to convert N_2O into nontoxic products of N_2 and O_2. Among a variety of tested catalysts, metals such as Cu, Fe and Co containing zeolite structures included MFI, MOR, FER, and Y showed promising activity features for N_2O decomposition [1–11].

Gold (Au) containing zeolite is one of the catalysts that have been verified for catalyzing the N_2O decomposition. Previously, experimental studies found that the Au/ZSM-5 can catalyze the decomposition of N_2O to N_2 even in the presence of O_2 [12]. Additionally, Au-zeolites also showed high activity for various reactions such as direct NO decomposition, CO oxidation and the water gas shift (WGS) reaction at low temperature [13–16]. The different oxidation states of Au species have been proposed and investigated as catalytic active sites in literature. Ichikawa and coworker [16,17] studied Au/NaY, Au/Na-MOR, and Au/Na–ZSM-5 zeolites by using CO adsorption and have concluded that Au^+ was the dominant active site for the decomposition of NO with CO and the water gas shift. Gao et al. [12] analyzed the Au/ZSM-5 zeolite by using FTIR, XRD, HRAEM and CO-TPR. They found that the Au^+ and Au^{3+} were the dominant gold species; however, the Au^+ was irreversibly transformed to Au^0 at 500 °C. In addition, Fierro-Gonzalez and Gates [14] have synthesized and characterized monomeric Au^+ and Au^{3+} complexes in NaY zeolite without zero valence Au clusters and also tested the activity for the NO reduction with CO. In that report, they found the Au^{3+} complex was more active than the Au^+ complex. Recently, Deka et al. [18] theoretically studied the carbon monoxide (CO) interaction with Au^0, Au^+ and Au^{3+} species supported on FAU zeolite by using density functional theory. They found that the interaction between Au species and CO is strongest in the case of Au^+ and weakest in the Au^0 case. These findings emphasize that the oxidation state of Au in zeolites seriously influences catalytic activity. It is, therefore, of interest to investigate the reaction of N_2O decomposition on different oxidation states of Au supported in zeolites.

To understand the catalytic and adsorption process in zeolite, van der Waals interactions play an important role on the structures and energetics in the reaction coordinates. Previously, we have successfully used the ONIOM method [19] for studying several reactions in zeolites [20–24]. However, the performance of this method is dependent on the right partition of the active region and environment, and the right combination of high and low level methods. Zhao and Truhlar have recently developed the new

* Corresponding author at: Laboratory for Computational and Applied Chemistry, Department of Chemistry, Faculty of Science and Center of Nanotechnology, Kasetsart University Research and Development Institute, Kasetsart University, Bangkok 10900, Thailand.
E-mail address: jumras.l@ku.ac.th (J. Limtrakul).

0009-2614/$ - see front matter © 2012 Elsevier B.V. All rights reserved.
http://dx.doi.org/10.1016/j.cplett.2012.11.058

meta-hybrid density functional M06 series [25], in which van der Waals interactions are taken into account in the parameterization. This method has been successfully used for investigating the adsorption and reaction mechanisms over zeolites [26–33] and also over other materials such as metal–organic frameworks material [34–36].

To the best of our knowledge, the decomposition of N_2O on different species of Au in zeolite has not been theoretically studied and compared previously. In this Letter, we report the theoretical investigation on the activity of the Au cation and Au atom supported ZSM-5 zeolite for the initial N–O bond breaking process of N_2O decomposition by using the M06-L method. Although, the comprehensive decomposition of N_2O is quite complicated [7], we preliminarily illustrate the molecular charge transfer during the N–O bond breaking state. The reaction mechanism and relative energies and structures of intermediates and transition states are discussed.

2. Models and method

The ZSM-5 zeolites were represented by the 12T cluster model that was generated from its lattice structures [37]. The 12T cluster model of ZSM-5, illustrated in Figures 1 and 2, covers the intersection at the interconnection between the straight channel and the zigzag channel. One aluminium atom was substituted for a silicon atom at the T12 site to generate the Brønsted acid site. In the model of Au^+ supported ZSM-5 (Au/ZSM-5), the Brønsted site of zeolite

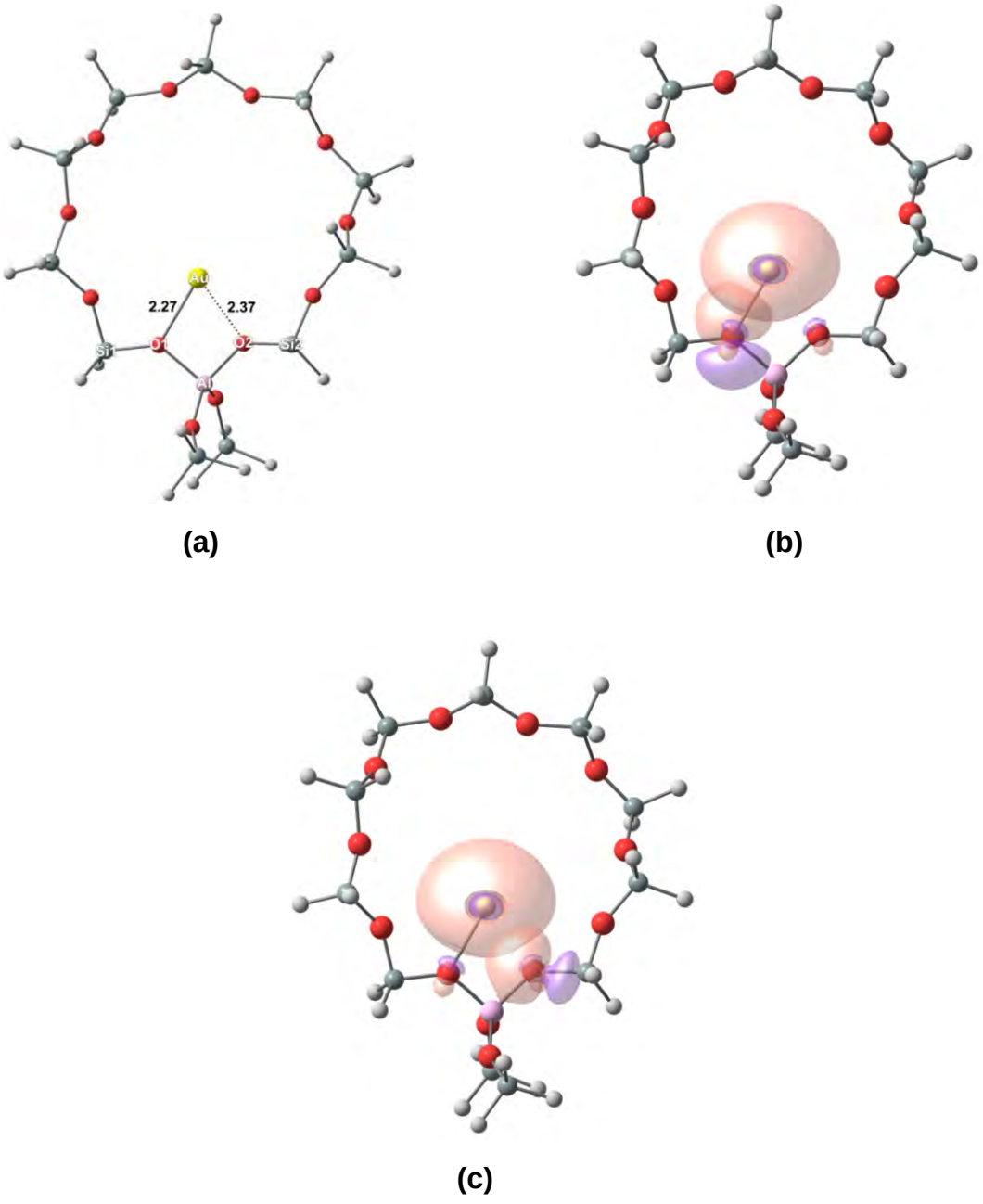

Figure 1. Optimized geometric parameters of the Au^+ supported ZSM-5 models (a) and the orbital interaction between the 6s orbital of Au^+ and the 2s, 2p orbitals of framework oxygens O1 (b) and O2 (c).

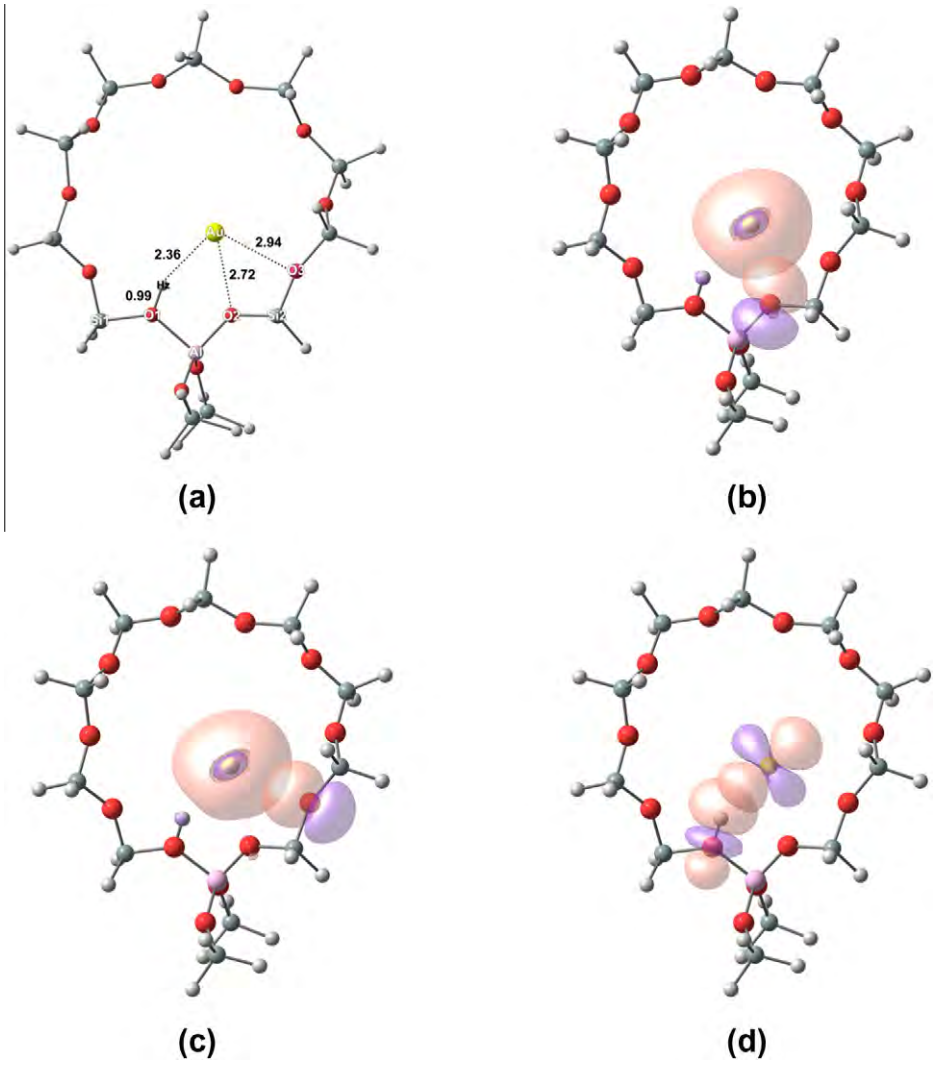

Figure 2. Optimized geometric parameters of the Au^0 supported ZSM-5 models (a) and the orbital interaction between the 6s orbital of Au^0 and the 2s, 2p orbitals of framework oxygens O2 (b) and O3 (c) and between the 5d orbital of Au^0 and the Brønsted proton (d).

is exchanged by the Au cation (Figure 1a). For the Au^0 supported ZSM-5 (Au/H-ZSM-5), an Au atom was placed next to the Brønsted site of zeolite (Figure 2a).

The M06-L density functional was used in all calculations. The basis set of 6-31G(d,p) was employed for the N_2O molecule and all zeolitic atoms, while the Au atom was described by the effective core potentials (ECP) of Dolg et al. [38]. During geometry optimizations, only the 5T active region and the adsorbates were allowed to relax while the rest of the structure is kept fixed at the crystallographic coordinates. Partial charges and population analysis were determined by the natural atomic orbital (NAO) and natural bond orbital (NBO) methods [39]. Frequency calculations were performed at the same level of theory to ensure that each transition structure has only one imaginary frequency which corresponds to the expected motion of atoms for each transition structure. All calculations were performed with the Gaussian 09 code [40].

3. Results and discussion

3.1. Structures of Au/ZSM-5 and Au/H-ZSM-5

We considered the high spin state and low spin state of the Au/ZSM-5 and Au/H-ZSM-5. The energy differences between these two states are 37.7 and 110.2 kcal/mol with a preference for the low spin state on both systems. The lowest spin state of the Au/ZSM-5 and Au/H-ZSM-5 is a singlet and doublet state, respectively (see Supporting Information). Optimized structures of Au/ZSM-5 and Au/H-ZSM-5 zeolites are illustrated in Figure 1a and 2a, respectively. Partial charges for these systems are tabulated in Table 1. In the Au/ZSM-5 zeolite, the Au cation (Au^+) is coordinated with the two oxygen bridging atoms of zeolite having the bond

Table 1
Partial charge on the reaction coordinated of N_2O decomposition on Au/ZSM-5 and Au/H-ZSM-5 zeolites.

Reaction coordinates	NPA charge (e)				
	Au	O1	N1	N2	N_2O
Au/ZSM-5					
Isolated	0.75	−0.30	0.39	−0.09	0.00
Ads_1	0.64	−0.39	0.45	0.03	0.09
TS_1	0.83	−0.48	0.16	0.10	−0.22
Prod_1	0.85	−0.31	−0.01	0.04	−0.28
Au/H-ZSM-5					
Isolated	−0.01	−0.30	0.39	−0.09	0.00
Ads_2	−0.02	−0.32	0.44	−0.09	0.02
TS_2	0.36	−0.53	0.12	−0.04	−0.45
Prod_2	0.41	−0.49	0.002	0.02	−0.46

distances of 2.27 and 2.37 Å for Au···O1 and Au···O2, respectively. The Al···Au distance is predicted to be 3.10 Å. The interaction of Au with ZSM-5 zeolite is also analyzed by using NBO analysis as shown in Figure 1b and c. We found the orbital interaction between the sp-orbital of zeolite framework oxygens (O1 and O2) and the s-orbital of the Au cation. The transfer of electrons from the framework oxygens to the Au cation is also observed. This leads to a decrease of the electron density in the 2s, 2p orbital of oxygens and an increase of the electron density in the 6s orbital of Au. Therefore, the partial atomic charge on the Au is reduced from +1 to +0.75*e*. These results indicate that the framework of ZSM-5 zeolite behaves as an electron donor. The complexation energy between Au^+ and the zeolite framework is predicted to be −133.4 kcal/mol.

As for the Au/H-ZSM-5 zeolite, the Au atom (Au^0) interacts with a Brønsted proton (Hz) and the oxygen bridging (O2) of the zeolite. The acidic bond (O1–Hz) of zeolite is calculated to be 0.99 Å. The calculated distances of Au···Hz, Au···O2 and Au···O3 are 2.36, 2.72 and 2.94 Å, respectively. The NBO analysis shows the orbital interaction between the d-orbital of supported Au and the Brønsted proton of zeolite and between the s-orbital of Au and the framework oxygens (Figure 2b–d). We also found the electron transfer from the 2s, 2p orbital of framework oxygens to the 6s orbital of Au and from the 5d orbital of Au to the Brønsted proton of zeolite. Because of a higher electron transfer for the former modes, the partial atomic charge on the Au atom is negative (−0.01*e*). The interaction energy between the Au atom and H-ZSM-5 is found to be endothermic of 6.1 kcal/mol, which is in the same trend as the theoretical observations for the interaction Au to FAU zeolite [18].

3.2. Adsorption of N_2O on Au/ZSM-5 and Au/H-ZSM-5 zeolites

The spin state crossing may play a role in the catalytic reactions. For a comprehensive inspection of the catalytic process of Au-based zeolite, we analyzed the reaction pathways along with two

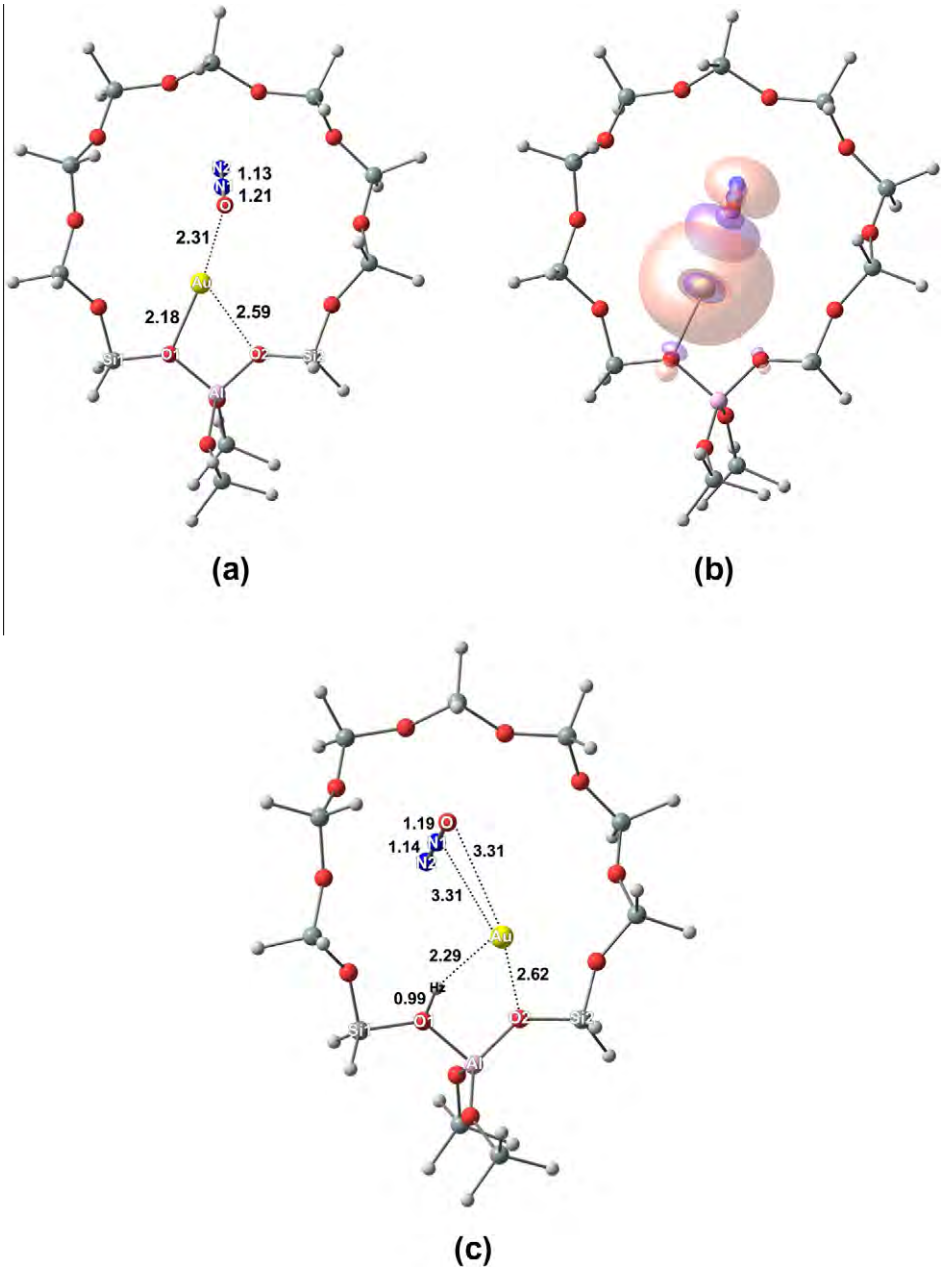

Figure 3. Optimized structures of the N_2O adsorption over Au/ZSM-5 (a, b) and Au/H-ZSM-5 (c) zeolites.

possible states of both systems which are singlet–triplet spin states for Au/ZSM-5 and doublet-quartet spin states for Au/H-ZSM-5, respectively (Figures S1 and S2). From the results of two spin states, we can clearly demonstrate that the catalytic process of N_2O decomposition over the natural and cationic forms of gold incorporated ZSM-5 framework proceed entirely in the low spin state of the system. Only the occurrence of intersystem crossing is found after the decomposition of N_2O on the Au/ZSM-5 catalysts, leading to the lowering endothermicity of reaction. Therefore, the following discussion of all complexes in reaction coordinates is obtained from the low spin state excepting the N_2O decomposed product that is acquired from the high spin state.

Figure 3 depicts the adsorption structure of N_2O interacted with the Au^+ of the Au/ZSM-5 and Au^0 of the Au/H-ZSM-5. Selected geometrical structures for the adsorption complexes are tabulated in Tables 2 and 3. In Au/ZSM-5, it can be seen that the N_2O molecule interacts with the Au^+ by its O lone pair electron with the O···Au distance of 2.31 Å (cf. Figure 3a). This interaction leads to the change of the structure of Au/ZSM-5. The distance of Au···O1 is contracted from 2.27 to 2.18 Å while the distance of Au···O2 is elongated by 0.22 Å. The NBO shows orbital interaction between the 6s orbital of the Au cation and the 2p orbital of the nitrous oxide O atom (Figure 3b). The electrons are transferred from N_2O to Au^+ in Au/ZSM-5 zeolite leading to the reduction of the positive charge on Au from +0.75*e* to +0.64*e* while the charge on the N_2O molecule becomes positive (Table 1). However, the partial charge of O1 compared to the isolated molecule is more negative (from −0.30*e* to −0.39*e*) by reason of the electrons induced from N1 and N2 to O1. The transfer of these electrons results in the elongation of the O–N1 bond of N_2O from 1.19 to 1.26 Å and contraction of the N1–N2 bond by 0.01 Å. These correspond to the red shifted stretching frequencies of adsorbed N_2O with respect to the isolated molecules of 64 and 15 cm^{-1} for υ_{ON} and υ_{NN}, respectively, which is a similar result to the previous calculation [41]. The adsorption energy for this complex is −15.9 kcal/mol.

For the case of Au/H-ZSM-5, the N_2O is weakly adsorbed on zeolite through interactions between O and N1 of the N_2O and the Au active site. The internuclear distances of Au···O and Au···N1 are comparable (Figure 3c). The adsorption interactions are weak so that we cannot observe the dominant orbital interaction between the Au atom and the adsorbed N_2O molecule. The structures of the Au/H-ZSM-5 zeolite differ slightly from the corresponding isolated structures while the adsorbed N_2O are not significantly altered (Table 3). The υ_{ON} and υ_{NN} in the N_2O adsorbed on Au/H-ZSM-5 are 1365 and 2399 cm^{-1}, respectively, which are close to their isolated stretching frequencies (υ_{ON} = 1371 cm^{-1} and υ_{NN} = 2405 cm^{-1}). The interatomic distance of Au···Hz and Au···O2 is reduced by 0.07 and 0.10 Å, respectively. The electron transfers from N_2O to the Au active site in Au/H-ZSM-5 are detected in a similar way to those of Au/ZSM-5 (Table 1). The negative charge of the Au atom is increased from −0.01*e* to −0.02*e* while the charge summation on N_2O is more positive (0.02*e*). The calculated adsorption energy is −5.5 kcal/mol, which is almost three times lower than that derived from the Au/ZSM-5 complex (−15.9 kcal/mol). The reason is that the electron donation from N_2O to Au in Au/H-ZSM-5 is lower than that in Au/ZSM-5.

Table 2
Optimized geometrical parameters of the species involved in the decomposition of N_2O on Au/ZSM-5.

Parameter	Isolated cluster	N_2O adsorption (Ads_1)	Transition state (TS_1)	Product (Prod_1)
Distances (Å)				
Au–Al	3.10	3.15	3.01	3.13
Au–O1	2.27	2.18	2.21	2.20
Au–O2	2.37	2.59	2.33	2.33
Au–O	–	2.31	1.96	1.92
Au–N1	–	3.04	3.19	3.13
N1–O	1.19	1.26	1.71	3.10
N1–N2	1.14	1.13	1.12	1.11
Angles (°)				
Al–Si1–O1	131.0	130.1	129.7	129.9
Al–Si2–O2	136.3	136.2	134.8	134.9
Au–O–N1	–	116.1	120.7	73.0
O–N1–N2	179.8	178.2	144.3	104.7

Table 3
Optimized geometrical parameters of the species involved in the decomposition of N_2O on Au/H-ZSM-5.

Parameter	Isolated cluster	N_2O adsorption (Ads_2)	Transition state (TS_2)	Product (Prod_2)
Distances (Å)				
Au–Al	3.85	3.80	3.40	3.52
Au–Hz	2.36	2.29	2.26	2.15
Au–O2	2.72	2.62	2.28	2.29
Au–O3	2.94	3.12	2.77	2.85
Au–O	–	3.31	2.04	1.95
Au–N1	–	3.31	2.97	3.39
O1–Hz	0.99	0.99	0.99	0.99
N1–O	1.19	1.19	1.52	3.03
N1–N2	1.14	1.14	1.16	1.11
Angles (°)				
Al–Si1–O1	130.2	131.3	130.8	133.4
Al–Si2–O2	134.6	134.9	131.4	128.8
Al–O1–Hz	112.1	113.0	112.5	114.0
Au–O–N1	–	80.0	112.0	82.8
O–N1–N2	179.8	179.5	121.3	132.3

3.3. N_2O Decomposition on Au/ZSM-5 and Au/H-ZSM-5 zeolites

After the N_2O molecule adsorbed on Au/ZSM-5 (Ads_1) and Au/H-ZSM-5 (Ads_2), it can be decomposed in a single step without intermediates via O–N bond breaking (Figure 4). Selected geometrical parameters and partial charge for the reaction in Au/ZSM-5 and Au/H-ZSM-5 are documented in Tables 2 and 3, respectively. At the transition states, the N–O bond of the adsorbed N_2O is cleaved and subsequently oxygen of the N_2O is transferred to the Au active site. In the Au/ZSM-5 zeolite (TS_1), the N–O bond is stretched while the O···Au distance is contracted, leading to the formation of a new bond (Table 2). The electrons are transferred from the Au active site in Au/ZSM-5 to the N_2O molecule. The positive partial charge of Au is increased from 0.64*e* to 0.83*e* and the charge summation on the N_2O molecule is more negative (Table 1). This trend is in agreement with the previous calculation of N_2O decomposition of Fe-BEA zeolite [42] and Fe embedding on graphene sheet [43]. The transition state is confirmed by the frequency calculation with one imaginary frequency at −422.6i cm^{-1}. The activation energy is calculated to be 41.9 kcal/mol. The transition state then proceeds by the deposition of an oxygen species on the Au center and the formation of a nitrogen molecule (Prod_1). In this product complex, the singlet spin state is changed to become a triplet state (cf. Figure S1). Furthermore, the result of the spin-crossing phenomenon leads to the lowering of the endothermicity of the reaction to −2.4 kcal/mol.

For the Au/H-ZSM-5 zeolite (TS_2), the N–O bond is increased from 1.19 to 1.52 Å and the Au–O distance is decreased from 3.31 to 2.04 Å. Comparable to the case of Au/ZSM-5, it is observed that the electron transfers from the Au^0 of Au/H-ZSM-5 to N_2O. The negative charge on Au becomes positive while the charge summation of N_2O is considered to be more negative (Table 1). Normal mode analysis reveals one imaginary frequency at −634.2i cm^{-1} associated with the transition state. Here the activation energy is 15.2 kcal/mol, which is significantly lower than the N_2O decomposition on Au/ZSM-5 reported above. Again, the surface oxygen

species is generated on the active Au center and a nitrogen molecule is also formed in the zeolite framework (Prod_2). The surface Au–O bond distance in the surface oxygen species is 1.95 Å. Comparing with the reaction over Au/ZSM-5 catalyst, the calculated energy of Au/H-ZSM-5 complex (Prod_2) with respect to the reactant is more exothermic than that of the other by −13.4 kcal/mol and no occurrence of intersystem crossing is observed.

The complete energy profiles for the N_2O decomposition on Au/ZSM-5 and Au/H-ZSM-5 zeolites are shown in Figure 5. Due to the nature of the N_2O molecule being that its LUMO is considered to be π^*-orbital with the anti-bonding of both N–O and N–N bonds, the dissociation of the N_2O molecule should occur by transferring electrons from the Au active center to the N_2O molecule to fill electrons on the anti-bonding of N–O, assisting the weakening of the N–O bond and, thus, making it easy to break. The tendency of this charge transfer mechanism was also previously suggested in literatures [44]. Furthermore, Stirling and co-worker [45] demonstrated that electron transfer from the metals atom to N_2O is a very important process for the reaction of transition metals with N_2O and NO_2. In our work, we found the similar charge transfer mechanism that was in literatures in both the Au/H-ZSM-5 and Au/ZSM-5 case. The charges are transferred from the Au active site

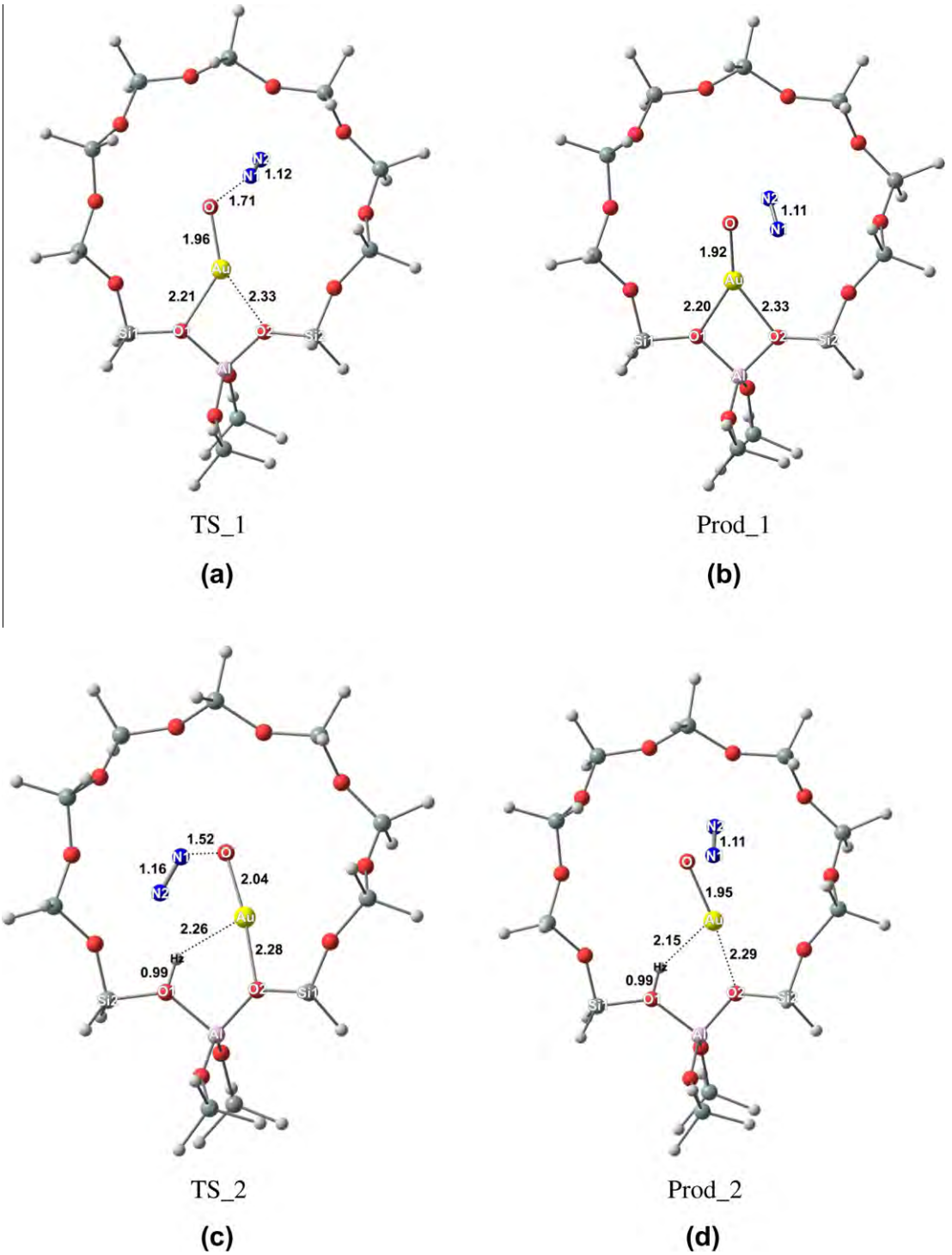

Figure 4. Optimized structures of transition states and products involved in the decomposition of N_2O over Au/ZSM-5 (a, b) and Au/H-ZSM-5 (c, d) zeolites.

to the N_2O molecule leading to a more positive charge of the Au active species supported on zeolite and a more negative N_2O molecule (Table 1). In the Au/H-ZSM-5 case, the charge difference between the adsorption and transition state complexes (q_{TS}–q_{Ads}) of Au and N_2O are +0.38*e* and −0.47*e*, respectively, which are higher than that of the Au/ZSM-5 case (+0.19*e* and −0.31*e* for Au and N_2O, respectively). This result indicates that the amount of charge transfer from the Au active site to N_2O in the Au/H-ZSM-5 case is higher than that of the Au/ZSM-5 case. This higher amount of charge transfer of Au/H-ZSM-5 leads to the higher activity for the N_2O breaking reaction. As a result, the activation energy for the decomposition of N_2O on Au/H-ZSM-5 zeolite is found to be much lower than on Au/ZSM-5 zeolite (Figure 5).

The N_2O decomposition over the metal-exchanged zeolites have been extensively investigated, especially the Fe-ZSM-5 catalyst [7,11,46–49]. Different forms of extra-framework Fe species in the zeolite are used to present the active site for N_2O decomposition reaction as summarized in Table S1 in the Supplementary Data. Significantly, the catalytic activity of Fe-ZSM-5 depends on the identity of Fe cationic species, leading to a wide range of the activation barrier for this reaction from 2 to 45 kcal/mol. From these works, the $[Fe]^+$ and $[Fe(OH)_2]^+$ are concluded to be the inactive sites for this reaction as remarked clearly by Heyden et. al. [7]. Therefore, the comparison of results in this Letter with the Fe-ZSM-5 catalyst, which is found to be an active catalyst for the decomposition of N_2O, could provide an ideal tendency of Au-ZSM-5 reactivity on this reaction. As a result, it could be concluded that the Au/ZSM-5 is considered not to be the candidate site for this reaction due to the involvement of the high-energy-demanded step. While the Au/ZSM-5 seems to be the inactive site, the Au/H-ZSM-5 can serve as the active center as considered from the mild activation height and exothermic process after decomposition. The activation energy is calculated to be 15.2 kcal/mol, which is in line with the values of the active forms of Fe-ZSM-5 zeolite. These findings would provide a better understanding of Au/H-ZSM-5 as a synergistic catalyst for the N_2O decomposition reaction.

3.4. Effect of zeolite framework on N_2O decomposition on Au/ZSM-5 and Au/H-ZSM-5

In order to investigate the effect of the ZSM-5 framework on the reaction on N_2O decomposition, we performed the single-point calculation by using the extended 120T cluster model (cf. Figure S3).

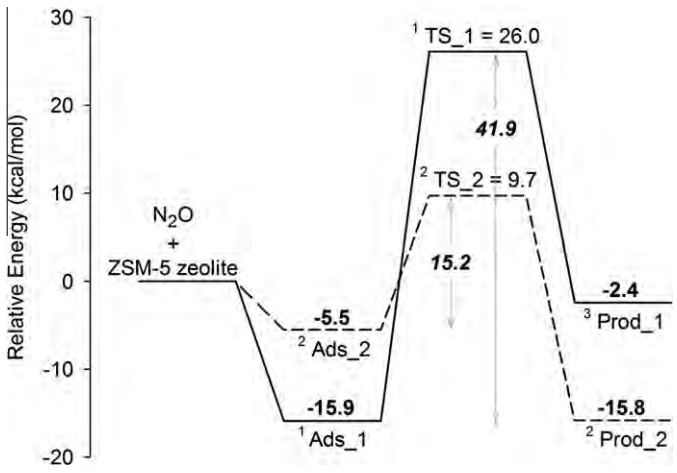

Figure 5. Energy profile for the N_2O decomposition for both zeolites: Au/ZSM-5 zeolite (solid line) and Au/H-ZSM-5 (dashed line) zeolite (energies are in kcal/mol). The superscript numbers in reaction profiles refer to the most stable spin state of each reaction complex.

The relative energies of the systems involved in the reaction are summarized in the Supplementary Data, Table S2. In the Au/ZSM-5 system, the adsorption energy is almost the same after increasing the extended framework (−15.9 to −16.4 kcal/mol). This might be due to the strong interaction between the oxygen of N_2O and Au^+ supported on ZSM-5 playing an important role for the adsorption energy of this complex instead of the long range interaction of the zeolite framework. In contrast to the Au/ZSM-5 system, the N_2O adsorption complexes in Au/H-ZSM-5 are more stabilized by the framework. The adsorption energy increases from −5.5 to −12.7 kcal/mol. This indicates that the zeolite framework contributes to the adsorption energy in the same way as the weak interaction between the Au^0 active site and the probe molecule. Nevertheless, when considering the activation energy of these systems, it remains almost unchanged by the confinement effect of the ZSM-5 framework. Activation energies for the reaction in the 120T model are calculated to be 42.9 and 18.5 kcal/mol for the Au/ZSM-5 and Au/H-ZSM-5 systems, respectively. These results show a similar trend to the computations from the 12T cluster model.

We also investigated the reaction without the whole zeolitic framework to evaluate the effect of the supported ZSM-5 framework on the catalytic activity of the Au species for N_2O decomposition. The single point calculations on the optimized structures were performed to avoid the effect of structural differences. The adsorption energies of N_2O are calculated to be −14.9 and −0.8 kcal/mol for Au^+ and Au^0, respectively, which are about 1 and 4 kcal/mol lower than those of the 12T cluster of Au/ZSM-5 and Au/H-ZSM-5, respectively. When considering the relative amount, we found that strong interaction between N_2O and Au^+ contributes about 90% of the adsorption energy, while the weak interaction of Au^0 provided ∼15% of the energy contribution in the 12T cluster and only 6% in the 120T framework. The results from the extended 120T cluster and the bare Au site lead to the conclusion that the adsorption of N_2O on Au/H-ZSM-5 is highly contributed by the ZSM-5 framework and the strong interaction between N_2O and the Au^+ active site plays a significant role for the Au/ZSM-5 zeolite. As per our expectation, the activation energies are calculated to be 54.7 and 32.8 kcal/mol for Au^+ and Au^0, respectively, which is higher than the case of the activation energies in the Au species supported by ZSM-5. This result confirms our finding mentioned earlier that the supported zeolite framework increases the activity of Au for N_2O decomposition by providing the charge distribution between the Au species and the zeolite which facilitate the charge transferring from Au to the N_2O molecule to break the N–O bond and also to stabilize all the species in the reaction coordinates as well, especially the transition state with respect to the bare Au system. This finding is in good agreement with our previous work, methane activation on Au^+ and Au^{2+} exchanged zeolites [50]. The zeolite framework reduced the activation energies obtained from the extreme case of bare Au ions.

4. Conclusion

The density functional calculations, M06-L including dispersion in the parameterization, has been employed for investigating the N_2O decomposition reaction over Au/ZSM-5 and Au/H-ZSM-5 zeolites. The reaction is proposed to proceed in a single step of the N_2O N–O bond breaking via electron to give the surface oxygen deposited on the Au active site and the nitrogen molecule. The calculated activation barriers for N_2O decomposition are observed to be 41.9 and 15.2 kcal/mol for the reaction over Au/ZSM-5 and Au/H-ZSM-5 zeolites, respectively. The latter activation energy is much lower than that of the former as a result of more charge transfer from the Au active species to the N_2O molecule found in the Au/H-

ZSM-5 as compared to the Au/ZSM-5 adduct. On the basis of these results, it can be concluded that the Au/H-ZSM-5 zeolite is more active for N_2O decomposition than the Au/ZSM-5 zeolite. We also found that the supported zeolite facilitates the charge transfer of the Au species and plays a role in stabilizing all of the species in the reaction coordinate as well as the transition state complexes over the bare Au system.

Acknowledgements

This work was supported in part by grants from the National Science and Technology Development Agency (NANOTEC Center for the Design of Nanoscale Materials for Green Nanotechnology and NSTDA Chair Professor), the Thailand Research Fund (to BB (MRG5480239), and SW (RGJ PhD), the Kasetsart University Research and Development Institute (KURDI), the Commission on Higher Education, Ministry of Education ('National Research University of Thailand' and 'Postgraduate Education and Research Programs in Petroleum and Petrochemicals and Advanced Materials') as well as under the program Strategic Scholarships for Frontier Research Network for the Joint Ph.D. Program Thai Doctoral degree from the Office of the Higher Education Commission, Thailand (to TM).

Appendix A. Supplementary data

Supplementary data associated with this article can be found, in the online version, at http://dx.doi.org/10.1016/j.cplett.2012.11.058.

References

[1] M. Shelef, Chem. Rev. 95 (1995) 209.
[2] S.A. Gomez, A. Campero, A. Martínez-Hernández, G.A. Fuentes, Appl. Catal. A 197 (2000) 157.
[3] H. Yahiro, M. Iwamoto, Appl. Catal. A 222 (2001) 163.
[4] J. Pérez-Ramírez, F. Kapteijn, G. Mul, J.A. Moulijin, Chem. Commun. (2001) 693.
[5] J. Pérez-Ramírez, F. Kapteijn, G. Mul, J.A. Moulijn, J. Catal. 208 (2002) 211.
[6] I. Melián-Cabrera, C. Mentruit, J.A.Z. Pieterse, R.W. van den Brink, G. Mul, F. Kapteijn, J.A. Moulijn, Catal. Commun. 6 (2005) 301.
[7] A. Heyden, B. Peters, A.T. Bell, F.J. Keil, J. Phys. Chem. B 109 (2005) 1857.
[8] M. Schwidder, M.S. Kumar, K. Klementiev, M.M. Pohl, A. Brückner, W. Grünert, J. Catal. 231 (2005) 314.
[9] M. Devades et al., Appl. Catal. B 67 (2006) 187.
[10] C. Chupin, A.C. van Veen, M. Konduru, J. Despres, C. Mirodals, J. Catal. 241 (2006) 103.
[11] P. Pantu, S. Pabchanda, J. Limtrakul, Chem. Phys. Chem. 5 (2004) 1901.
[12] Z. Gao, Q. Sun, H. Chen, X. Wang, W.M.H. Sachtler, Catal. Lett. 72 (2001) 1.
[13] S. Qiu, R. Ohnishi, M. Ichikawa, J. Chem. Soc. Chem. Commun. (1992) 1425.
[14] J.C. Fierro-Gonzalez, B.C. Gates, J. Phys. Chem. B 108 (2004) 16999.
[15] T.M. Salama, T. Shido, R. Ohnishi, M. Ichikawa, J. Chem. Soc. Chem. Commun. (1994) 2749.
[16] M.M. Mohamed, T.M. Salama, M. Ichikawa, J. Colloid Interface Sci. 224 (2000) 366.
[17] S. Qiu, R. Ohnishi, M. Ichikawa, J. Phys. Chem. 98 (1994) 2719.
[18] A. Deka, R.C. Deka, A. Choudhury, Chem. Phys. Lett. 490 (2010) 184.
[19] M. Svensson, S. Humbel, R.D.J. Froese, T. Matsubara, S. Sieber, K. Morokuma, J. Phys. Chem. A 100 (1996) 19357.
[20] S. Namuangruk, P. Pantu, J. Limtrakul, J. Catal. 225 (2004) 523.
[21] S. Namuangruk, P. Pantu, J. Limtrakul, ChemPhysChem 6 (7) (2005) 1333.
[22] T. Maihom, S. Namuangruk, T. Nanok, J. Limtrakul, J. Phys. Chem. C 112 (2008) 12914.
[23] B. Jansang, T. Nanok, J. Limtrakul, J. Phys. Chem. B 110 (2006) 12626.
[24] S. Namuangruk, P. Khongpracha, P. Pantu, J. Limtrakul, J. Phys. Chem. B 110 (2006) 25950.
[25] Y. Zhao, D.G. Truhlar, Acc. Chem. Res. 41 (2008) 157.
[26] T. Maihom, B. Boekfa, J. Sirijaraensre, T. Nanok, M. Probst, J. Limtrakul, J. Phys. Chem. C 113 (2009) 6654.
[27] B. Boekfa, S. Choomwattana, P. Khongpracha, J. Limtrakul, Langmuir 25 (22) (2009) 12990.
[28] C. Kumsapaya, K. Bobuatong, P. Khongpracha, Y. Tantirungrotechai, J. Limtrakul, J. Phys. Chem. C 113 (2009) 16128.
[29] T. Maihom, P. Pantu, C. Tachakritikul, M. Probst, J. Limtrakul, J. Phys. Chem. C 114 (2010) 7850.
[30] B. Boekfa, P. Pantu, M. Probst, J. Limtrakul, J. Phys. Chem. C 114 (2010) 15061.
[31] S. Wannakao, B. Boekfa, P. Khongpracha, M. Probst, J. Limtrakul, ChemPhysChem 11 (2010) 3432.
[32] K. Bobuatong, M. Probst, J. Limtrakul, J. Phys. Chem. C 114 (2010) 21611.
[33] S. Wannakao, P. Khongpracha, J. Limtrakul, J. Phys. Chem. A 115 (2011) 12486.
[34] S.J. Kolmann, B. Chan, M.J.T. Jordan, Chem. Phys. Lett. 467 (2008) 126.
[35] R.B. Getman, J.H. Miller, K. Wang, R.Q. Snurr, J. Phys. Chem. C 115 (2011) 2066.
[36] T. Maihom, S. Choomwattana, P. Khongpracha, M. Probst, J. Limtrakul, ChemPhysChem 13 (2012) 245.
[37] H. van Koningsveld, H. van Bekkum, J.C. Jansen, Acta Crystallogr. B 43 (1987) 127.
[38] M. Dolg, H. Stoll, H. Preuss, R.M. Pitzer, J. Phys. Chem. 97 (1993) 5852.
[39] A.E. Reed, L.A. Curtiss, F. Weinhold, Chem. Rev. 88 (1988) 899.
[40] M.J. Frisch et al., Gaussian 09, Revision A.02, Gaussian Inc., Wallingford CT, 2009.
[41] A. Sierraalta, R. Hernandez-Andara, E. Ehrmann, J. Phys. Chem. B 110 (2006) 17912.
[42] N. Liu, B. Chen, Y. Li, R. Zhang, X. Liang, Y. Li, Z. Lei, J. Phys. Chem. C 115 (2011) 12883.
[43] S. Wannakao, T. Nongnual, P. Khongpracha, T. Maihom, J. Limtrakul, J. Phys. Chem. C 116 (2012) 16992.
[44] W.B. Tolman, Angew. Chem. Int. Ed. 49 (2010) 1018.
[45] A. Stirling, J. Am. Chem. Soc. 124 (2002) 4058.
[46] A. Heyden, A.T. Bell, F.J. Keil, J. Catal. 233 (2005) 26.
[47] N. Hansen, A. Heyden, A.T. Bell, F.J. Keil, J. Phys. Chem. C 111 (2007) 2092.
[48] N. Hansen, A. Heyden, A.T. Bell, F.J. Keil, J. Catal. 248 (2007) 213.
[49] H. Guesmi, D. Berthomieu, B. Bromley, B. Coq, L. Kiwi-Minsker, Phys. Chem. Chem. Phys. 12 (2010) 2873.
[50] S. Wannakao, C. Warakulwit, K. Kongpatpanich, M. Probst, J. Limtrakul, ACS Catal. 2 (2012) 986.

Aldol Condensation of Acetaldehyde over H-ZSM-5 Zeolite: An advanced DFT approach

*Bundet Boekfa[1,2,3,4] and Jumras Limtrakul[2,3,4,5]**

[1]Department of Chemistry, Faculty of Liberal Arts and Science, Kasetsart University, Kamphaeng Saen Campus, Nakhon Pathom 73140, Thailand
[2]Center for Advanced Studies in Nanotechnology and Its Applications in Chemical, Food and Agricultural Industries, Kasetsart University, Bangkok 10900, Thailand
[3]Center of Nanotechnology, Kasetsart University Research Development Institute, Kasetsart University, Bangkok 10900, Thailand
[4]NANOTEC Center for Nanoscale Materials Design for Green Nanotechnology, Kasetsart University, Bangkok 10900, Thailand
[5]Department of Chemistry and National Center of Excellence for Petroleum, Petrochemicals and Advanced Materials, Faculty of Science, Kasetsart University, Bangkok 10900, Thailand

*Corresponding author's e-mail address: jumras.l@ku.ac.th

Introduction

Zeolite is one of the most important heterogeneous catalysts, especially for the petrochemical industry. Among the various pore zeolites, ZSM-5 is a particularly significant catalyst for being used for many organic reactions such as hydrocarbon cracking, isomerization and aldol condensation.[1-10] The aldol condensation is a salient C-C bond forming reaction. Aldol condensation can be easily catalyzed with the specific pore of zeolite to produce mesityl oxide.[11-14] The mesityl oxide can be hydrogenated to produce methyl isobutyl ketone, which is widely used as an organic solvent for paints, lacquers, etc.

Tautomerization or Keto-Enol Isomerization is an important reaction for organic synthesis due to its being an initial step of Aldol Condensation.[8-10] The keto-enol isomerization of acetaldehyde and acetone has been reported both experimentally and theoretically. [15-21] The acetone tautomerization on different zeolites, namely H-FER, H-ZSM-5 and H-MCM-22 have been calculated with the M06 functional.[20] These studies have provided us with understanding of the adsorption, and reaction mechanism and the confinement effect with different pore sizes of zeolites. The confinement effect is being proposed to cover the interaction between the zeolite framework and the adsorbing molecule.[22]

The adsorption and reaction mechanism with the confinement effect of zeolite have been successfully studied with M06 functional. [20,23-30] We found that neglecting the extended zeolite framework resulted in discrepancies between the cluster and the actual zeolite behaviors. The recent development of new density functionals have incorporated a dispersion interaction into account, a contribution that is essential for accurate predictions of noncovalent interaction that normally is not included in DFT such as the popular B3LYP functional, and thus has brought adsorption and the chemical reaction of zeolite within reach of deriving accurate results. [20,23,31-33] Many new DFT have been developed and applied in the zeolite such as M06 family[31-34], DFT-D scheme proposed by Grimme [35-37], ωB97X-D by Chai and Head-Gordon's [38]. Recently, the ωB97X-D functional, is a long-range corrected hybrid functional optimized to include dispersion correction, has been successfully applied to study the adsorption of alcohol and nitrile in H-ZSM-5 zeolite.[39]

In this study, the adsorption and aldol condensation reaction of acetaldehyde have been systematically explored using advanced density functional methods. A large cluster of zeolite serving as a nanometer-sized chemical reactor has been modeled by the well calibrated ONIOM scheme. The Brønsted acid active site is treated with the MP2 method while the outer framework zeolite is calculated with various new DFT: B3LYP, cam-B3LYP, M06-2X and ωB97X-D functionals. This study will be benchmark for understanding the aldol reaction and the effect of the confinement effect.

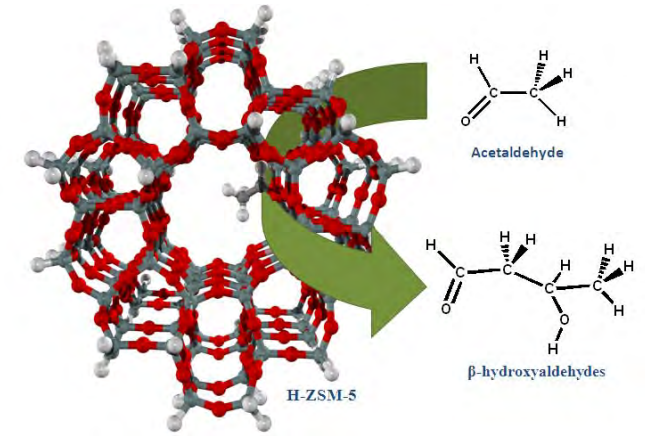

Figure 1. Model for aldol condensation of acetaldehyde on the H-ZSM-5 zeolite.

Method

The adsorption and aldol condensation reaction of acetaldehyde on H-ZSM-5 have been explored using well calibrated ONIOM schemes. The inner layer representing the Brønsted acid site, where the chemical reaction occurred, is optimized with MP2 while the outer layer representing the zeolite framework is evaluated with different density functionals namely B3LYP, cam-B3LYP, M06-2X and ωB97X-D. The combined method can be referred as: ONIOM(MP2:B3LYP), ONIOM(MP2:cam-B3LYP), ONIOM(MP2:M06-2X) and ONIOM(MP2:ωB97X-D). The basis set employed being 6-31G(d,p) and more accurate energies were improved by single point calculations at a higher level of theory with the basis set of 6-311+G(2df,2p). An Al atom is selected to substitute the Si atom at the T12 position to generate the Brønsted acid site. The frequency calculations are calculated to ensure that all transition structures derived, each has only one imaginary frequency corresponding to the reaction pathway. All calculations were performed using the Gaussian 09 code. [40]

Results and Discussion

The adsorption of acetaldehyde on H-ZSM-5 zeolite

The adsorption of acetaldehyde on H-ZSM-5 zeolite is calculated with the ONIOM(MP2:B3LYP), ONIOM(MP2:cam-B3LYP), ONIOM(MP2:M06-2X) and ONIOM(MP2:ωB97X-D). The acetaldehyde on H-ZSM-5 zeolite structure is illustrated in Fig. 1a. Acetaldehyde is adsorbed on the zeolite by forming a strong hydrogen bonding interaction between the carbonyl group (O3) and the acidic of the Brønsted acid site (Hz). The adsorption energies of acetaldehyde on H-ZSM-5 are evaluated to be -19.1, -19.8, -21.7 and -23.2 kcal/mol for ONIOM(MP2:B3LYP), ONIOM(MP2:cam-B3LYP), ONIOM(MP2:M06-2X) and ONIOM(MP2:ωB97X-D), respectively.

In comparison with the adsorption of acetone on H-ZSM-5, the calculated adsorption energies are calculated to be -19.6, -20.5, -24.9 and -26.6 kcal/mol for ONIOM(MP2:B3LYP), ONIOM(MP2:cam-B3LYP), ONIOM(MP2:M06-2X) and ONIOM(MP2:ωB97X-D), respectively. The adsorption energies are still lower than experimental one of -31.1 kcal/mol. By increasing the model to ONIOM(5T:34T), the adsorption energies are -27.0 and -31.3 kcal/mol for ONIOM(MP2:M06-2X) and ONIOM(MP2:ωB97X-D), respectively. The results derived via the ONIOM(MP2:ωB97X-D) have compared well with experimental ones. Thus this level of theory will be employed for the adsorption of acetaldehyde on H-ZSM-5 and their corresponding reaction mechanisms.

Table 1. Comparison of the adsorption energy, ΔE_{ads}, (kcal/mol) along the adsorption of acetaldehyde on H-ZSM-5 zeolite with ONIOM calculation.

Method	5T	5T:23T
ONIOM(MP2:B3LYP)	-17.3	-19.1
ONIOM(MP2:cam-B3LYP)	-17.3	-19.8
ONIOM(MP2:M06-2X)	-17.3	-21.7
ONIOM(MP2:ωB97X-D)	-17.8	-23.2

The Aldol condensation reaction of Acetaldehyde on H-ZSM-5 zeolite

The reaction of acetaldehyde on H-ZSM-5 is composed of two steps: the tautomerization reaction and the aldol condensation reaction. The ONIOM(5T:23T) is calculated with the MP2:ωB97X-D approach. First, the acetaldehyde adsorbs on H-ZSM-5 via the hydrogen bond (Fig. 3a). The Brønsted O1-Hz bond distance is lengthened from 0.97 to 1.03 Å. The carbonyl double bond (O3-C1) is lengthened from 1.21 to 1.24 Å. The O1---Hz bond distance is about 1.52 Å. The adsorption energy is -23.2 kcal/mol.

The tautomerization or keto-enol isomerization is the first reaction step (Fig. 2). The mechanism is processed via the double proton transfer. At the transition state (Fig. 3b), the proton Bronsted acid (Hz) completely transfers to the oxygen of the carbonyl group (O3). The O1-Hz bond increases to 1.80 Å. The O3-Ca bond distance increases to 1.31 Å. The proton of acetone (H1) is transferred to the oxygen of the zeolite. The C2-H1 bond distance increases to 1.43 Å. Only one imaginary frequency at -1007.5i corresponds with the pathway. The activation energy is 24.8 kcal/mol. The energy is reasonable because the previous acetone tautomerization on H-ZSM-5 is calculated to be 20.5 kcal/mol. Enol is the product of this reaction (Fig. 3c). The enol interacts with zeolite via the hydrogen bond between the π of the double bond and the proton of zeolite. The relative energy is -6.6 kcal/mol.

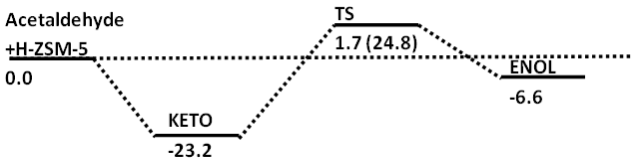

Figure 2. Energies profile of the tautomerization of acetaldehyde on H-ZSM-5 zeolite calculated from MP2:ωB97X-D (kcal/mol).

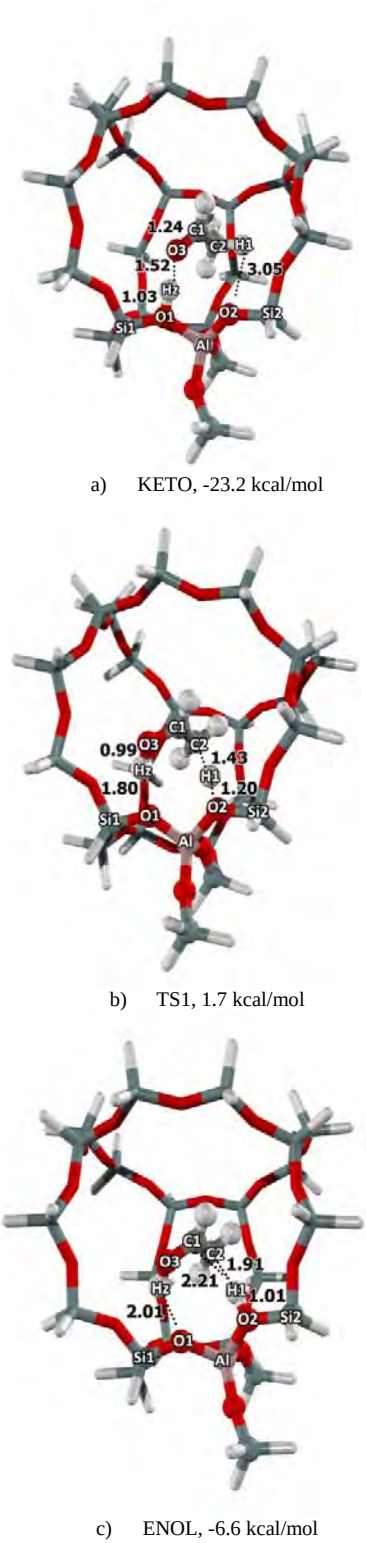

a) KETO, -23.2 kcal/mol

b) TS1, 1.7 kcal/mol

c) ENOL, -6.6 kcal/mol

Figure 3. Molecular structures of the tautomerization of acetaldehyde on H-ZSM-5 zeolite calculated from MP2:ωB97X-D (kcal/mol): a)keto, b) TS1 and c) enol.

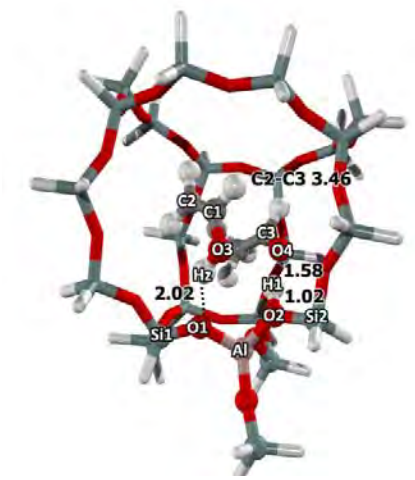

a) CO-AD, -24.4 kcal/mol

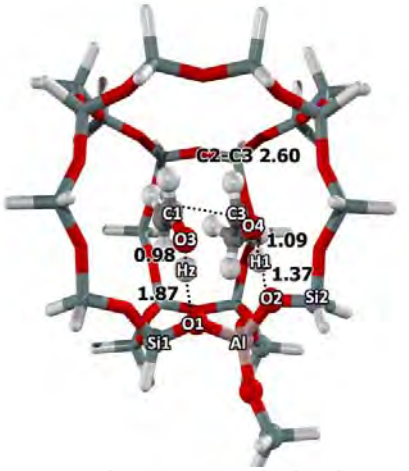

b) TS2, -20.6 kcal/mol

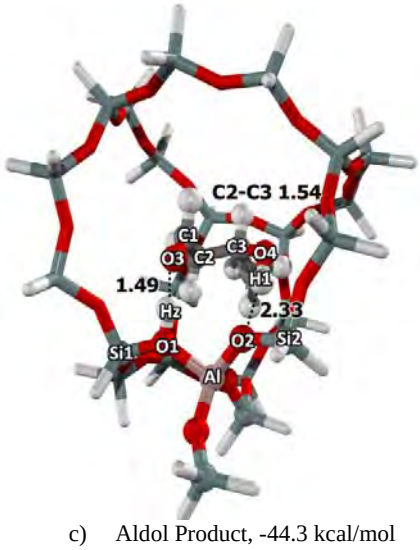

c) Aldol Product, -44.3 kcal/mol

Figure 4. Molecular structures of the aldol condensation of acetaldehyde on H-ZSM-5 zeolite calculated from MP2:ωB97X-D (kcal/mol): a)CO-AD, b) TS2 and c) Aldol Product.

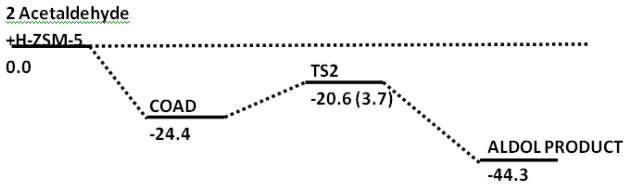

Figure 5. Energies profile of the aldol condensation of acetaldehyde on H-ZSM-5 zeolite calculated from MP2:ωB97X-D (kcal/mol).

For the aldol condensation, the reaction is via the C-C bond formation between the enol product and the other acetaldehyde (Fig. 4). The acetaldehyde adsorbs on the proton zeolite due to the stronger adsorption between the carbonyl group of acetaldehyde and the proton of zeolite than the enol product (Fig. 4a). The energy for the co-adsorption step is -24.4 kcal/mol. At the transition state (Fig. 4b), the C2-C3 bond is forming. The C2-C3 is changed from 3.46 Å (CO-AD) to 2.60 Å (TS2) and to 1.54 Å (Aldol Product). At this transition state, the O2-H1 bond is breaking and the O1-Hz is forming while the O1-Hz is forming and the O3-H1 is breaking. The imaginary frequency at -111.9i corresponds with the pathway. The activation energy is 3.7 kcal/mol. The activation energy for this step is lower than the tautomerization (24.8 kcal/mol). The aldol product (Fig. 4c), β-hydroxyaldehydes or aldehyde-alcohols, is found with the relative energy -44.3 kcal/mol.

Conclusions

The adsorption and aldol condensation reaction of acetaldehyde over H-ZSM-5 zeolite have been investigated using the ONIOM model. The adsorption energies are calculated to be -19.1, -19.8, -21.7 and -23.2 kcal/mol for ONIOM(MP2:B3LYP), ONIOM(MP2:cam-B3LYP), ONIOM(MP2:M06-2X) and ONIOM(MP2:ωB97X-D), respectively. The model is shown to be accurate in predicting the adsorption energy compared to the experimental estimate. The aldol condensation is composed of two steps: the tautomerization reaction and the aldol condensation reaction. The first step, tautomerization, is the rate determining step and requires an activation energy of 24.8 kcal/mol. As for the aldol condensation, it requires an activation barrier of only 3.7 kcal/mol. Our findings derived in this study suggest that the ONIOM(MP2:ωB97X-D) model approach is able to provide an accurate and practical model for exploring the adsorption and mechanism of the reaction of zeolites.

Acknowledgement. This work was supported in part by grants from the National Science and Technology Development Agency (NSTDA Chair Professor funded by the Crown Property Bureau under the management of the National Science and Technology Development Agency and NANOTEC Center for Nanoscale Materials Design for Green Nanotechnology funded by the National Nanotechnology Center), the Thailand Research Fund (TRF), and the Commission on Higher Education, Ministry of Education (the "National Research University Project of Thailand (NRU)" and the "National Center of Excellence for Petroleum, Petrochemical and Advanced Materials (NCE-PPAM)"). The support from the Kasetsart University Research and Development Institute (KURDI) and Graduate School Kasetsart University are also acknowledged.

References

(1) Smit, B.; Maesen, T. L. M. *Nature* **2008**, *451*, 671.
(2) Bhan, A.; Iglesia, E. *Acc. Chem. Res.* **2008**, *41*, 559.
(3) Luzgin, M. V.; Rogov, V. A.; Arzumanov, S. S.; Toktarev, A. V.; Stepanov, A. G.; Parmon, V. N. *Angewandte Chemie - International Edition* **2008**, *47*, 4559.
(4) Corma, A. *J. Catal.* **2003**, *216*, 298.
(5) Yaluris, G.; Rekoske, J. E.; Aparicio, L. M.; Madon, R. J.; Dumesic, J. A. *J. Catal.* **1995**, *153*, 65.
(6) Andy, P.; Gnep, N. S.; Guisnet, M.; Benazzi, E.; Travers, C. *J. Catal.* **1998**, *173*, 322.
(7) Venuto, P. B. *Microporous Materials* **1994**, *2*, 297.
(8) Evans, D. A.; Nelson, J. V.; Vogel, E.; Taber, T. R. *J. Am. Chem. Soc.* **1981**, *103*, 3099.
(9) Salvapati, G. S.; Ramanamurty, K. V.; Janardanarao, M. *J. Mol. Catal.* **1989**, *54*, 9.
(10) Li, C. J. *Chem. Rev. (Washington, DC, U. S.)* **1993**, *93*, 2023.
(11) Xu, T.; Munson, E. J.; Haw, J. F. *J. Am. Chem. Soc.* **1994**, *116*, 1962.
(12) Biaglow, A. I.; Sepa, J.; Gorte, R. J.; White, D. *J. Catal.* **1995**, *151*, 373.
(13) Panov, A. G.; Fripiat, J. J. *J. Catal.* **1998**, *178*, 188.
(14) Dumitriu, E.; Hulea, V.; Fechete, I.; Auroux, A.; Lacaze, J. F.; Guimon, C. *Microporous Mesoporous Mater.* **2001**, *43*, 341.
(15) Rodríguez-Santiago, L.; Vendrell, O.; Tejero, I.; Sodupe, M.; Bertran, J. *Chem. Phys. Lett.* **2001**, *334*, 112.
(16) Wu, C. C.; Lien, M. H. *J. Phys. Chem.* **1996**, *100*, 594.
(17) Lee, D.; Kim, C. K.; Lee, B. S.; Lee, I.; Lee, B. C. *J. Comput. Chem.* **1997**, *18*, 56.
(18) Cucinotta, C. S.; Ruini, A.; Catellani, A.; Stirling, A. *ChemPhysChem* **2006**, *7*, 1229.
(19) Solans-Monfort, X.; Bertran, J.; Branchadell, V.; Sodupe, M. *J. Phys. Chem. B* **2002**, *106*, 10220.
(20) Boekfa, B.; Pantu, P.; Probst, M.; Limtrakul, J. *J. Phys. Chem. C* **2010**, *114*, 15061.
(21) Boekfa, B.; Sirijareansre, J.; Pantu, P.; Limtrakul, J. *Stud. Surf. Sci. Catal.* **2004**, *154 B*, 1582.
(22) Derouane, E. G.; Fripiat, J. G. *J. Phys. Chem.* **1987**, *91*, 145.
(23) Boekfa, B.; Choomwattana, S.; Khongpracha, P.; Limtrakul, J. *Langmuir* **2009**, *25*, 12990.
(24) Wannakao, S.; Boekfa, B.; Khongpracha, P.; Probst, M.; Limtrakul, J. *ChemPhysChem* **2010**, *11*, 3432.
(25) Kongpatpanich, K.; Nanok, T.; Boekfa, B.; Probst, M.; Limtrakul, J. *Phys. Chem. Chem. Phys.* **2011**, *13*, 6462.
(26) Phuakkong, O.; Bobuatong, K.; Pantu, P.; Boekfa, B.; Probst, M.; Limtrakul, J. *ChemPhysChem* **2011**, *12*, 2160.
(27) Wannakao, S.; Khongpracha, P.; Limtrakul, J. *J. Phys. Chem. A* **2011**, *115*, 12486.
(28) Choomwattana, S.; Maihom, T.; Boekfa, B.; Pantu, P.; Limtrakul, J. *Can. J. Chem. Eng.* **2012**, *90*, 865.
(29) Wannakao, S.; Warakulwit, C.; Kongpatpanich, K.; Probst, M.; Limtrakul, J. *ACS Catalysis* **2012**, *2*, 986.
(30) Wattanakit, C.; Nokbin, S.; Boekfa, B.; Pantu, P.; Limtrakul, J. *J. Phys. Chem. C* **2012**, *116*, 5654.
(31) Zhao, Y.; Truhlar, D. G. *Theor. Chem. Acc.* **2008**, *120*, 215.
(32) Zhao, Y.; Truhlar, D. G. *J. Phys. Chem. C* **2008**, *112*, 6860.
(33) Zhao, Y.; Truhlar, D. G. *Acc. Chem. Res.* **2008**, *41*, 157.
(34) Zhao, Y.; Schultz, N. E.; Truhlar, D. G. *J. Chem. Theory Comput.* **2006**, *2*, 364.
(35) Grimme, S. *J. Comput. Chem.* **2004**, *25*, 1463.
(36) Grimme, S.; Antony, J.; Schwabe, T.; Mück-Lichtenfeld, C. *Organic and Biomolecular Chemistry* **2007**, *5*, 741.
(37) Grimme, S.; Antony, J.; Ehrlich, S.; Krieg, H. *J. Chem. Phys.* **2010**, *132*.
(38) Chai, J. D.; Head-Gordon, M. *Phys. Chem. Chem. Phys.* **2008**, *10*, 6615.
(39) Van Der Mynsbrugge, J.; Hemelsoet, K.; Vandichel, M.; Waroquier, M.; Van Speybroeck, V. *J. Phys. Chem. C* **2012**, *116*, 5499.
(40) M. J. Frisch, G. W. T., H. B. Schlegel, G. E. Scuseria, M. A. Robb, J. R. Cheeseman, G. Scalmani, V. Barone, B. Mennucci, G. A. Petersson, H. Nakatsuji, M. Caricato, X. Li, H. P. Hratchian, A. F. Izmaylov, J. Bloino, G. Zheng, J. L. Sonnenberg, M. Hada, M. Ehara, K. Toyota, R. Fukuda, J. Hasegawa, M. Ishida, T. Nakajima, Y. Honda, O. Kitao, H. Nakai, T. Vreven, J. A. Montgomery, Jr., J. E. Peralta, F. Ogliaro, M. Bearpark, J. J. Heyd, E. Brothers, K. N. Kudin, V. N. Staroverov, R. Kobayashi, J. Normand, K. Raghavachari, A. Rendell, J. C. Burant, S. S. Iyengar, J. Tomasi, M. Cossi, N. Rega, J. M. Millam, M. Klene, J. E. Knox, J. B. Cross, V. Bakken, C. Adamo, J. Jaramillo, R. Gomperts, R. E. Stratmann, O. Yazyev, A. J. Austin, R. Cammi, C. Pomelli, J. W. Ochterski, R. L. Martin, K. Morokuma, V. G. Zakrzewski, G. A. Voth, P. Salvador, J. J. Dannenberg, S. Dapprich, A. D. Daniels, Ö. Farkas, J. B. Foresman, J. V. Ortiz, J. Cioslowski, and D. J. Fox In *Gaussian 09, Revision A.02, Gaussian, Inc., Wallingford CT.* 2009.

SELECTIVE OXIDATION OF METHANE TO METHANOL OVER CATALYTIC Fe-ZSM-5 ZEOLITE: A DFT (M06-L) STUDY

*Bundet Boekfa[1,3,4,5],Thana Maihom[2,3,4,5], Sippakorn Wannakao[2,3,4,5] and Jumras Limtrakul[2,3,4,5]**

[1]Department of Chemistry, Faculty of Liberal Arts and Science, Kasetsart University, Kamphaeng Saen Campus, Nakhon Pathom 73140, Thailand
[2]Department of Chemistry and National Center of Excellence for Petroleum, Petrochemicals and Advanced Materials, Faculty of Science, Kasetsart University, Bangkok 10900, Thailand
[3]Center for Advanced Studies in Nanotechnology and Its Applications in Chemical, Food and Agricultural Industries, Kasetsart University, Bangkok 10900, Thailand
[4]Center of Nanotechnology, Kasetsart University Research Development Institute, Kasetsart University, Bangkok 10900, Thailand
[5]NANOTEC Center of Excellence, National Nanotechnology Center, Kasetsart University, Bangkok 10900, Thailand
*Corresponding author's e-mail address: jumras.l@ku.ac.th

Introduction

Zeolites are outstanding solid catalysts for their activity and selectivity.[1-6] They are of tremendous interest for their exceptional range of applications for adsorption, separation and catalysis zeolite supported metal oxide catalysts provide high activity for nitrous oxide decomposition and methane oxidation. [7-8] With metal oxide modified zeolite such as Fe-Zeolite[7-9] and Cu-Zeolite, [10-12] the conversion of methane to methanol can occur. For example, Fe-ZSM-5 as the catalyst has been used for methane to methanol with nitrous oxide as an oxidant. [7-8] Subsequently, nitrous oxide decomposition under high temperature generates the highly selective and active surface oxygen or α-oxygen. The α-oxygen is used for oxidation of methane to produce methanol at room temperature. [13-14]

To obtain detailed molecular information regarding the mechanism, theoretical study has been used to study the reaction of methane to methanol.[15-18] Previously, the ONIOM(our-Own-N-layered Integrated molecular Orbital + molecular Mechanics) (B3LYP:UFF) method has been used to study the reaction of methane to methanol and nitrous oxide decomposition.[15-16,19] To avoid the error from the overestimated van der Waals interactions from the universal force field and the weak interaction from the small quantum cluster of B3LYP method, the full quantum cluster, M06 functional[20-22], has been used to study the adsorption and reaction in the zeolite pore.[23-24] Recently, the reaction inside modified metal-zeolite catalysts such as VO_2-MCM-22 and Au-FAU have been successfully studied with the M06-L functional. [25-26] The results compared well with experiment ones and the sophisticated MP2 method.

In this study, the full optimized 34T quantum cluster of Fe-ZSM-5 is used to study the selective oxidation of methane to methanol and decomposition of nitrous oxide. This model can be used to represent the confinement effect of the zeolite framework.[23,27] We used the density functional theory, M06-L, to study the adsorption and reaction mechanism.

Models and Method

The Fe-ZSM-5 zeolite is used to study the selective oxidation of methane to methanol. The 34T quantum cluster is used to represent the pore structure of ZSM-5. [23,27] A silicon atom was substituted with an aluminium atom at the most favorable position (T12) and the iron cation $[FeO_2]^+$ was placed at the Brønsted acid site.[16] In the model, the surface oxygen atoms are terminated by the H atom. We optimized all 34T quantum clusters, and only the terminal hydrogen atoms are kept fixed with the crystallographic structure. [28]

The 34T quantum cluster was treated with the M06-L functional.[20] The Si, Al, C, O and H atoms were calculated with the 6-31G(d,p) level of theory while the Fe atom was calculated with the effective core potential basis of Stuttgart and Bohn. The total spin was kept constant at the sextet state. Structure optimizations were carried out using the Gaussian 09 program. [29]

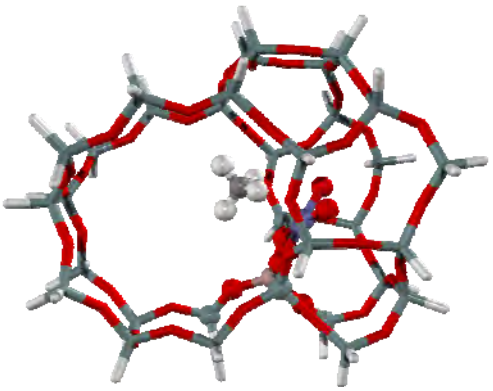

(a)

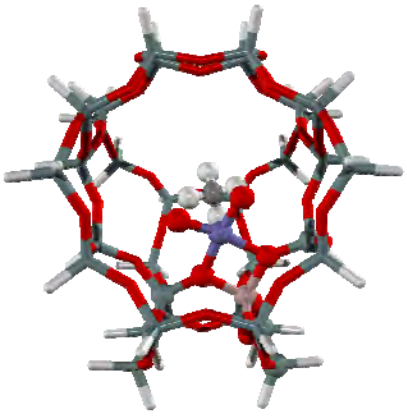

(b)

Figure 1. The 34T model cluster of Fe-ZSM-5 with methane adsorption optimized with the M06-L functional: (a) viewed from the straight channel and (b) viewed from the zigzag channel.

Results and Discussion

The optimized 34T quantum cluster of Fe-ZSM-5 zeolite is shown in Figure 1. This model covers the components of both zigzag and straight channels connected with the intersection where the probe molecule prefers to locate. The model was carefully tested to represent the framework effect of zeolite. The average Si-O distance is about 1.62 Å, which compared well with experiment data of 1.59 Å.[28] The Al-O distance is about 1.73 Å. The iron atom (Fe) is coordinated by two oxygen bridge atoms of the zeolites with the bond distances (Fe-O) of 2.00 and 2.02 Å. The Fe ··· Al distance is 2.81 Å, which agrees well with the experiment finding of 2.9 Å.[30] The oxygen atoms (O1 and O2) are bonded with the iron atom with distances of 1.67 and 1.68 Å respectively.

The methane molecule is located in the ZSM-5 zeolite at the intersection cavity [AD, Figure 2A]. The molecule is adsorbed on the $[FeO_2]^+$ active site of Fe-ZSM-5 zeolite. The distance between the methane molecule and the anion oxygen is about 2.73 Å. The C-H bond distance of methane is increased from 1.09 Å in the gas phase to 1.10 Å. The adsorption energy is calculated to be -8.7 kcal/mol.

After the methane adsorbs on the $[FeO_2]^+$ active site of the Fe-ZSM-5 zeolite, the methane can be transformed to the methanol product by two reaction steps: the methane hydrogen abstraction and the methanol formation. We also studied the reoxidation of the Fe-ZSM-5 catalyst by using nitrous oxide decomposition.

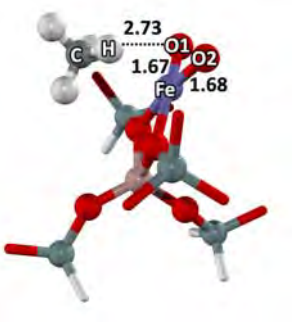

a) AD, ΔE=-8.7 kcal/mol

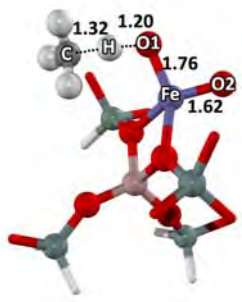

b) TS1, ΔE=15.5 kcal/mol

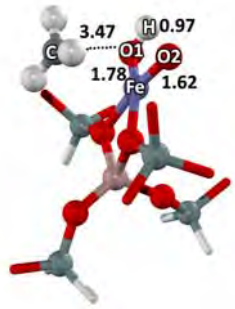

c) IN, ΔE=-3.7 kcal/mol

Figure 2. Molecular structure of the methane hydrogen abstraction on Fe-ZSM-5: (a) AD, (b) TS1 and (c) IN. Distances are in Å and energies are in kcal/mol.

The reaction begins with the activation of the methane C-H bond by the oxygen atom of the $[FeO_2]^+$ active site. At the transition state [TS1, Figure 2B], the O1 ··· H is forming and the H-C is breaking. The O1 ··· H and H ··· C bond distances are 1.20 and 1.32 Å, respectively. The Fe-O1 distance increases by about 0.13 Å. The imaginary frequency of 172i cm^{-1} of the transition state corresponds to the movement of the hydrogen atom from the carbon of methane to the oxygen of the $[FeO_2]^+$ active site. The apparent activation energy of this step is 15.5 kcal/mol and the actual activation energy is 24.2 kcal/mol. By spin density analysis, we found that the intermediate at this step is methyl radical. The methyl radical intermediate [IN1, Figure 2C], has a relative energy of -3.7 kcal/mol. The H ··· C bond distance is about 3.47 Å.

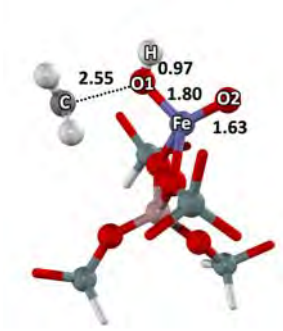

a) TS2, ΔE=4.0 kcal/mol

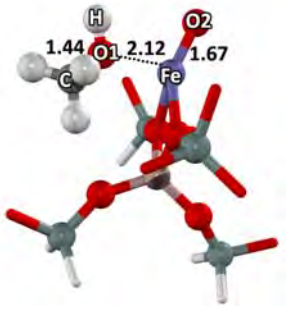

b) PR, ΔE=-47.4 kcal/mol

Figure 3. Molecular structure of the methanol formation on Fe-ZSM-5: (a) TS2 and (b) PR. Distances are in Å and energies are in kcal/mol.

The methyl radical intermediate can be converted to methanol through transition state [TS2, Figure 3A]. At the transition state, the imaginary frequency of 158i cm^{-1} shows the formation of the C-O bond and the breaking the Fe-O bond. The C ··· O and Fe ··· O bond distances are 2.55 and 1.80 Å, respectively. This step requires an activation energy of only 7.7 kcal/mol. The methanol product is strongly adsorbed on the $[FeO]^+$ active site with the relative energy of -47.4 kcal/mol. The release of the product is found to be an important step. The methanol can be desorbed from the $[FeO]^+$ active site with desorption energy of 33.4 kcal/mol.

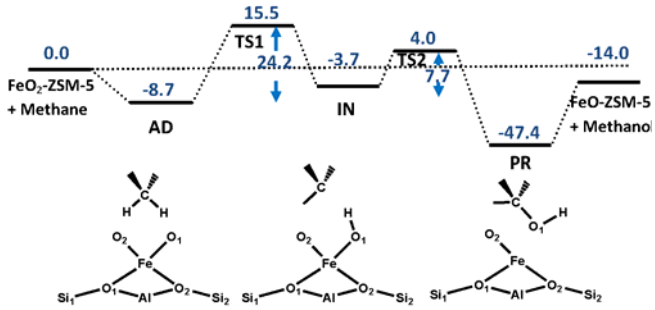

Figure 4. Energy profile for the oxidation of methane to methanol over Fe-ZSM-5 zeolite.

For the last step, the nitrous oxide is used as the reoxidizing agent of the Fe-ZSM-5. N_2O adsorbs on the $[FeO]^+$ active site [AD2, Figure 5A] with an adsorption energy -14.2 kcal/mol which agrees well with the experiment data of -16 kcal/mol.[31] The imaginary frequency of 776i cm^{-1} of the transition state [TS3, Figure 5B] shows the N-O bond of the nitrous oxide breaking and a new Fe-O bond forming. This step requires an activation energy of 32.9 kcal/mol. The nitrogen molecule can be removed from the catalyst with desorption energy of only 5 kcal/mol.

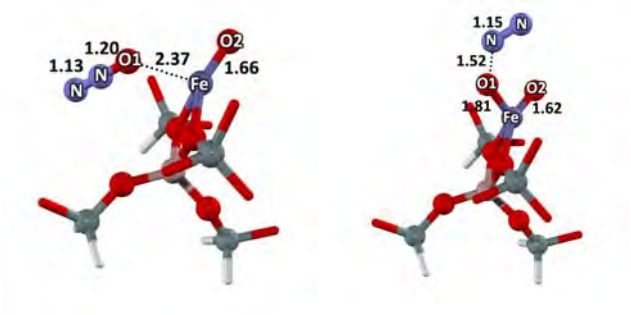

a) AD2, ΔE=-14.2 kcal/mol b) TS3, ΔE=18.7 kcal/mol

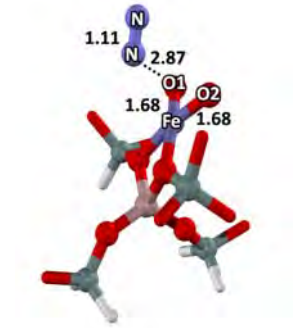

c) PR2, ΔE=-21.3 kcal/mol

Figure 5. Molecular structure of the reoxidation of the Fe-ZSM-5 Catalyst by using nitrous oxide decomposition: (a) AD2, (b) TS3 and (c) PR2. Distances are in Å and energies are in kcal/mol.

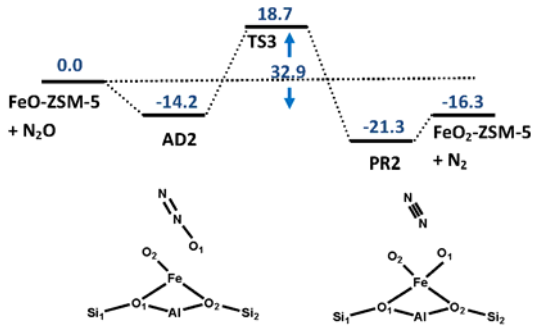

Figure 6. Energy profile for the reoxidation of the Fe-ZSM-5 catalyst by using nitrous oxide decomposition.

Conclusion

The Fe-ZSM-5 zeolite has been used to study the conversion of methane to methanol which is an alternative important fuel. The fully optimized 34 tetrahedral quantum cluster is used to represent the nanopore of Fe-ZSM-5 zeolite. The method used is the M06-L/6-31G(d,p) level of theory. The adsorption energy of methane on the $[FeO_2]^+$ active site of Fe-ZSM-5 is calculated to be -8.7 kcal/mol. The reaction mechanism composed of two reaction steps: the methane hydrogen abstraction and the methanol formation. The activation energies are calculated to be 24.2 and 7.7 kcal/mol, respectively. The reoxidation of the Fe-ZSM-5 catalyst using nitrous oxide decomposition requires an activation energy of 32.9 kcal/mol. We, therefore, studied the complete oxidation reaction mechanism inside the zeolite pore.

Acknowledgement. This work was supported in part by grants from the National Science and Technology Development Agency (2009 NSTDA Chair Professor funded by the Crown Property Bureau under the management of the National Science and Technology Development Agency and NANOTEC Center of Excellence funded by the National Nanotechnology Center), the Thailand Research Fund (TRF), and the Commission on Higher Education, Ministry of Education (the "National Research University Project of Thailand (NRU)" and the "National Center of Excellence for Petroleum, Petrochemical and Advanced Materials (NCE-PPAM)"). The support from the Kasetsart University Research and Development Institute (KURDI) and Graduate School Kasetsart University are also acknowledged.

References

(1) Bhan, A.; Iglesia, E. *Acc. Chem. Res.* **2008**, *41*, 559-567.
(2) Corma, A. *J. Catal.* **2003**, *216*, 298-312.
(3) Derouane, E. G. *J. Mol. Catal. A: Chem.* **1998**, *134*, 29-45.
(4) Lonsinger, S. R.; Chakraborty, A. K.; Theodorou, D. N.; Bell, A. T. *Catal. Lett.* **1991**, *11*, 209-217.
(5) Smit, B.; Maesen, T. L. M. *Nature* **2008**, *451*, 671-678.
(6) Venuto, P. B. *Microporous Materials* **1994**, *2*, 297-411.
(7) Pannov, G. I.; Sobolev, V. I.; Kharitonov, A. S. *J. Mol. Catal.* **1990**, *61*, 85-97.
(8) Sobolev, V. I.; Dubkov, K. A.; Panna, O. V.; Panov, G. I. *Catal. Today* **1995**, *24*, 251-252.
(9) Michalkiewicz, B. *Appl. Catal., A* **2004**, *277*, 147-153.
(10) Alayon, E. M.; Nachtegaal, M.; Ranocchiari, M.; Van Bokhoven, J. A. *Chem. Commun. (Cambridge, U. K.)* **2012**, *48*, 404-406.
(11) Beznis, N. V.; Weckhuysen, B. M.; Bitter, J. H. *Catal. Lett.* **2010**, *138*, 14-22.
(12) Smeets, P. J.; Hadt, R. G.; Woertink, J. S.; Vanelderen, P.; Schoonheydt, R. A.; Sels, B. F.; Solomon, E. I. *J. Am. Chem. Soc.* **2010**, *132*, 14736-14738.
(13) Dubkov, K. A.; Starokon, E. V.; Paukshtis, E. A.; Volodin, A. M.; Panov, G. I. *Kinet. Catal.* **2004**, *45*, 202-208.
(14) Starokon, E. V.; Parfenov, M. V.; Pirutko, L. V.; Abornev, S. I.; Panov, G. I. *J. Phys. Chem. C* **2011**, *115*, 2155-2161.
(15) Pabchanda, S.; Pantu, P.; Limtrakul, J. *J. Mol. Catal. A: Chem.* **2005**, *239*, 103-110.
(16) Pantu, P.; Pabchanda, S.; Limtrakul, J. *ChemPhysChem* **2004**, *5*, 1901-1906.
(17) Knops-Gerrits, P. P.; Goddard Iii, W. A. *J. Mol. Catal. A: Chem.* **2001**, *166*, 135-145.

(18) Liang, W.; Bell, A. T.; Head-Gordon, M.; Chakraborty, A. K. *J. Phys. Chem. B* **2004**, *108*, 4362-4368.
(19) Pantu, P.; Boekfa, B.; Sunpetch, B.; Limtrakul, J. *Chem. Eng. Commun.* **2008**, *195*, 1477-1485.
(20) Zhao, Y.; Truhlar, D. G. *Theor. Chem. Acc.* **2008**, *120*, 215-241.
(21) Zhao, Y.; Truhlar, D. G. *Acc. Chem. Res.* **2008**, *41*, 157-167.
(22) Zhao, Y.; Truhlar, D. G. *J. Phys. Chem. C* **2008**, *112*, 6860-6868.
(23) Boekfa, B.; Pantu, P.; Probst, M.; Limtrakul, J. *J. Phys. Chem. C* **2010**, *114*, 15061-15067.
(24) Wattanakit, C.; Nokbin, S.; Boekfa, B.; Pantu, P.; Limtrakul, J. *J. Phys. Chem. C* **2012**, *116*, 5654-5663.
(25) Wannakao, S.; Boekfa, B.; Khongpracha, P.; Probst, M.; Limtrakul, J. *ChemPhysChem* **2010**, *11*, 3432-3438.
(26) Wannakao, S.; Khongpracha, P.; Limtrakul, J. *J. Phys. Chem. A* **2011**, *115*, 12486-12492.
(27) Boekfa, B.; Choomwattana, S.; Khongpracha, P.; Limtrakul, J. *Langmuir* **2009**, *25*, 12990-12999.
(28) Van Koningsveld, H.; Van Bekkum, H.; Jansen, J. C. *Acta Crystallographica* **1987**, *B43*, 127-132.
(29) M. J. Frisch, G. W. T., H. B. Schlegel, G. E. Scuseria, M. A. Robb, J. R. Cheeseman, G. Scalmani, V. Barone, B. Mennucci, G. A. Petersson, H. Nakatsuji, M. Caricato, X. Li, H. P. Hratchian, A. F. Izmaylov, J. Bloino, G. Zheng, J. L. Sonnenberg, M. Hada, M. Ehara, K. Toyota, R. Fukuda, J. Hasegawa, M. Ishida, T. Nakajima, Y. Honda, O. Kitao, H. Nakai, T. Vreven, J. A. Montgomery, Jr., J. E. Peralta, F. Ogliaro, M. Bearpark, J. J. Heyd, E. Brothers, K. N. Kudin, V. N. Staroverov, R. Kobayashi, J. Normand, K. Raghavachari, A. Rendell, J. C. Burant, S. S. Iyengar, J. Tomasi, M. Cossi, N. Rega, J. M. Millam, M. Klene, J. E. Knox, J. B. Cross, V. Bakken, C. Adamo, J. Jaramillo, R. Gomperts, R. E. Stratmann, O. Yazyev, A. J. Austin, R. Cammi, C. Pomelli, J. W. Ochterski, R. L. Martin, K. Morokuma, V. G. Zakrzewski, G. A. Voth, P. Salvador, J. J. Dannenberg, S. Dapprich, A. D. Daniels, Ö. Farkas, J. B. Foresman, J. V. Ortiz, J. Cioslowski, and D. J. Fox; Gaussian 09, Revision A.2, Gaussian, Inc., Wallingford CT, 2009.
(30) Choi, S. H.; Wood, B. R.; Ryder, J. A.; Bell, A. T. *J. Phys. Chem. B* **2003**, *107*, 11843-11851.
(31) Wood, B. R.; Reimer, J. A.; Bell, A. T. *J. Catal.* **2002**, *209*, 151-158.

ISOMERIZATION MECHANISM OF *m*-XYLENE TO *p*-XYLENE ON H-ITQ-22: A DFT MECHANISTIC STUDY

Bundet Boekfa[1,2,4,5] *and* Jumras Limtrakul[2,3,4,5]*

[1]Department of Chemistry, Faculty of Liberal Arts and Science, Kasetsart University, Kamphaeng Saen Campus, Nakhon Pathom 73140, Thailand
[2]Center for Advanced Studies in Nanotechnology and Its Applications in Chemical, Food and Agricultural Industries, Kasetsart University, Bangkok 10900, Thailand
[3]Department of Chemistry, Faculty of Science, National Center of Excellence for Petroleum, Petrochemicals and Advanced Materials, Kasetsart University, Bangkok 10900, Thailand
[4]Center of Nanotechnology, Kasetsart University Research Development Institute, Kasetsart University, Bangkok 10900, Thailand
[5]NANOTEC Center of Excellence, National Nanotechnology Center, Kasetsart University, Bangkok 10900, Thailand
*Corresponding author's e-mail address: jumras.l@ku.ac.th

Introduction

Zeolites are important industrial nanostructure materials with a wide range of applications such as separation, catalysis and ion-exchange[1-4]. These materials are used as catalysts for petrochemical industries, namely hydrocarbon cracking, oligomerization and isomerization[1-5]. ITQ-22 (IWR) is a new multipore zeolite[6] which is constructed with 8- (small pore), 10- (medium pore) and 12- (large pore) membered rings. This zeolite has proved to be an outstanding catalysis for alkylation of benzene with isopropanol or propylene, disproportionation of xylene to toluene and trimethylbenzenes, and isomerization of *m*-xylene to *p*-xylene[6].

p-xylene is a high value aromatic material for the production of synthetic fibers [7]. Many catalysts for the isomerization of xylene have been developed to produce *p*-xylene, and many zeolites such as H-ZSM-5, H-MOR, H-BEA and H-MCM-22 are used with a high percentage of *p*-xylene[8-14]. ITQ-22 zeolite possessing a three-dimensional structure with three different pore sizes has proved to be a good shape-selective catalyst for isomerization of *m*-xylene to *p*-xylene[6]. This is similar to 10MR pore zeolite (H-ZSM-5) and also produces low trimethylbenzene which is similar to 12MR pore zeolite (H-MOR, H-BEA). In order to explore the detailed chemical reactions that occur inside the shape-selective catalyst, it is essential to study the confinement effect. The confinement effect, which is mainly composed of dispersive van der Waals interactions, has been proposed by Derouane[15] to explain the interaction between zeolite and the adsorbed molecule. Recently, the zeolite confinement effect on the adsorption and reactions have been successfully studied by the new density functional theory, M06-2X[16-22]. In this work, we study the reaction mechanism of *m*-xylene to *p*-xylene on H-ITQ-22 zeolite. The large quantum cluster is used to represent the zeolite structure. This study will enable us to understand the reaction mechanism of isomerization of xylene in the ITQ-22 zeolite.

Method

The adsorption and reaction of *m*-xylene to *p*-xylene on H-ITQ-22 zeolite have been studied with the M06-2X functional with 6-31G9d,p) basis set. The quantum cluster model was taken from the lattice structure of ITQ-22 zeolite. The 42T quantum cluster of H-ITQ-22 is modeled to cover the intersection between the 12-MR straight channel and the 10-MR window (cf. Figure 1). An Al atom is selected to substitute the Si atom at the T1 position to generate the Brønsted acid site. Only terminated hydrogen atoms (Si-H) are kept fixed with the crystallographic structure[6]. The frequency calculations were performed to ensure that an obtained transition structure has only one imaginary frequency corresponding to the reaction pathway. All calculations were performed using the Gaussian 03[23] code incorporated with the Minnesota Density Functional module 3.1 by Zhao and Truhlar[21].

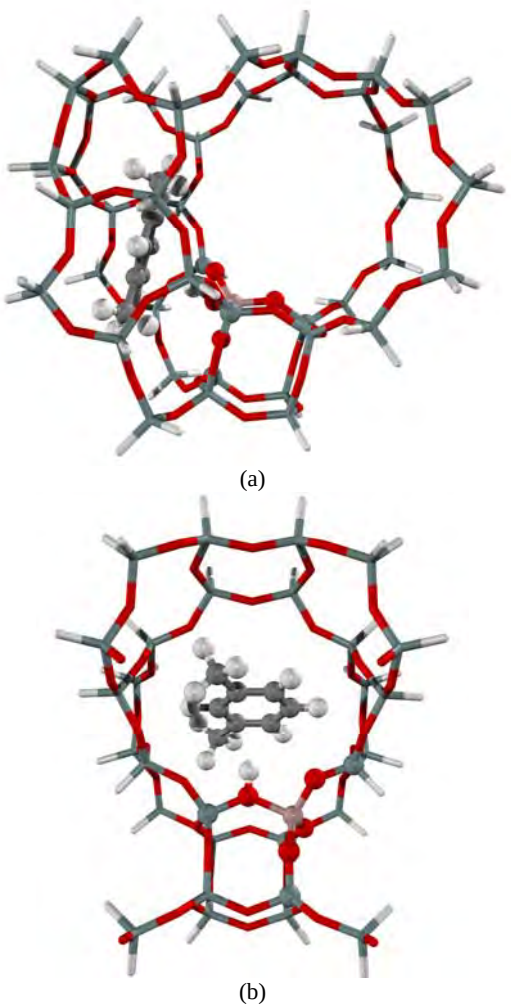

(a)

(b)

Figure 1. Presentation of *m*-xylene on H-ITQ-22 models the 42T quantum cluster: (a) view from the straight channel (12MR) and (b) view from the intersection region (10- and 12-MR).

Results and Discussion

The optimized structures of H-ITQ-22 zeolite are illustrated in Fig. 1. The O1-Hz Brønsted acid bond distance is predicted to be 0.97 Å. The average Si-O distance is calculated to be 1.63 Å, which compared well with the experiment data of 1.61 Å[6]. The average Al-O distance is calculated to be 1.76 Å. The Al ··· Hz distance is 2.38 Å, which again compared well with the experimental values of 2.38-2.48 Å[24].

The *m*-xylene molecule prefers to adsorb on the Brønsted acid site via the π-bond interaction of the double bond of benzene as shown in Figure 3A. The Brønsted acid bond distance is increased by 0.02 Å. The distances between the double bond carbon and the Brønsted acid (C1···Hz and C2···Hz) are 2.27 and 2.38 Å, respectively. The adsorption energy is calculated to be -23.9 kcal/mol. which is in the range of the experimental data of -20.4 kcal/mol for the adsorption of ethylbenzene in H-FAU zeolite[25] and -19.6 kcal/mol for the adsorption of *p*-xylene on siliceous zeolite [26-27].

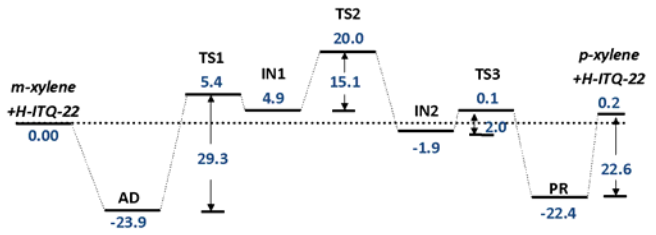

Figure 2. Potential energy diagram of the isomerization of *m*-xylene to *p*-xylene on the H-ITQ-22 calculated with M06-2X functional (kcal/mol).

The mechanism of isomerization for *m*-xylene to *p*-xylene in H-ITQ-22 was proposed to proceed in three steps, namely: 1) the protonation of *m*-xylene, 2) the methyl shift of protonated *m*-xylene, and 3) the proton back to zeolite and desorption of *p*-xylene. Figure 2 shows the reaction mechanism for the isomerization of *m*-xylene to *p*-xylene.

Protonation of *m*-xylene adsorption complex. In the first step, the adsorbed *m*-xylene [Figure 3A, AD] is protonated by the acidic proton of the H-ITQ-22 zeolite. At the transition state [Figure 3B, TS1], the Hz is shifted to the C1 atom of xylene and the tertiary carbenium ion is formed. The Brønsted acid O1-Hz distance is increased from 0.99 Å to 1.67 Å and the Hz ··· C1 is decreased from 2.27 Å to 1.25 Å. The C1-C2 bond distance is elongated by 0.03 Å. The activation energy for this step is evaluated to be 29.3 kcal/mol. By comparing the protonation of the *m*-xylene step with the other two steps: the methyl shift of protonated *m*-xylene, and the proton back to zeolite and desorption of *p*-xylene, this step is proposed to be the rate determining step of the reaction. The proton Brønsted acid is completely transferred to the carbon of *m*-xylene, the protonated *m*-xylene [Figure 3C, IN1] is formed with a relative energy of 4.9 kcal/mol as evidenced from the O1-Hz and Hz-C1 bond distances (2.04 Å and 1.17 Å, respectively).

Methyl Shift of protonated *m*-xylene. In this step, the methyl group (at C3) is shifted from the C1 atom to the C2 atom of the adsorbing molecule, the transition state complex is formed [see TS2 of Figure 3D] as observed by the breaking of the C1-C3 bond and the forming of the C2-C3 bond. The C1-C3 and C2-C3 bond distances are 1.85 and 1.89 Å, respectively. This step requires activation energy of only 15.0 kcal/mol and the protonated *p*-xylene is derived [Figure 4A, IN2].

Proton back to the zeolite and desorption of *p*-xylene. In the last step, the proton back to anionic zeolite from the protonated *p*-xylene and the product of *p*-xylene is formed over the H-ITQ-22. At the transition state [Figure 4B, TS3], the hydrogen atom of protonated *p*-xylene, H2, is shifted back to the oxygen atom of the anionic zeolite framework. The C2-H2 and H2-O2 bond lengths are 1.24 and 1.59 Å, respectively. This step is very much facile and it requires an activation energy of only 2.0 kcal/mol. The *p*-xylene product [Figure 4C, PR] interacts with the H-ITQ-22 via a π-bond interaction of the C1-C2 bond with a relative energy of -22.4 kcal/mol. The desorption energy of *p*-xylene on H-ITQ-22 is predicted to be 22.6 kcal/mol. The *m*-xylene to *p*-xylene isomerization is an endothermic reaction. The heat of reaction is calculated to be 0.10 kcal/mol.

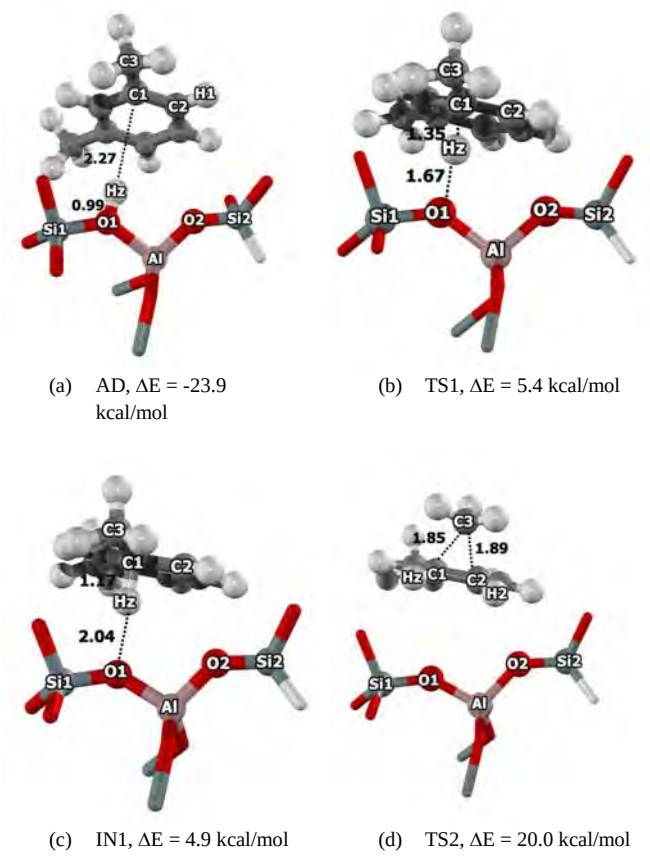

(a) AD, ΔE = -23.9 kcal/mol

(b) TS1, ΔE = 5.4 kcal/mol

(c) IN1, ΔE = 4.9 kcal/mol

(d) TS2, ΔE = 20.0 kcal/mol

Figure 3. Optimized structure of *m*-xylene isomerization to *p*-xylene on H-ITQ-22 zeolite: a) the adsorption complex(AD), b) the transition structure (TS1), c)the protonated *m*-xylene (IN1) and d) the transition structure (TS2). Distances are in Ås.

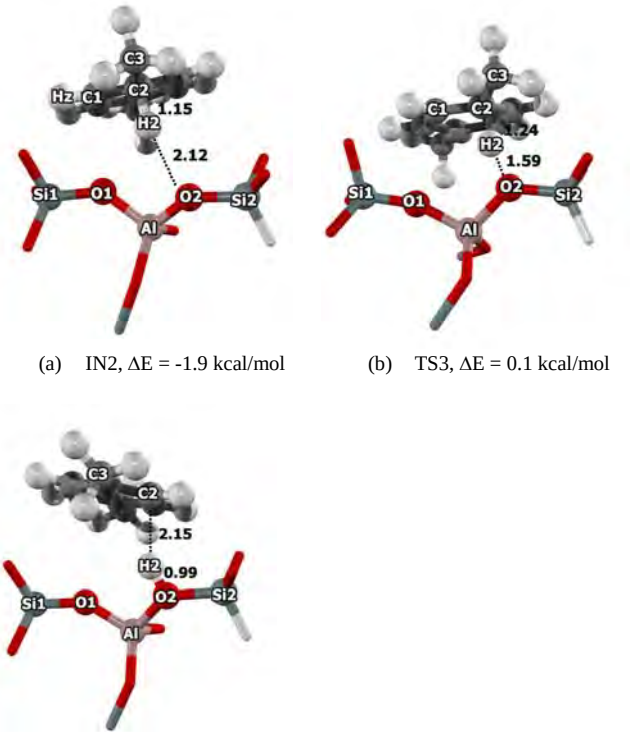

(a) IN2, ΔE = -1.9 kcal/mol (b) TS3, ΔE = 0.1 kcal/mol

(c) PR, ΔE = -22.4 kcal/mol

Figure 4. Optimized structure of *m*-xylene isomerization to *p*-xylene on H-ITQ-22 zeolite: a) the protonated *p*-xylene (IN2), b) the transition structure (TS3) and c) the *p*-xylene product (PR). Distances are in Ås.

Conclusion

The adsorption and isomerization reaction of *m*-xylene to *p*-xylene on H-ITQ-22 has been studied using the M06-2X/6-31G(d,p) functional. The adsorption energy of *m*-xylene is calculated to be -23.9 kcal/mol, which is in the range of experimental data. The isomerization of *m*-xylene to *p*-xylene in H-ITQ-22 was proposed to be in three steps of mechanism, namely: 1) the protonation of *m*-xylene, 2) the methyl shift of protonated *m*-xylene, and 3) the proton back to zeolite and desorption of *p*-xylene. The first step is the rate-determining step with activation energy 29.3 kcal/mol. This study will provide detailed understanding for the adsorption and reaction mechanism of xylene isomerization in the H-ITQ-22 zeolite.

Acknowledgement. This work was supported in part by grants from the National Science and Technology Development Agency (2009 NSTDA Chair Professor funded by the Crown Property Bureau under the management of the National Science and Technology Development Agency and NANOTEC Center of Excellence funded by the National Nanotechnology Center), Kasetsart University Research and Development Institute (KURDI), the Thailand Research Fund (TRF), and the Commission on Higher Education, Ministry of Education (the "National Research University Project of Thailand (NRU)" and the "National Center of Excellence for Petroleum, Petrochemical and Advanced Materials (NCE-PPAM)"). The authors are grateful to Donald G. Truhlar and Yan Zhao for their support with the M06-2X functional.

References

(1) Bhan, A.; Iglesia, E. *Acc. Chem. Res.* **2008**, *41*, 559-567.
(2) Corma, A. *J. Catal.* **2003**, *216*, 298-312.
(3) Smit, B.; Maesen, T. L. M. *Nature (London, U. K.)* **2008**, *451*, 671-678.
(4) Venuto, P. B. *Microporous Mater.* **1994**, *2*, 297-411.
(5) Yaluris, G.; Rekoske, J. E.; Aparicio, L. M.; Madon, R. J.; Dumesic, J. A. *J. Catal.* **1995**, *153*, 65-75.
(6) Corma, A.; Rey, F.; Valencia, S.; Jorda, J. L.; Rius, J. *Nat. Mater.* **2003**, *2*, 493-497.
(7) Kaeding, W. W.; Chu, C.; Young, L. B.; Weinstein, B.; Butter, S. A. *J. Catal.* **1981**, *67*, 159-174.
(8) Chiche, B.; Finiels, A.; Gauthier, C.; Geneste, P.; Graille, J.; Pioch, D. *J. Org. Chem.* **1986**, *51*, 2128-2130.
(9) Kaeding, W. W.; Chu, C.; Young, L. B.; Butter, S. A. *J. Catal.* **1981**, *69*, 392-398.
(10) Martens, J. A.; Perez-Pariente, J.; Sastre, E.; Corma, A.; Jacobs, P. A. *Applied Catalysis* **1988**, *45*, 85-101.
(11) Mirth, G.; Cejka, J.; Lercher, J. A. *J. Catal.* **1993**, *139*, 24-33.
(12) Vos, A. M.; Rozanska, X.; Schoonheydt, R. A.; van Santen, R. A.; Hutschka, F.; Hafner, J. *J. Am. Chem. Soc.* **2001**, *123*, 2799-2809.
(13) Wu, P.; Komatsu, T.; Yashima, T. *Microporous Mesoporous Mater.* **1998**, *22*, 343-356.
(14) Yuan, W.; Lin, Y. S.; Yang, W. *J. Am. Chem. Soc.* **2004**, *126*, 4776-4777.
(15) Derouane, E. G.; Chang, C. D. *Microporous Mesoporous Mater.* **2000**, *35-36*, 425-433.
(16) Kumsapaya, C.; Bobuatong, K.; Khongpracha, P.; Tantirungrotechai, Y.; Limtrakul, J. *J. Phys. Chem. C* **2009**, *113*, 16128-16137.
(17) Maihom, T.; Boekfa, B.; Sirijaraensre, J.; Nanok, T.; Probst, M.; Limtrakul, J. *J. Phys. Chem. C* **2009**, *113*, 6654-6662.
(18) Boekfa, B.; Choomwattana, S.; Khongpracha, P.; Limtrakul, J. *Langmuir* **2009**, *25*, 12990-12999.
(19) Boekfa, B.; Pantu, P.; Probst, M.; Limtrakul, J. *J. Phys. Chem. C* **2010**, *114*, 15061-15067.
(20) Wannakao, S.; Boekfa, B.; Khongpracha, P.; Probst, M.; Limtrakul, J. *ChemPhysChem* **2010**, *11*, 3432-3438.
(21) Zhao, Y.; Truhlar, D. G. *Theor. Chem. Acc.* **2008**, *120*, 215-241.
(22) Zhao, Y.; Truhlar, D. G. *J. Phys. Chem. C* **2008**, *112*, 6860-6868.
(23) Frisch, M. J.; Trucks, G. W.; Schlegel, H. B.; Scuseria, G. E.; Robb, M. A.; Cheeseman, J. R.; Montgomery, J. A., Jr.; Vreven, T.; Kudin, K. N.; Burant, J. C.; Millam, J. M.; Iyengar, S. S.; Tomasi, J.; Barone, V.; Mennucci, B.; Cossi, M.; Scalmani, G.; Rega, N.; Petersson, G. A.; Nakatsuji, H.; Hada, M.; Ehara, M.; Toyota, K.; Fukuda, R.; Hasegawa, J.; Ishida, M.; Nakajima, T.; Honda, Y.; Kitao, O.; Nakai, H.; Klene, M.; Li, X.; Knox, J. E.; Hratchian, H. P.; Cross, J. B.; Adamo, C.; Jaramillo, J.; Gomperts, R.; Stratmann, R. E.; Yazyev, O.; Austin, A. J.; Cammi, R.; Pomelli, C.; Ochterski, J. W.; Ayala, P. Y.; Morokuma, K.; Voth, G. A.; Salvador, P.; Dannenberg, J. J.; Zakrzewski, V. G.; Dapprich, S.; Daniels, A. D.; Strain, M. C.; Farkas, O.; Malick, D. K.; Rabuck, A. D.; Raghavachari, K.; Foresman, J. B.; Ortiz, J. V.; Cui, Q.; Baboul, A. G.; Clifford, S.; Cioslowski, J.; Stefanov, B. B.; Liu, G.; Liashenko, A.; Piskorz, P.; Komaromi, I.; Martin, R. L.; Fox, D. J.; Keith, T.; Al-Laham, M. A.; Peng, C. Y.; Nanayakkara, A.; Challacombe, M.; Gill, P. M. W.; Johnson, B.; Chen, W.; Wong, M. W.; Gonzalez, C.; Pople, J. A. *Gaussian 03, revision B.05; Gaussian, Inc.: Pittsburgh, PA*, 2003.

(24) Klinowski, J. *Chem. Rev.* **1991**, *91*, 1459-1479.
(25) Coker, E. N.; Jia, C.; Karge, H. G. *Langmuir* **2000**, *16*, 1205-1210.
(26) Richards, R. E.; Rees, L. V. C. *Zeolites* **1988**, *8*, 35-39.
(27) Yan, T. Y. *Industrial and Engineering Chemistry Research* **1989**, *28*, 572-576.

Reaction Mechanism of Isomerization of 1-Butene to Isobutene over Multipore H-ITQ-22 Zeolite: A DFT Study

Bundet Boekfa[1,2,4], Piti Treesukol[1,2,4] and Jumras Limtrakul[2,3,4]*

[1]Chemistry Department, Faculty of Liberal Arts and Science, Kasetsart University Kamphaeng Saen Campus, Nakhon Pathom 73140, Thailand
[2]Center for Advanced Studies in Nanotechnology and Its Applications in Chemical, Food and Agricultural Industries, Kasetsart University, Bangkok 10900, Thailand
[3]Laboratory for Computational and Applied Chemistry, Department of Chemistry, Faculty of Science and Center of Nanotechnology, Kasetsart University Research and Development Institute, Kasetsart University, Bangkok 10900, Thailand
[4]NANOTEC Center of Excellence, National Nanotechnology Center, Kasetsart University, Bangkok 10900, Thailand
[*]Corresponding author: Tel.: +662 562 5555 ext 2169, Fax: +662 562 5555 ext 2176, E-mail address: jumras.l@ku.ac.th

Introduction

Zeolites are widely used for their range of applications in petroleum refineries and petrochemical industries[1-4]. With their size- and shape-selectivity and their ability, zeolites are the catalysts of choice for petrochemical catalysts such as hydrocarbon cracking, isomerization and oligomerization[1-3,5]. ITQ-22 (IWR) is a new synthetic multipore zeolite[6] with a pore structure that comprises 8-, 10- and 12-membered-ring pores of 4.52 x 3.32, 5.86 x 4.98 and 6.66 x 6.66 Å, respectively. This zeolite has proved to be an outstanding catalyst for isomerization-disproportionation of m-xylene, and alkylation of benzene with isopropanol and propylene[6].

1-butene isomerization over acidic catalysts is an important reaction for the production of isobutene, a raw material for methyl *tert*-butyl ether (MTBE) and ethyl *tert*-butyl ether (ETBE) production[7-12]. Many zeolites such as Ferrierite, ZSM-5 and Theta-1 zeolite[8,11] have been already used for those reactions. Corma et al. proposed the mechanism for this reaction on Theta-1 zeolite as a monomolecular mechanism[13]. Their activation energy is calculated to be 33-34 kcal/mol, which compares well with the experimental value of 30 kcal/mol. Tuma et al. used the hybrid MP2:DFT to study adsorption of the 1-butene, isobutene, *tert*-butyl cation and their alkoxide species in H-zeolite[14-15]. These studies lead us to understand the reaction in the specific pore of zeolite.

The zeolite framework effect or confinement effect, which is mainly composed of dispersive van der Waals interactions, has been proposed by Derouane[16] to explain the interactions between the zeolite framework and the adsorbed molecule. The conventional DFT functions are not able to describe the van der Waals effect from the zeolite framework. Recently, we have studied a number of adsorptions and reactions in the zeolite framework by using the recently developed M06-functionals including dispersion energy[17-24]. We found that these functionals can be used to describe the confinement effect of the zeolite framework. Combined with a second-order Møller-Plesset perturbation theory (MP2), the ONIOM (MP2:M06-2X) can successfully elucidate the adsorption and reaction mechanism of aliphatic, aromatic and heterocyclic compounds[20].

In this study, we examine the framework effects of this new multipore zeolite, H-ITQ-22, for the 1-butene isomerization into isobutene on the H-ITQ-22 zeolite by means of the well calibrated scheme of ONIOM (MP2:M06-2X). This study will provide the detailed understanding for the adsorption and reaction mechanism of butane isomerization in this new zeolite framework.

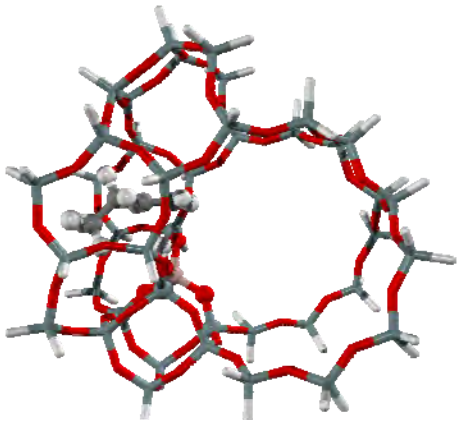

Figure 1. Presentation of 1-butene on H-ITQ-22 models 5T:42T ONIOM model. Atoms treated with the MP2 level of theory are shown in balls, whereas the areas treated with the M06-2X functional are shown in wireframes.

Methodology

The adsorption and reaction of 1-butene on H-ITQ-22 zeolite have been studied with an ONIOM model[25]. An Al atom is selected to substitute the Si atom at the T1 position. The active 5T (T means tetrahedral of Si or Al atoms) represents the Brønsted acid site assigned to be the inner layer, where the extended 42T model is the outer layer. The 5T inner layer of the ONIOM model is calculated with the MP2/6-31G(d,p) level of theory while the 42T outer layer is performed with the M06-2X/6-31G(d,p) level of theory[20]. The ONIOM 5T:42T is shown in Fig. 1. Only the active region, $AlSi_4O_4H$ and the probe molecule are allowed to relax while the rest is kept fixed with the crystallographic structure[6]. All calculations were performed using the Gaussian 03 program[26] incorporated with the Minnesota Density Functionals module 3.1 by Zhao and Truhlar[17-18].

Results and Discussion

Butane and 1-butene adsorptions onto the Brønsted acid site of H-ITQ-22. The ONIOM model for the H-ITQ-22 zeolite is illustrated in Fig. 1. The 42T quantum cluster is modeled to cover the intersection cavity (10T and 12T) where the guest molecule prefers to locate. The inner-layer 5T cluster, representing the Brønsted acid site, is calculated with the MP2 calculation while the outer-layer 42T cluster, representing the framework of zeolite, is calculated with the M06-2X functional. The acidic O1-Hz distance is calculated to be 0.97 Å. The Al ··· Hz bond distance is about 2.37 Å, which agrees well with the experiment data (2.38-2.48 Å)[27].

The optimized structures of butane and 1-butene on H-ITQ-22 zeolite are shown in Figures 2a and 2b, respectively. The butane molecule adsorbs in the 10T pore of H-ITQ-22 via interactions between the alkyl group and the Brønsted acid site of zeolite. The acidic O1-Hz bond distance is almost the same as in the isolated zeolite (0.97 Å). The distance between the carbon atom of butane and the Brønsted acid site (C2 ··· Hz) distance is 2.79 Å. The adsorption energy of butane on H-ITQ-22 is calculated to be -11.8 kcal/mol. This energy compares well with the experimental data of -11.9 kcal/mol for butane on H-MOR zeolite[28] and -12.6 kcal/mol for butane H-ZSM-5 zeolite[29].

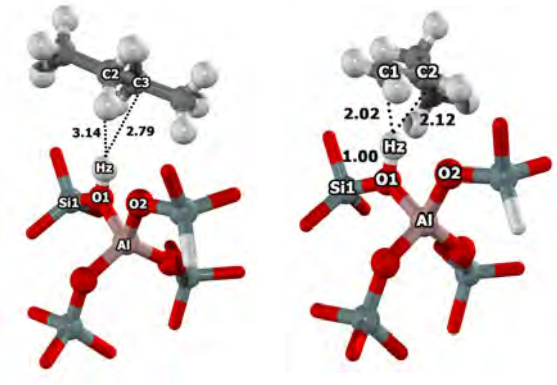

(a) Butane, ΔE= -11.8 kcal/mol

(b) 1-butene, ΔE= -20.5 kcal/mol

Figure 2. Optimized structure of butane (a) and 1-butene (b) on H-ITQ-22 zeolite. Distances are in Ås.

The 1-butene molecule prefers to adsorb on the Brønsted acid site via the π-bond interaction of the double bond carbons. The acidic O1-Hz bond distance is increased to 1.00 Å. The distances between the double bond carbon and the Brønsted acid site (C1 - - Hz and C2 - - Hz) are 2.02 and 2.12 Å, respectively. The calculated adsorption energy is -20.6 kcal/mol. Only the adsorption of ethene on H-FAU from the experiment is reported to be -9.1 kcal/mol by Cant and Hall[30]. With the greater acidity of H-ITQ-22 and the larger probe molecule, our calculated adsorption energy of 1-butene on H-ITQ-22 is in the range of experimental data.

1-butene Isomerization to Isobutene on H-ITQ-22 The isomerization reaction of 1-butene to isobutene on H-ITQ-22 is proposed as a stepwise mechanism via 4 steps: 1) the secondary alkoxide intermediate formation via the protonation of 1-butene, 2) the cyclic transition state via the methyl shift and the primary alkoxide intermediate formation, 3) the *tert*-carbenium cation formation via the proton shift and 4) the protonation back to zeolite and desorption of isobutene. Fig. 3 shows the energies profile for the 1-butene isomerization reaction.

The 1-butene molecule is adsorbed in the intersection pore at the 10T position of ITQ-22 [AD, Figure 2b] with an adsorption energy of -20.5 kcal/mol. The first transition state [TS1, Figure 4a] is the secondary alkoxide intermediate formation. The Brønsted acid O1-Hz bond is broken and the strong covalent bond O2-C2 is formed. This step requires an activation energy of about 17.1 kcal/mol. The intermediate [IN1, Figure 4b] strongly interacts with zeolite with a relative energy of -27.0 kcal/mol. The second transition state [TS2, Figure 4c] is the cyclic transition state via the methyl shift. The C4 atom breaks the bond with the C3 atom and forms a bond with the C2 atom. This corresponds with the breaking of the O2-C2 bond and the forming of the O2-C3 bond. The activation energy is calculated to be 30.4 kcal/mol. The primary alkoxide intermediate [IN2, Figure 4d] is the product with a relative energy of -27.7 kcal/mol.

The third transition state [TS3, Figure 5a] is the proton transfer from C2 to C3 with an activation energy of 38.2 kcal/mol. This step is the rate determining step of the 1-butene isomerization reaction

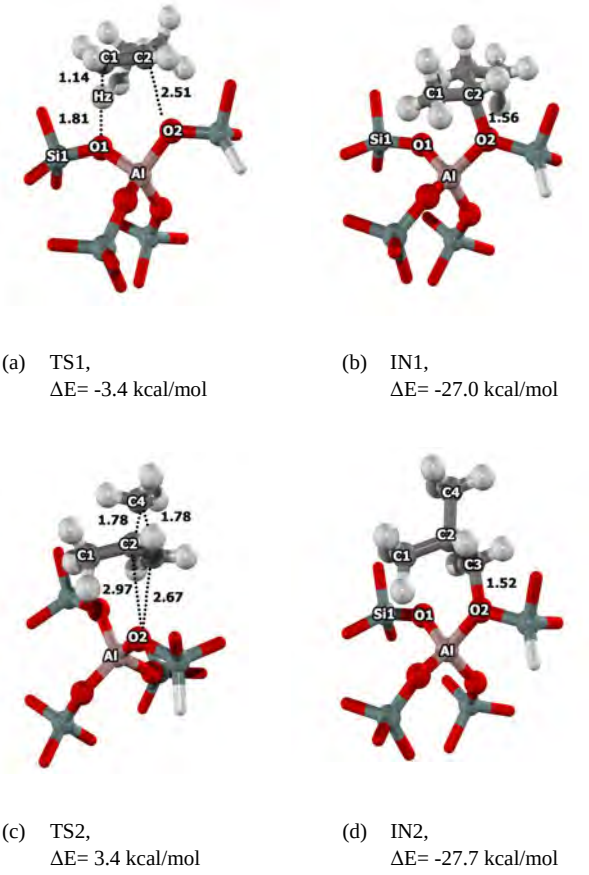

(a) TS1, ΔE= -3.4 kcal/mol

(b) IN1, ΔE= -27.0 kcal/mol

(c) TS2, ΔE= 3.4 kcal/mol

(d) IN2, ΔE= -27.7 kcal/mol

Figure 4. Optimized structure of 1-butene isomerization to isobutene on H-ITQ-22 zeolite: a) the transition structure (TS1), b) the secondary alkoxide intermediate (IN1), c) the transition structure (TS2), d) the primary alkoxide intermediate (IN2). Distances are in Ås.

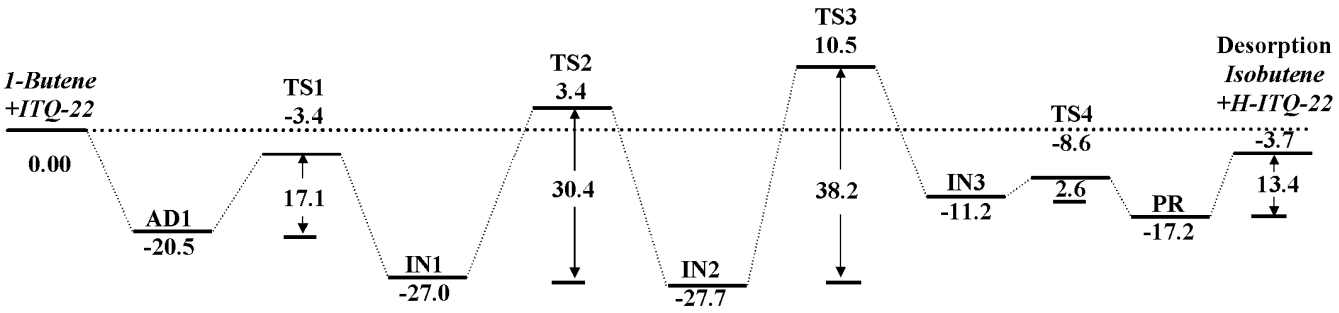

Figure 3. Potential energy diagram of the 1-butene to isobutene on the 5T:42T ONIOM (MP2:M06-2X) method (kcal/mol).

and gives the *tert*-butyl carbenium ion product [IN3, Figure 5b]. The *tert*-butyl carbenium is not stable and can move easily to isobutene via the forth transition state [TS4, Figure 5c]. The activation energy is only 2.6 kcal/mol. The isobutene product is adsorbed on H-ITQ-22 via a π-bonding interaction with a relative energy -17.2 kcal/mol [PR, Figure 5d]. The desorption energy of isobutene on H-ITQ-22 is 13.4 kcal/mol. The 1-butene isomerization to isobutene is an exothermic reaction with a heat of reaction (ΔH) of 4.1 kcal/mol.

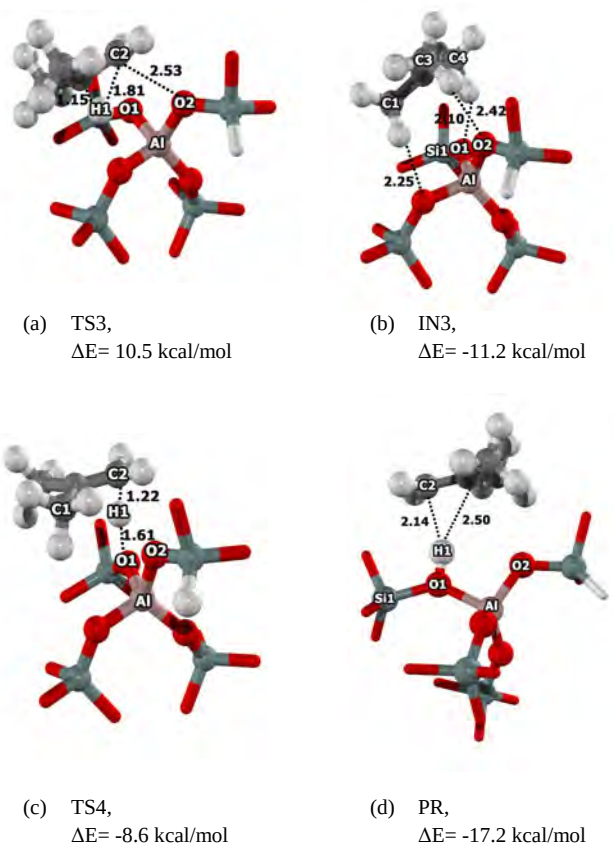

(a) TS3, ΔE= 10.5 kcal/mol

(b) IN3, ΔE= -11.2 kcal/mol

(c) TS4, ΔE= -8.6 kcal/mol

(d) PR, ΔE= -17.2 kcal/mol

Figure 5. Optimized structure of 1-butene isomerization to isobutene on H-ITQ-22 zeolite: a) the transition structure (TS3), b) the *tert*-butyl carbenium cation (IN3), c) the transition structure (TS4), d) the product isobutene adsorption (PR). Distances are in Ås.

Energetic Analysis between quantum cluster MP2 and ONIOM (MP2:M06-2X) The energies profile for 1-butene isomerization to isobutene on H-ITQ-22 is shown in Figure 3 and the energies are shown in Table 1. The adsorption energies are calculated to be -20.5 and -11.2 kcal/mol for 5T:42T and 5T, respectively. The framework increases the adsorption energy by about 45%. The reaction mechanism of 1-butene to isobutene is proposed to be step four of the mechanisms. Without the framework effect, the activation energies are calculated to be 25.4, 51.3, 46.3 and 0.6 kcal/mol on the 5T cluster with the MP2 calculation. The activation energies are decreased to be 17.1, 30.4, 38.2 and 2.6 kcal/mol with the 5T:42T ONIOM (MP2:M06-2X). The framework stabilizes the transition structure by as much as 30-40 % and the values are in the range of the experimental data. We suggest that the ONIOM (MP2:M06-2X) is practical for the study of the framework effect on the adsorption and reaction mechanism in the ITQ-22 zeolite.

Table 1. The Contribution Analysis on the 1-butene isomerization on 5T:42T of ITQ-22 calculated with the ONIOM (MP2:M06-2X). Intrinsic activation energies are in parenthesis. Energies are in kcal/mol.

Model	5T:42T	5T // 5T:42T
Method	ONIOM (MP2:M06-2X)	MP2//ONIOM (MP2:M06-2X)
AD	-20.5	-11.2
TS1	-3.4 (17.1)	14.2 (25.4)
IN1	-27.0	-24.7
TS2	3.4 (30.4)	26.6 (51.3)
IN2	-27.7	-24.9
TS3	10.5 (38.2)	21.4 (46.3)
IN3	-11.2	4.6
TS4	-8.6 (2.6)	5.2(0.6)
PR	-17.2	7.9

Conclusions

The adsorption and isomerization reaction of 1-butene on H-ITQ-22 were theoretically studied using the ONIOM (MP2:M06-2X) approach. The adsorption energy of 1-butene on H-ITQ-22 is calculated to be -20.5 kcal/mol, which is in the range of experimental data. The reaction mechanism of 1-butene isomerization is proposed to be in four steps: 1) the secondary alkoxide intermediate formation via the protonation of 1-butene, 2) the cyclic transition state via the methyl shift and the primary alkoxide intermediate formation, 3) the *tert*-carbenium cation formation via the proton shift and 4) the protonation back to zeolite and desorption of isobutene. The activation energies are calculated to be 17.1, 30.4, 38.2 and 2.6 kcal/mol, respectively. The rate determining step is the *tert*-carbenium cation formation. This multi-pore H-ITQ-22 zeolite is suggested as one of the candidate materials for selective isomerization of 1-butene to isobutene and should be of particular interest to the petrochemical industry.

Acknowledgement. This work was supported in part by grants from the National Science and Technology Development Agency (2009 NSTDA Chair Professor funded by the Crown Property Bureau under the management of the National Science and Technology Development Agency and NANOTEC Center of Excellence funded by the National Nanotechnology Center), Kasetsart University Research and Development Institute (KURDI), the Thailand Research Fund (TRF), and the Commission on Higher Education, Ministry of Education (the "National Research University Project of Thailand (NRU)" and the "National Center of Excellence for Petroleum, Petrochemical and Advanced Materials (NCE-PPAM)"). The authors are grateful to Donald G. Truhlar and Yan Zhao for their support with the M06-2X functional.

References

(1) Bhan, A.; Iglesia, E. *Acc. Chem. Res.* **2008**, *41*, 559.
(2) Corma, A. *J. Catal.* **2003**, *216*, 298.
(3) Smit, B.; Maesen, T. L. M. *Nature (London, U. K.)* **2008**, *451*, 671.
(4) Venuto, P. B. *Microporous Mater.* **1994**, *2*, 297.
(5) Yaluris, G.; Rekoske, J. E.; Aparicio, L. M.; Madon, R. J.; Dumesic, J. A. *J. Catal.* **1995**, *153*, 65.
(6) Corma, A.; Rey, F.; Valencia, S.; Jorda, J. L.; Rius, J. *Nat. Mater.* **2003**, *2*, 493.
(7) Andy, P.; Gnep, N. S.; Guisnet, M.; Benazzi, E.; Travers, C. *J. Catal.* **1998**, *173*, 322.
(8) Guisnet, M.; Andy, P.; Gnep, N. S.; Benazzi, E.; Travers, C. *J. Catal.* **1996**, *158*, 551.

(9) Houžvička, J.; Hansildaar, S.; Ponec, V. *J. Catal.* **1997**, *167*, 273.
(10) Jousse, F.; Leherte, L.; Vercauteren, D. P. *Mol. Simul.* **1996**, *17*, 175.
(11) Meriaudeau, P.; Bacaud, R.; Ngoc Hung, L.; Vu, A. T. *J. Mol. Catal. A: Chem.* **1996**, *110*.
(12) Mériaudeau, P.; Tuan, V. A.; Le, N. H.; Szabo, G. *J. Catal.* **1997**, *169*, 397.
(13) Boronat, M.; Viruela, P.; Corma, A. *Phys. Chem. Chem. Phys.* **2001**, *3*, 3235.
(14) Tuma, C.; Kerber, T.; Sauer, J. *Angew. Chem.-Int. Edit.* **2010**, *49*, 4678.
(15) Tuma, C.; Sauer, J. *Phys. Chem. Chem. Phys.* **2006**, *8*, 3955.
(16) Derouane, E. G.; Chang, C. D. *Microporous Mesoporous Mater.* **2000**, *35-36*, 425.
(17) Zhao, Y.; Truhlar, D. G. *J. Phys. Chem. C* **2008**, *112*, 6860.
(18) Zhao, Y.; Truhlar, D. G. *Acc. Chem. Res.* **2008**, *41*, 157.
(19) Bobuatong, K.; Probst, M.; Limtrakul, J. *J. Phys. Chem. C* **2010**, *114*, 21611.
(20) Boekfa, B.; Choomwattana, S.; Khongpracha, P.; Limtrakul, J. *Langmuir* **2009**, *25*, 12990.
(21) Boekfa, B.; Pantu, P.; Probst, M.; Limtrakul, J. *J. Phys. Chem. C* **2010**, *114*, 15061.
(22) Maihom, T.; Boekfa, B.; Sirijaraensre, J.; Nanok, T.; Probst, M.; Limtrakul, J. *J. Phys. Chem. C* **2009**, *113*, 6654.
(23) Pantu, P.; Boekfa, B.; Limtrakul, J. *J. Mol. Catal. A: Chem.* **2007**, *277*, 171.
(24) Wannakao, S.; Boekfa, B.; Khongpracha, P.; Probst, M.; Limtrakul, J. *ChemPhysChem* **2010**, *11*, 3432.
(25) Dapprich, S.; Komiromi, I.; Byun, K. S.; Morokuma, K.; Frisch, M. J. *THEOCHEM* **1999**, *461-462*, 1.
(26) Frisch, M. J.; Trucks, G. W.; Schlegel, H. B.; Scuseria, G. E.; Robb, M. A.; Cheeseman, J. R.; Montgomery, J. A., Jr.; Vreven, T.; Kudin, K. N.; Burant, J. C.; Millam, J. M.; Iyengar, S. S.; Tomasi, J.; Barone, V.; Mennucci, B.; Cossi, M.; Scalmani, G.; Rega, N.; Petersson, G. A.; Nakatsuji, H.; Hada, M.; Ehara, M.; Toyota, K.; Fukuda, R.; Hasegawa, J.; Ishida, M.; Nakajima, T.; Honda, Y.; Kitao, O.; Nakai, H.; Klene, M.; Li, X.; Knox, J. E.; Hratchian, H. P.; Cross, J. B.; Adamo, C.; Jaramillo, J.; Gomperts, R.; Stratmann, R. E.; Yazyev, O.; Austin, A. J.; Cammi, R.; Pomelli, C.; Ochterski, J. W.; Ayala, P. Y.; Morokuma, K.; Voth, G. A.; Salvador, P.; Dannenberg, J. J.; Zakrzewski, V. G.; Dapprich, S.; Daniels, A. D.; Strain, M. C.; Farkas, O.; Malick, D. K.; Rabuck, A. D.; Raghavachari, K.; Foresman, J. B.; Ortiz, J. V.; Cui, Q.; Baboul, A. G.; Clifford, S.; Cioslowski, J.; Stefanov, B. B.; Liu, G.; Liashenko, A.; Piskorz, P.; Komaromi, I.; Martin, R. L.; Fox, D. J.; Keith, T.; Al-Laham, M. A.; Peng, C. Y.; Nanayakkara, A.; Challacombe, M.; Gill, P. M. W.; Johnson, B.; Chen, W.; Wong, M. W.; Gonzalez, C.; Pople, J. A. *Gaussian 03, revision B.05; Gaussian, Inc.: Pittsburgh, PA*, 2003.
(27) Klinowski, J. *Chem. Rev.* **1991**, *91*, 1459.
(28) Eder, F.; Stockenhuber, M.; Lercher, J. A. *J. Phys. Chem. B* **1997**, *101*, 5414.
(29) Yoda, E.; Kondo, J. N.; Domen, K. *J. Phys. Chem. B* **2005**, *109*, 1464.
(30) Cant, N. W.; Hall, W. K. *J. Catal.* **1972**, *25*, 161.